Induction Generator Wind Energy Research Program and Adaptive Power Factor Controller

Bonneville
POWER ADMINISTRATION

March 1987

INDUCTION GENERATOR WIND ENERGY RESEARCH PROGRAM

AND

ADAPTIVE POWER FACTOR CONTROLLER

FINAL TECHNICAL REPORT DOE/BP/22849--1

CONTRACT NUMBER: 80 BP 22849 DE90 011858

October 1, 1983 - December 31, 1986

Prepared For

BONNEVILLE POWER ADMINISTRATION
Portland, Oregon

Project Manager: N.G. Butler

&

SOUTHERN CALIFORNIA EDISON COMPANY
Rosemead, California

Project Manager: R.J. Yinger

by

S.S. Venkata & M.A. El-Sharkawi

UNIVERSITY OF WASHINGTON
Seattle, WA 98195

Acknowledgements

Several persons and organizations contributed to the successful completion of the work documented in this report and the development of the report itself. We wish to express our immense appreciation to Mr. Nicholas G. Butler, BPA, for his constant support, active participation, and the various constructive suggestions he provided us throughout the project period. We are also thankful to Mr. Douglas Seely and Mr. Bill Meyers for expressing confidence in our work by means of continued support for the contract.

Secondly, we wish to thank Mr. Robert J. Yinger, Mr. Michael Wehrey, Mr. Robert Scheffler, Dr. Kirby C. Holte and Mr. Roy L. Schellenberg, of Southern California Edison Company, for their support in the development and field testing of both 50-kVAR and 300-kVAR APFCs. We also express our gratitude to Mr. John Kelly and Mr. Darrell Bone, for their valuable assistance in the field.

Thirdly, we wish to thank the following graduate students who performed the "real" work: Mr. Ming-Liang Chen, Mr. Gregory Fissel, Mr. Disbeng Pei, Mr. Subramanian V. Vadari, Mr. Timothy J. Williams. Without the assistance of Mr. John Schulz (Technician), we could not have fabricated and installed all the APFCs. We also thank Ms. Carmen Leon for her patience in typing this report.

Finally, we wish to acknowledge the equipment gifts provided by John Fluke Manufacturing Company (digital multimeters and other instrumentation), Hewlett-Packard Company (HP 87 based data acquisition system). These were immensely useful throughout the course of the project.

CONTENTS

ILLUSTRATIONS

TABLES

SUMMARY

Overview

Several wind power stations consisting of clusters of wind turbines with induction generators in 20 to 400-kW range are emerging in several places in the United States. In larger stations such as in the Tehachapi pass area, east of Bakersfield in Southern California, there are already thousands of machines feeding real power into the Southern California Edison (SCE) Company's system. Similar but smaller stations can also be found in Oregon and Hawaii [1-6]. Many more are expected to spring up in the Pacific Northwest as well as in other parts of the United States by the year 2000. Table 1.1 shows the growth pattern of wind energy generation in the United States. [7].

Table 1.1 Wind Energy Generation in U.S.

Year	Cumulative Installed (MW)	Planned (MW)
1983	87	
1984	230	
1985	600	
1986	1,100	
1990		2,000
2000		5,000

Thus there is a great potential for wind energy. However, there are several problems associated with wind turbine systems. First and foremost is the tremendous demand of reactive power drawn by these three-phase induction generators from the utility. In most cases the amount of reactive power needed by these machines often exceeds the amount of real power they generate [6]. Secondly, most manufacturers of

the wind turbine systems are using standard induction motors as generators, resulting in less than optimum performance.

Recognizing, and consequently concerned with these problems, Bonneville Power Administration (BPA) funded a research contract with the University of Washington (UW) to investigate effective and practical solutions. This contract was initiated in January 1983 and it was completed in December 1986. The summary and findings of these two-part investigations on the intermediate-size wind turbines is the subject of this final report.

The first part is devoted to the investigation of viable schemes to improve the steady-state performance of commercially-available induction machines as generators. Initital efforts during FY 1983 were directed to the survey of wind energy systems manufacturers as well as motor manuafacturers who supplied the induction machines to the former. It was clear from these surveys and UW's previous investigations on small wind machines [8] that the existing machines' performance characteristics, particularly efficiency and power factor, when they are operated as generators, could be improved by combining the following four factors in several desirable ways: the direction of rotation, the supply voltage phase sequence, the insertion of a series capacitor in each auxiliary winding, and the incorporation of proper phase shift between the main and auxiliary windings on the same phase belt. During the following three years (FY 84 to 86) the work proceeded on the development of suitable mathematical models and their simulation on a computer, experimental investigation of the performance characteristics on a laboratory size (6-kW) generator in the UW Energy Systems

Laboratory to validate the models, and the identification of viable generator schemes. The results indicated that two schemes can provide better performance than the conventional mode of operation of the generator. At the same time, suitable techniques were developed to investigate the economic feasibility and reliability of the induction generators and wind turbine systems.

Significant effort was directed to the second part of the project which dealt with the investigation of ways to alleviate the reactive power drain from the utility grid by scores of these wind turbine generators. The development of a 7.5-kVAR, 480-V, three-phase, Adaptive Power Factor Controller (APFC) was initiated during the FY 1983. The feasibility of the APFC concept was successfully demonstrated by the UW research group in their Energy Systems Laboratory by thoroughly testing the controller on a 6.0-kW, induction generator [1].

Encouraged by the success of the 7.5-kVAR APFC, SCE joined BPA in the development of a 50-kVAR, 480-V, three-phase, APFC in the Summer of 1984. The APFC was tested successfully at the UW laboratory. It is currently connected to a 50-kW induction generator located in the SCE's Devers Wind Energy R&D Center near Palm Springs, California. Preliminary tests at the SCE site indicated that the intended performance was well verified even during the starting and braking of the turbine, and when the turbine and the feeder were suddenly disconnected from the grid. Further monitoring of the device is continuing. The field data, collected for more than a year, supported the reliable operation of the device. Both devices have been modified

several times to assure best performance and to reduce unnecessary complexities.

Subsequently, in July 1985, BPA and SCE jointly initiated the development of a 300-kVAR, 480-V, three-phase APFC for continuously compensating the reactive power needs of a group of seven horizontal-axis wind turbine machines, each rated 65-kW, connected to a common bus. The APFC was installed at the Oak Creek Energy Systems Inc. wind power station located in Tehachapi Pass, California, in May 1986. The field testing program is continuing successfully. The field data gathered did prove the intended performance of the device.

PROJECT GOAL AND OBJECTIVES

The primary goal of the project is to assure efficient and effective use of electric energy in the Pacific Northwest. With this goal in mind, two major objectives were defined. These were:

1) To identify and evaluate ways and means of improving the steady-state performance characteristics of commercially-available three-phase induction machines for the generator mode of operation.

2) To demonstrate the use of APFCs as an efficient and practical solution for alleviating the effects of excessive reactive power consumed by the induction generators in wind power stations.

REPORT ORGANIZATION

This report is organized into two major parts. Part I reports on the details of the induction generator evaluation. It is divided into the following five chapters: Survey of Induction Generators; Model

Development and Simulation of Generator Performance; Experimental Investigations on Induction Generators; Economic Feasibility Analysis of Induction Generators and Wind Turbine Systems; and Reliability Assessment of Induction Generators and Wind Turbine Systems.

Part II of the report deals entirely with the APFC work. It also contains the following five chapters on the development and demonstration of the APFC concept: Concept Development, Design and Demonstration of 7.5-kVAR Adaptive Power Factor Controller; Design and Fabrication of 50-kVAR Open-Loop APFC (OL-APFC) and Transient Simulation; Installation and Field Testing of 50-kVAR , OL-APFC at Southern California Edison's Devers Site; Development and Design of a 300-kVAR Closed-Loop APFC (CL-APFC); and Installation and Field Testing of 300-kVAR CL-APFC at Oak Creek Energy Systems Wind Park, Tehachapi, California.

PROJECT SUMMARY, RESULTS, CONCLUSIONS AND RECOMMENDATIONS

Part I: Wind Turbine Induction Generator Evaluation

1. Chapter 1 summarizes the results of a survey of eight wind turbine manufacturers and ten induction motor manufacturers. Chronologically, the following five categories of induction machines have emerged since 1955: U-frame motors, T-frame motors, energy-efficient motors, multi-speed generators and high-efficiency generators. The U-frame motors, energy-efficient motors and high-efficiency generators are too expensive for wind turbine manufacturers and wind farm developers to consider. Therefore, they have opted for commercially-available T-frame motors instead. Unfortunately, these motors do not possess desirable

performance characteristics for the generator mode of operation. The UW group concluded that by adopting simple, inexpensive, practical and operational modifications to these T-frame machines, their performance as generators can be improved.

2. Most of the T-frame machines used in wind turbine applications have two windings per phase on the same stator belt to realize dual-voltage operation. Chapter 2 summarizes the development of three models for these machines with the following four factors included: (i) supply voltage sequence (abc or acb), (ii) direction of rotation (ccw or cw), (iii) insertion of a fixed capacitor in series with each auxiliary winding and (iv) incorporation of proper phase shift between the main and auxiliary winding on the same phase belt. A systematic computer simulation of the model identified two viable schemes which can provide improvement in generator performance.

3. In order to validate the models, extensive experimental investigations were carried out on a 7.5-hp, three-phase, NEMA class-B, induction motor (6.0-kW as a generator). An accurate, micro-processor-based data acquisition system was fabricated to record each set of readings simultaneously. Based on the results obtained, the following conclusions were made:

a) The efficiency of the generator for the two proposed schemes increased by 1 to 2 percentage points over the conventional connection scheme in the intended range of operation.

b) The power factor of the machine improved substantially, though not optimally, due to the insertion of a fixed capacitor in the same operational range.

4. Chapter 4 provides a concise summary of a methodology for assessing the economic feasibility of using induction generators in wind energy conversion systems (WECS). In recommending the present worth method, the analysis includes such factors as accurate energy calculations, different tariff rates, tax credits, income-tax, accelerated depreciation and inflation. The application of the methodology to a practical 50-kW system indicates its payback period is about 3 years.

5. The use of the fault tree methodology was demonstrated to determine the reliability indices of induction generators and WECS in which they are used. The constant failure rates of components were accelerated by a factor of 1.4 to account for hostile environmental conditions under which the wind turbine systems operate. Chapter 5 succintly describes the technique and includes other relevant details.

Part II Adaptive Power Factor Controller (APFC)

6. The APFC was conceived as an adaptive, local, reactive power compensating device to alleviate the effects of reactive power demanded by the induction generators in wind power stations. The magnitude of reactive power drawn by a wind turbine fluctuates rapidly due to changing wind speed. The APFC, being an electronic device, can rapidly and adaptively switch to meet this situation without introducing harmonics or transients into the system. It can achieve close to unity power factor at the point of installation regardless of the variation in the real or reactive power of the induction generator. It can also be adjusted to maintain a power factor less than unity if so desired.

Other functional characteristics of the APFC are: it avoids self-excitation and overvoltage problems; it compensates the reactive power needs in each phase separately and, hence, it can be applied to unbalanced three-phase systems; it is modular to fit various sizes of compensations and, finally, it is simple and may be cost-effective in certain applications.

The concept was proved feasible by building a fractional VAR APFC in the UW laboratory and testing it against a single-phase fractional hp induction motor. The detailed summary of the concept is delineated in Chapter 1 of Part II of this report.

7. The first three-phase, OL-APFC rated at 7.5-kVAR, 480-V was then designed and fabricated. The details of this development along with the test results may be found in Chapter 1. This device was developed to possess three binary stages of switching, yielding eight discrete and equal steps of compensation.

8. The first practical OL-APFC was developed with hardware funds provided by SCE, and engineering development funds borne by BPA. The device, rated at 50-kVAR, 480-V, was also provided with three binary stages of compensation, but with individual phase control and switching. The device has been operating successfully since it was installed during the Summer of 1985 at SCE's Devers test site located near Palm Springs, California. The field data accumulated with an IBM-PC/XT based system for 1,400 hours of operation indicated that it can adaptively compensate the reactive power needs of a 50-kW, vertical-axis, wind machine manufactured by DAF-INDAL Inc. Chapter 2 summarizes this development

together with the results of the transient simulation analysis of the switching circuit.

9. The installation and field testing program results of this 50-kVAR OL-APFC are reported in Chapter 3. As mentioned earlier, the steady-state data collected proved the intended performance and reliability of the device.

10. The various versions and sizes of APFCs developed thus far were open-loop in design, with which it was not possible to verify whether the right number of capacitors was switched every desired moment or not. The UW team has recently developed a 300-kVAR closed-loop APFC design, the details of which are summarized in Chapter 4.

11. Encouraged by the 50-kW program results, the UW team proceeded to build a 300-kVAR, 480-V, CL-APFC to compensate a cluster of seven horizontal-axis wind machines at the Oak Creek Energy Systems Wind Farm in the Tehachapi Pass area as mentioned earlier. This device has four binary stages of compensation, yielding sixteen steps of discrete control. It was also designed to switch each phase independently. It was installed in May of 1986. A similar IBM-PC/XT system, as was installed in the Devers site, has the capability of monitoring the generator group's 18 electrical performance variables. The field data gathered to date indicated flawless performance of the device. With the exception of some SCR failures. The cause of these failures has been analysed and design changes have been made to eliminate future failures. Details on this version of the APFC are summarized in Chapter 5.

SUPPLEMENTARY READING MATERIAL

Additional details on the contents of this final report can be found in the following references [1,2,9-18].

PART 1

WIND TURBINE INDUCTION GENERATOR EVALUATION

CHAPTER 1

SURVEY OF WIND TURBINE INDUCTION GENERATORS

1.1 Introduction

This task was undertaken during FY 1983 to compile and evaluate the status of induction generators used in intermediate-size wind turbine systems. Separate surveys were conducted for wind turbine system manufacturers and induction motor manufacturers.

1.2 Survey of Wind Turbine Manufacturers

The following eight manufacturers were contacted through a one-page survey form and a transmittal letter explaining the purpose of the survey: 1) DAF INDAL, Canada; 2) Enertech, Norwich, VT; 3) Flowind, Kent, WA; 4) Hamilton, Los Angeles, CA; 5) Hydro-Stoch, Millville, CA; 6) Jay Carter, Burkburnett, TX; and 8) Wind Energy Systems, Buffalo, NY. Based on the response provided by five of these companies, the following generalizations may be made:

1) Intermediate-size wind turbine generators are generally equipped with squirrel-cage induction machines, which are simpler to build, rugged, cheaper and can be more easily synchronized with the utility supply than their synchronous counterparts.

2) The cut-in speed of these machines is in the range of 6 to 10 mph. The cut-out speeds are in the range of 40 to 50 mph, with rated or less than rated power generation occuring at this speed. Both horizontal and vertical axis machines are used.

3) Large wind farms are emerging in some parts of the U. S., particularly on the west coast. Thousands of machines have been installed, most of which are equipped with induction generators in the range of 20 to 400 kW. For example, in the State of California wind farms are located in three main areas: Altamont Pass, east of San Francisco; San Gorgonio Pass, east of Los Angeles near Palm Springs; and Tehachapi Pass east of Bakersfield. Additional wind farms are also located in Oregon and Hawaii.

4) Most of these systems are interconnected to the respective utility grid at the primary distribution voltage (for example, 15-kV) level. Since standard NEMA design B induction machines (with a power factor profile of 0.45 to 0.8 lagging in the expected operational range) are used, these systems draw a significant amount of reactive power from the utility system. In some cases, the manufacturers provide partial compensation with fixed capacitors, which is not an optimum solution.

5) Generally, intermediate-size wind turbine systems do not have precision speed-control mechanisms, since they cannot be economically justified.

1.3 Survey of Motor Manufacturers

Since most wind turbine manufacturers were utilizing standard three-phase induction motors as generators, this survey was undertaken in a similar manner as indicated earlier, to obtain a comprehensive understanding of these machines. The following eleven manufacturers

were contacted: Baldor, General Electric, Lesson, Lincoln, Marathon, Reliance, Sterling, TECO, Toshiba, U. S. Electric and Westinghouse. In response, they provided their catalogs and information germane to wind turbine systems.

The following trends have occured in the development of induction motors in the past three to four decades.

1) U-frame motors: These were introduced in 1955. These were basically liberal designs and had Class A insulation with 105 degrees C hot spot temperature rating. Their operating current and flux densities were lower, resulting in a larger frame size for a given output. The power factor and the efficiency profiles were moderately better. Presently available U-frame machines are equipped with synthetic insulating materials and are expected to have a better life expectancy than their earlier models [19].

2) T-frame motors: These came into existence in 1965. Stimuli for the T-frame program came from technological advances that demanded motor re-rating and an overall national economy that dictated it. The re-rating program was initiated by National Electric Manufacturers Association (NEMA). The intent was to include the changes in the frame assignment, shaft dimensions, and insulation class. Some of the characteristics of the T-frame machines include optimum design for minimal material, higher current and flux density, and smaller frame size. The T-frame motors were

designed for better insulation, life expectancy, and a marked gain in bearing performance [19].

3) Energy efficient motors: The escalation of oil prices and the attendant increase in cost of electric power since 1974 made it increasingly expensive to use motors with lower efficiency. Electric power rates have increased at an average of 11.5% per year since 1972 [20]. Therefore, several manufacturers initiated programs for developing energy-efficient motors. In order to decrease machine losses, lower current and flux densities were adopted resulting in increased efficiency. Such expensive energy efficient motors have 10 to 30% higher initial cost compared to conventional machines, with a payback period of 12 to 24 months [21].

4) Multi-speed generators: Single-winding, dual-speed (for example 1,200/1,800 r/min) machines are manufactured for discrete speed-control applications. Apparently, these generators provide greater efficiency even at lower speeds. These machines are manufactured to operate as motors but are used as generators for several renewable applications. The maximum size available is 375-kW [22].

5) High Efficiency Generators: These machines are specifically designed for generator applications with lower flux density values. Also, better materials such as high permeability silicon steel laminations and Class C insulation, are used in the manufacturing process. The result is reduced loss and

slightly higher efficiency than conventional induction generators. However, this development is not attractive for wind-farm developers because of their higher first cost [23].

In summary, U-frame motors, energy efficient-motors, and high efficiency generators are considered to be too expensive by wind turbine manufacturers. Therefore, they have adopted commercially available NEMA Design Class B, T-frame motors instead. Unfortunately, these motors do not possess desirable performance characteristics for the generator mode of operation. To be specific, these motors have an almost flat efficiency profile varying between 75% to 88% depending on the size and the load, the smaller values being valid for lower sizes and reduced loads [24]. In a similar manner, the corresponding power factor profile varies between 45% and 80% exhibiting a similar trend as the efficiency profile. Because the reactive demand of these generators is higher than in the motor mode of operation for the same slip speed [14], the power factor profile will further deteriorate in the generator mode of operation. For these reasons, an in-depth investigation of commercially available induction motors in the 25-500 hp class was undertaken. The summary of the various aspects, such as their performance improvement, economic feasibility and reliability assessment, are reported in Chapters 2 through 5.

CHAPTER 2

MECHANISMS FOR IMPROVING INDUCTION GENERATOR PERFORMANCE

2.1 Introduction

Most of the manufacturers of intermediate-size turbine generators (20-kW to 400-kW) are using standard induction motors as generators. This is because of the ability of the induction machine to perform over a limited variable speed range during its operation compared with a synchronous generator which must maintain constant speed. Due to the gusty nature of the wind, energy conversion systems need to be flexible in their ability to respond, both, mechanically and electrically to the significant moment-by-moment variation in power, available and extracted from the wind. The induction machine fulfills this need very well. In addition they are simpler to build, rugged, cheaper, and can be more easily synchronized with the utility supply than their synchronous counterparts. However, these generators used in wind turbine or wind energy conversion systems, must be designed to be cost-effective, fail-safe, and posses maximum performance indices (such as efficiency and power factor) over their entire operational range. At present it is not clear whether the commercially available induction motors, used as generators, can meet the required standards for wind, small-hydro and other applications. Therefore, based on the experience of the UW research group with single-phase generators [8,25], it was conjectured that simple and practical modifications to available induction motors

can improve their efficiency and power factor profile. The findings of this investigation are summarized in this chapter.

2.2 The Conjecture

Suitable combination of the following design and operational factors, if implemented on commercially available three-phase induction machines used as generators, can yield better steady-state performance.

1) supply voltage sequence (abc or acb),
2) direction of rotation (ccw or cw),
3) symmetric insertion of series capacitors in each auxiliary winding, and
4) incorporation of proper phase-shift between each of the main and auxiliary winding voltages.

2.3 Identification of Schemes for Performance Improvement

Commercially available machines used in wind turbine systems usually have dual windings per phase on the same phase belt and they are intended for dual-voltage operation (for example, 220/440-V) as shown in Figure 2.1. These NEMA Design Class B motors have squirrel-cage rotors. They are also designed to rotate in the counter-clockwise (ccw) direction, looking from the load side of the shaft, under normal conditions of operation.

Figure 2.2 shows six of the twelve stator schemes realized after considering all the four factors listed in Sec. 2.2, representing "abc"

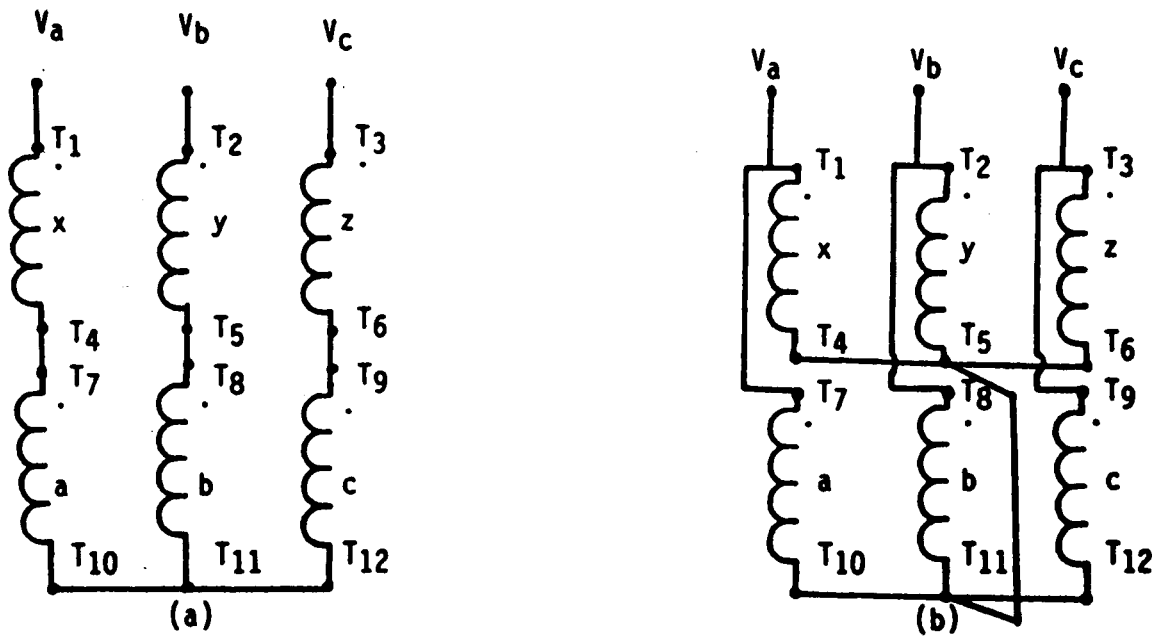

Figure 2.1 Arrangement of stator coils in a dual-winding, three-phase induction machine.
(a) 440-V connection.
(b) 220-V connection.

Scheme	Stator Connections with Main and Auxiliary Coils in-phase	Scheme	Stator Connections with Normal Main and Reversed Auxiliary Coils
I	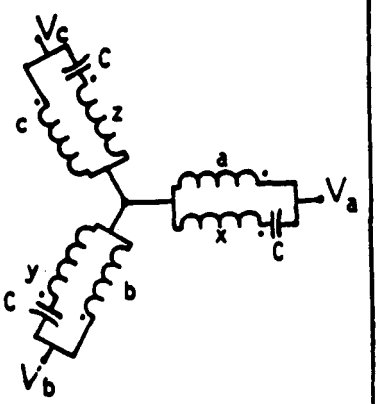	II	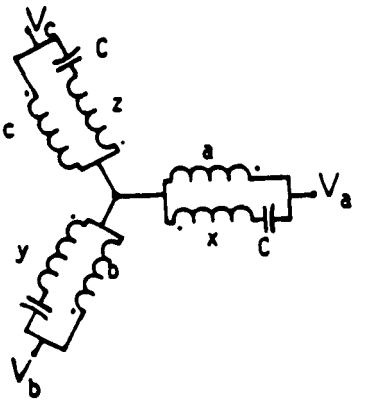
III	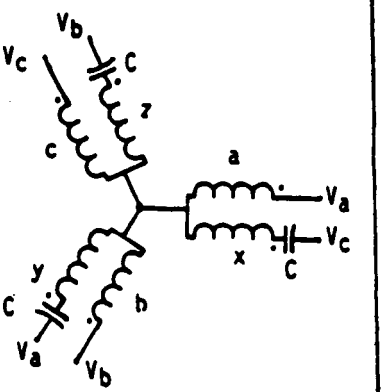	IV	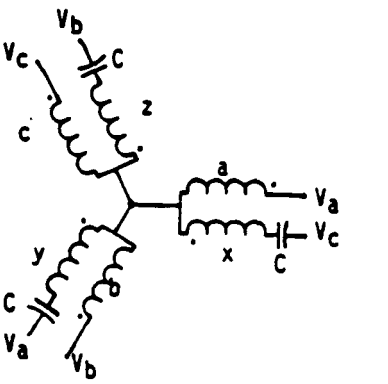
V	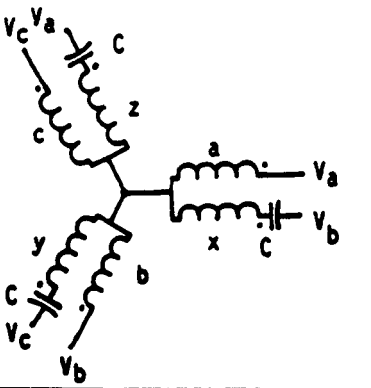	VI	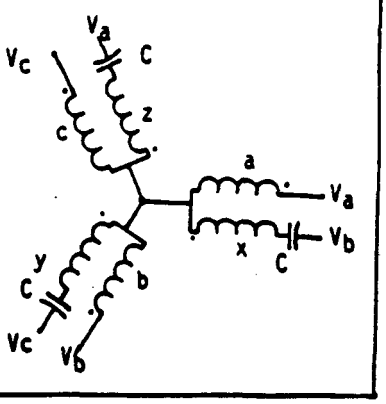

Figure 2.2 **Different stator connections and applied voltages for abc sequence and CCW direction of rotation.**

Legend: a,b,c: Main Windings
x,y,z: Auxiliary Windings
In Scheme III, Main Winding Voltages lag the corresponding auxiliary winding voltages by 120^{o}.

phase sequence and "ccw" rotation. The other six schemes correspond to "acb" phase sequence and clockwise "cw" direction of rotation.

2.4 Induction Generator Model Development

With six coupled coils in the rotor, a mathematical model for the steady-state performance evaluation of the three-phase induction generator can be developed. Using Kirchhoff's voltage law, the generalized matrix model for the generator in phase (ph) variable form is:

$$\bar{V}_{ph} = [R]_{ph}\, \bar{I}_{ph} + p\, [L]_{ph}\, \bar{I}_{ph} = [Z]_{ph}\, \bar{I}_{ph} \qquad (2.1)$$

In eq. (2.1), the 6 stator currents were defined to be positive for generator operation. The 6 rotor currents were defined in the opposite sense. The above matrix equation when expanded contains 12 linear equations with time-varying coefficients. The $[Z]_{ph}$ matrix is a quasi-steady-state matrix in the sense that both 'p' = d(.)/dt operator terms as well as steady-state impedance terms occur together and it is a standard practice [26,27]. In order to transform the phase variable model to a complete steady-state model, the familiar symmetrical component transformation as defined below was utilized.

$$\text{Let} \quad \bar{V}_{ph} \triangleq [S_{12}]\, \bar{V}_{PNO} \qquad (2.2)$$

$$\text{and} \quad \bar{I}_{ph} \triangleq [S_{12}]\, \bar{I}_{PNO} \qquad (2.3)$$

where $$[S_{12}] \triangleq \begin{bmatrix} [S_3] & & & \\ & [S_3] & & \\ & & [S_3] & \\ & & & [S_3] \end{bmatrix} \quad (2.4)$$

In equation (2.4)

$$[S_3] = \frac{1}{\sqrt{3}}$$

0	P	N	
1	1	1	a
a	a^2	1	b
a^2	a	1	c

(2.5)

where $$a \triangleq \epsilon^{j(2\pi/3)} \text{ and } a^2 \triangleq \epsilon^{j(4\pi/3)} \quad (2.6)$$

Substitution of equations (2.2) and (2.3) in (2.1) yields a matrix system of equation,

$$\bar{V}_{PN0} = [S_{12}]^{-1} [Z]_{ph} [S_{12}] \bar{I}_{PN0}$$

$$= [Z]_{PN0} \bar{I}_{PN0} \quad (2.7)$$

Equation (2.7) when expanded becomes equation (2.8), which is the final mathematical model sought. For details on this development, and the explanation of various terms in equation (2.8), see reference [9].

2.5 Application of Model to Test Machine

The machine tested at the UW Energy Systems Laboratory was a 7.5-hp (6.0-kW generator rating), 220/440-V, 20/10-A, 60-Hz, 1,800 r/min, three-phase, NEMA Design Class B induction motor. The machine parameters required for simulating the model on a computer were obtained

$$\bar{V}_{PNO} = [Z]_{PNO} \bar{I}_{PNO} \tag{2.8}$$

		Stator main (sm) Psm	Nsm	Osm	Stator auxiliary (sa) Psa	Nsa	Osa	Rotor main (rm) Prm	Nrm	Orm	Rotor auxiliary (ra) Pra	Nra	Ora	
Stator main (sm)	V_{Psm}	$R_s + jX_{ds}$	0	0	jX_{ds}	0	0	jX_m	0	0	jX_m	0	0	I_{Psm}
	V_{Nsm}	0	$R_s + jX_{ds}$	0	0	jX_{ds}	0	0	jX_m	0	0	jX_m	0	I_{Nsm}
	V_{Osm}	0	0	$R_s + jX_{Os}$	0	0	0	0	0	0	0	0	0	I_{Osm}
Stator aux. (sa)	V_{Psa}	jX_{ds}	0	0	$R_s + jX_{ds} + Z_R$	0	0	jX_m	0	0	jX_m	0	0	I_{Psa}
	V_{Nsa}	0	jX_{ds}	0	0	$R_s + jX_{ds} + Z_R$	0	0	jX_m	0	0	jX_m	0	I_{Nsa}
	V_{Osa}	0	0	0	0	0	$R_s + jX_{os} + Z_R$	0	0	0	0	0	0	I_{Osa}
Rotor main (rm)	V_{Prm}	jsX_m	0	0	jsX_m	0	0	$R_r + jsX_r$	0	0	jsX_r	0	0	I_{Prm}
	V_{Nrm}	0	$j(2-s)X_m$	0	0	$j(2-s)X_m$	0	0	$R_r + j(2-s)X_{dr}$		0	$j(2-s)X_r$	0	I_{Nrm}
	V_{Orm}	0	0	0	0	0	0	0	0	$R_r + jX_{or}$	0	0	0	I_{Orm}
Rotor aux. (ra)	V_{Pra}	jsX_m	0	0	jsX_m	0	0	jsX_r	0	0	$R_r + jsX_{dr}$	0	0	I_{Pra}
	V_{Nra}	0	$j(2-s)X_m$	0	0	$j(2-s)X_m$	0	0	$j(2-s)X_r$	0	0	$R_r + j(2-s)X_{dr}$	0	I_{Nra}
	V_{Ora}	0	0	0	0	0	0	0	0	0	0	0	$R_r + jX_{or}$	I_{Ora}

NOTE: For explanation of symbols, please see reference [9].

by conducting the required tests following IEEE standards for testing [28].

A computer program was generated in Fortran 77 language to document the mathematical model and to evaluate the generator's performance characteristics. The machine saturation and losses, which are nonlinear functions of appropriate voltages and currents, were properly accounted for in the simulation process.

2.6 Summary of Results

When all the twelve schemes (identified in Sec. 2.3) for the generator operation were simulated for the test machine, only two resulted in the best performance. Scheme III shown in Figure 2.2 is one of them. On the other hand, scheme V and one other scheme exhibited the worst performance of the generator. The simulation studies were conducted for two discrete values of 75-, and 100-μF per phase capacitor in series with each auxiliary winding.

Table 2.1 shows the results obtained for the conventional, operational scheme of the generator without modifying any of the four factors mentioned in Section 2.3. Table 2.2 lists the corresponding results for schemes III and V with 75-μF capacitor connected in series with the auxiliary windings. The results are highlighted for one particular speed of 1,836 r/min., which is quite close to the rated operating speed for this class of four-pole machine. All these results are also presented in graphical format, along with the corresponding experimental results, in Chapter 3. Suitable conclusions based on these results are also made in that chapter.

Table 2.1

Calculated Performance Characteristics of the Conventional Induction Generator

Speed (r/min)	Line Current (A)	P_t (W)	Q_t (VAR)	Power Factor	Efficiency(%)	Torque (lb-in)	Remarks
1,804.0	9.67	543.	3,641.	0.148	61.4	41.4	Dir:CCW
1,808.0	10.19	1,170.	3,696.	0.302	76.1	71.8	Seq:abc
1,812.0	10.98	1,799.	3,769.	0.431	81.5	103.0	Class-
1,816.0	12.00	2,431.	3,861.	0.533	83.8	134.9	ical
1,820.0	13.19	3,063.	3,972.	0.611	84.9	167.5	Scheme
1,824.0	14.51	3,695.	4,102.	0.669	85.3	200.7	
1,828.0	15.94	4,327.	4,251.	0.713	85.3	234.5	
1,832.0	17.45	4,957.	4,420.	0.746	85.0	268.8	
1,836.0	19.02	5,585.	4,608.	0.771	84.6	303.7	
1,840.0	20.64	6,209.	4,815.	0.790	84.1	339.0	

List of Various Losses in Watts

Speed (r/min)	Main wdg copper losses	Aux. wdg copper losses	Rotor copper losses	Core losses	Stray load losses	Rot. losses	Total losses	Remarks
1,804.0	42.1	42.1	4.2	185.0	27.9	40.0	341.2	Dir:CCW
1,808.0	46.7	46.7	16.8	185.0	31.8	40.0	367.1	Seq:abc
1,812.0	54.3	54.3	38.2	185.0	38.0	40.0	409.7	Class-
1,816.0	64.8	64.8	68.3	185.0	46.2	40.0	468.9	ical
1,820.0	78.3	78.3	107.3	185.0	56.1	40.0	544.9	Scheme
1,824.0	94.8	94.8	155.4	185.0	67.7	40.0	637.7	
1,828.0	114.4	114.4	212.6	185.0	80.8	40.0	747.1	
1,832.0	137.1	137.1	278.9	185.0	95.2	40.0	873.3	
1,836.0	162.8	162.8	354.6	185.0	110.9	40.0	1016.1	
1,840.0	191.7	191.7	439.4	185.0	127.8	40.0	1175.7	

Note:

P_t is the total three-phase power delivered at the generator terminals.
Q_t is the total three-phase reactive power delivered at the generator.
Torque is the quantity measured at the generator shaft.

Table 2.2

Calculated Performance Characteristics of Scheme III and V With 75-Microfarads/Phase in Series With the Auxiliary Winding

Speed (r/min)	Current (A)			Voltage (V)		P_t (W)	Q_t (VAR)	Efficiency (%)	Power Factor	Remarks
	I_m	I_a	I_l	V_c	V_w					
1804.0	3.47	6.47	3.02	229.1	139.9	607.6	966.3	58.9	0.532	Dir:CCW
1808.0	3.33	6.42	4.22	227.4	136.2	1335.4	883.1	76.4	0.834	Seq:abc
1812.0	4.19	6.37	5.78	225.5	132.3	2066.2	753.8	82.9	0.939	Scheme III
1816.0	5.64	6.31	7.50	223.3	128.2	2795.9	577.6	85.7	0.979	
1820.0	7.35	6.24	9.28	220.9	124.0	3519.9	354.0	86.8	0.995	
1824.0	9.17	6.17	11.11	218.4	119.6	4233.7	83.3	87.1	1.000	
1828.0	11.05	6.09	12.95	215.6	115.1	4932.7	-234.0	86.9	0.999	
1832.0	12.96	6.01	14.81	212.6	110.5	5612.4	-596.4	86.5	0.994	
1836.0	14.87	5.92	16.65	209.4	105.7	6268.6	-1002.1	85.7	0.987	
1840.0	16.79	5.82	18.48	206.1	100.9	6897.1	-1448.6	84.9	0.979	
1804.0	5.82	6.75	3.03	238.8	148.7	607.6	966.3	53.5	0.532	Dir:CW
1808.0	7.56	6.83	4.23	241.9	153.3	1335.4	883.1	68.4	0.834	Seq:acb
1812.0	9.41	6.92	5.80	244.8	157.8	2066.2	753.8	73.8	0.939	
1816.0	11.31	6.99	7.51	247.6	162.3	2795.9	577.6	76.2	0.979	Scheme V
1820.0	13.25	7.07	9.30	250.2	166.7	3519.9	354.1	77.2	0.995	
1824.0	15.21	7.14	11.13	252.6	171.0	4233.7	83.3	77.5	1.000	
1828.0	17.18	7.20	12.97	254.8	175.1	4932.7	-234.0	77.3	0.999	
1832.0	19.14	7.26	14.82	256.8	179.1	5612.4	-596.4	76.9	0.994	
1836.0	21.09	7.31	16.67	258.6	183.0	6268.6	-1002.1	76.3	0.987	
1840.0	23.03	7.35	18.50	260.2	186.7	6897.1	-1448.6	75.6	0.979	

Speed (r/min)	Main wdg cu.losses	Aux wdg cu.losses	Rotor cu.losses	Core losses	Stray losses	Rot. losses	Total losses	Remarks
1804.0	21.7	75.4	51.0	205.2	30.2	40.0	423.5	Dir:CCW
1808.0	20.0	74.3	49.5	199.3	28.8	40.0	411.8	Seq:abc
1812.0	31.7	73.0	55.0	193.2	34.2	40.0	427.1	Scheme III
1816.0	57.3	71.6	67.7	187.1	44.5	40.0	468.3	
1820.0	97.1	70.1	87.8	181.0	58.4	40.0	534.4	
1824.0	151.3	68.5	115.4	174.9	75.2	40.0	625.3	
1828.0	219.7	66.8	150.4	168.8	94.8	40.0	740.5	
1832.0	302.1	64.9	192.7	162.8	116.9	40.0	879.5	
1836.0	398.2	63.0	242.1	157.0	141.4	40.0	1041.8	
1840.0	507.4	61.0	298.4	151.3	168.2	40.0	1226.2	
1804.0	61.0	81.9	75.0	219.9	49.6	40.0	527.4	Dir:CW
1808.0	102.8	84.1	98.1	227.8	65.3	40.0	618.2	Seq:acb
1812.0	159.2	86.1	128.8	235.9	84.0	40.0	734.0	Scheme V
1816.0	230.3	88.1	167.1	244.1	105.5	40.0	875.1	
1820.0	316.1	89.9	213.1	252.4	129.7	40.0	1041.2	
1824.0	416.4	91.7	266.8	260.7	156.4	40.0	1232.0	
1828.0	531.0	93.3	327.8	269.0	185.7	40.0	1446.8	
1832.0	659.4	94.8	395.9	277.2	217.3	40.0	1684.5	
1836.0	800.8	96.1	470.9	285.2	251.1	40.0	1944.0	
1840.0	954.4	97.2	552.1	293.1	286.9	40.0	2223.7	

Note: P_t = total three-phase power delivered at the terminals
Q_t = total three-phase reactive power delivered at the terminals
I_m = main winding current
I_a = auxiliary winding current
I_l = line current
V_c = voltage across capacitor
V_w = voltage across auxiliary winding only

CHAPTER 3

EXPERIMENTAL VERIFICATION OF INDUCTION GENERATOR PERFORMANCE IMPROVEMENT

3.1 Introduction

In order to verify the induction generator model presented in Chapter 2, extensive experimental investigations were conducted on the 6.0-kW test induction machine available at the UW Energy Systems Laboratory. The experimental set-up is briefly described in Sec. 3.2 and the summary of the results together with salient conclusions and limitations of the proposed schemes are highlighted in Sec. 3.3. Sec. 3.4 concludes with recommendations.

3.2 Description of Experimental Set-up

Fig.3.1 Shows the block diagram of the experimental arrangement. Fig.3.2 shows the photographic views of the test set-up. The system consists of a dc drive motor, pulleys and belts, a high-precision torque transducer, an ac induction generator, analog meters, a digital instrumentation panel, and a data acquisition system. The dc motor is supplied from a 125-V dc source and the power produced by the induction generator is delivered to the 3-phase, 60-Hz, utility system through an autotransformer.

In designing the experimental sep-up, accuracy of the measurements was the primary concern. Therefore Fluke digital meters, with $\pm$ 0.1 to

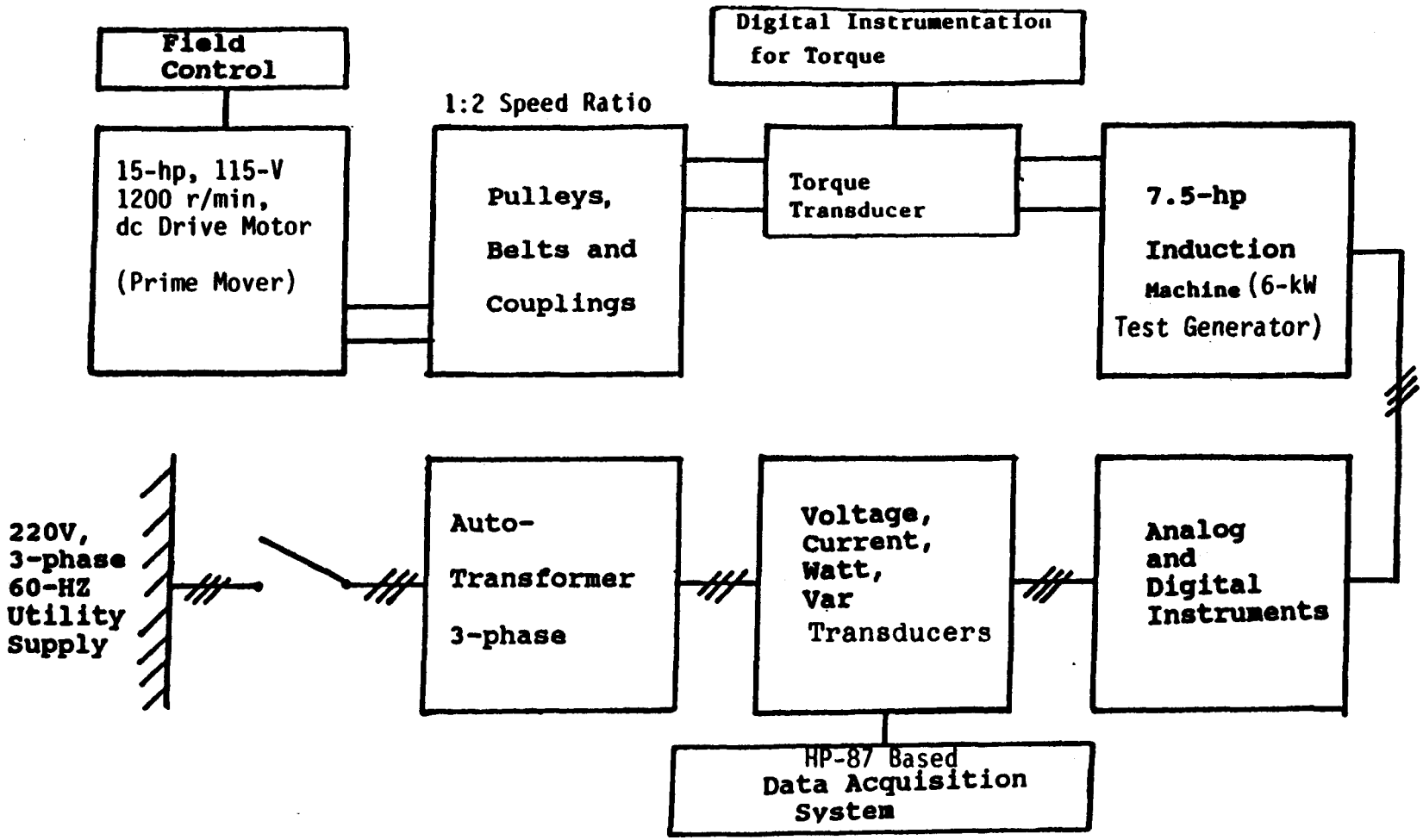

Figure 3.1 Block diagram of the experimental set-up

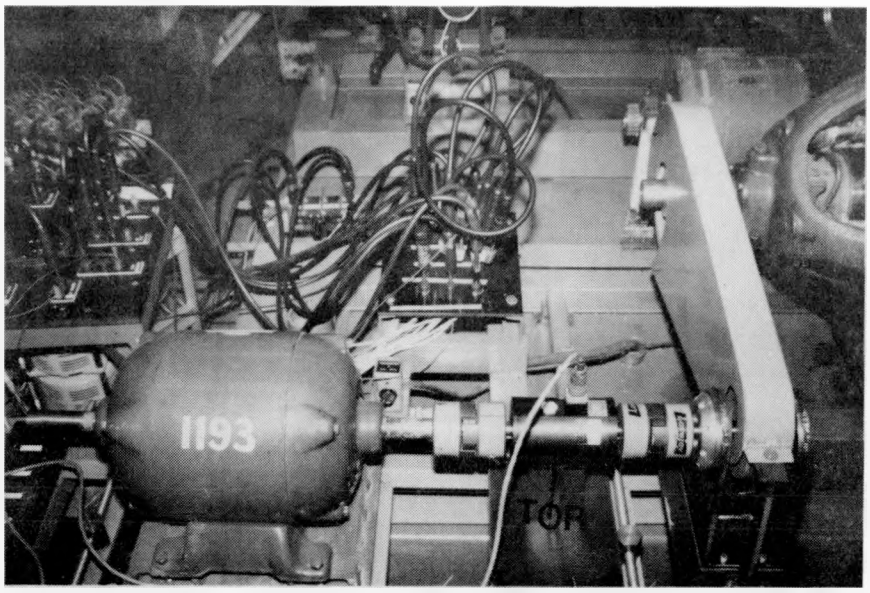

a) Induction generator and torque transducer
1193: Induction Generator
TOR: Torque Transducer

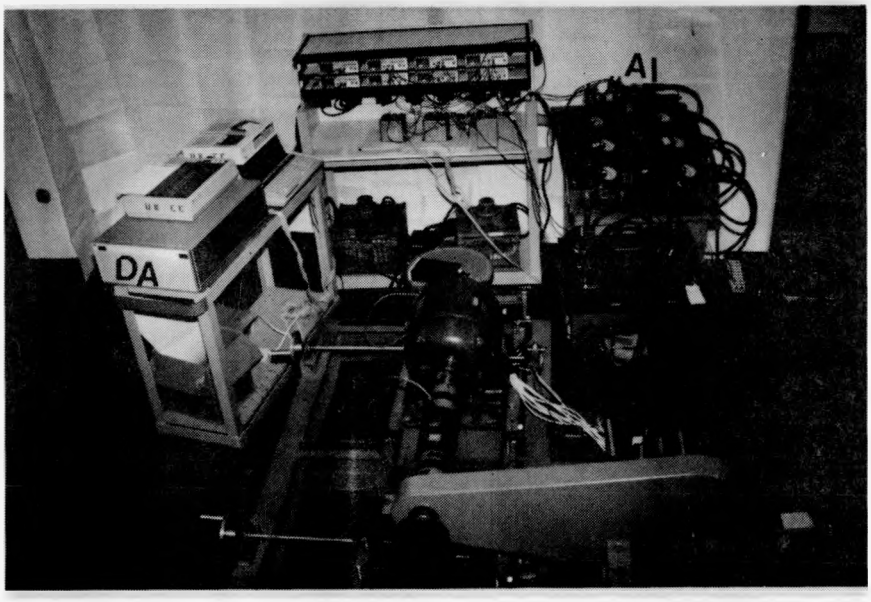

b) Overall view of the test facility
DA: Data Acquisition System
DI: Digital Instrumentation
AI: Analog Instrumentation

Figure 3.2 Photographic View of Experimental Set-Up

1% accuracy, were used for all voltage and current measurements. Dynamometer type meters with ± 0.5% accuracy were used for both real and reactive power measurements. The torque measurement deserves a special mention. A high-precision torque transducer consisting of (1) Lebow 1600 series torque sensor and (2) Daytronic model 3270 digital indicator was selected. The sensor is a strain-gauge, and the transducer works on the rotating transformer principle. The output is through an LED display with ± 0.1% accuracy. All electric transducers, manufactured by Scientific Columbus Inc., were also selected for their ± 0.1% accuracy.

Since it was very difficult to record all 18 measurements simultaneously for a given operating point, a data acquisition system (DA) was conceived and installed. It consists of an HP-87XM microcomputer, an HP-6942A multiprogrammer, an HP-9121 disk unit and an HP-82905B printer. All the instruments were properly calibrated for both static and dynamic conditions.

Interactive software was developed in BASIC to gather the data automatically and to immediately evaluate machine performance indices at each operating point.

3.3 Summary of Induction Generator's Performance Results

Figures 3.3 and 3.4 summarize the important results obtained from both the model simulation presented in Chapter 2 and the experimental investigations described briefly in this chapter. The following salient observations and conclusions may be drawn from these two plots:

1. The efficiency of the generator with Scheme III is on the average 1 to 2 percentage points higher than for the

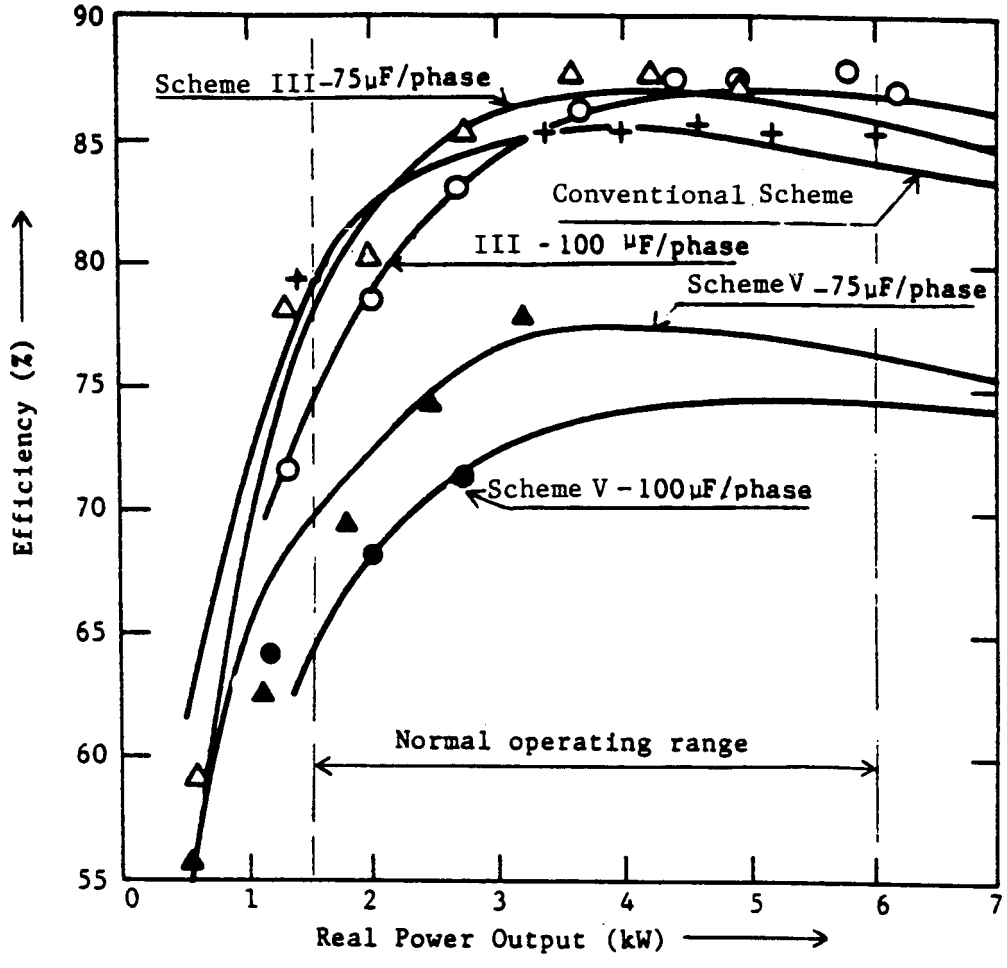

—: Calculated values for all cases
+: Measured values for conventional scheme
△: Measured values for Scheme III, 75 μF/phase
▲: Measured values for Scheme V, 75 μF/phase
○: Measured values for Scheme III, 100 μF/phase
●: Measured values for Scheme V, 100 μF/phase

Figure 3.3 Plot of Efficiency Versus Real Power Output for Conventional Scheme, Schemes III and V

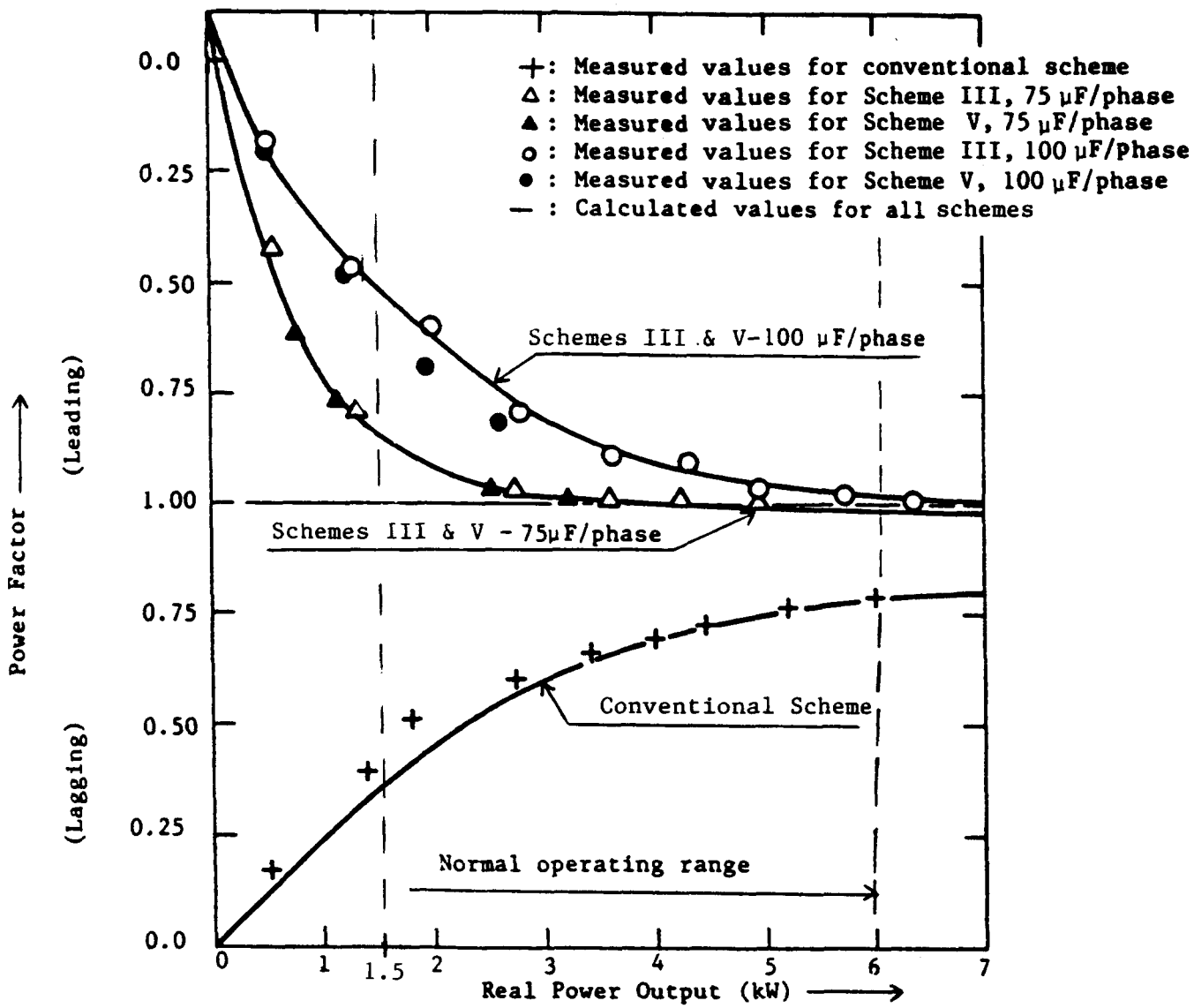

Figure 3.4 Plot of Power Factor Versus Real Power Output for Conventional Scheme, Schemes III and V

conventional case. This is the most important finding of these investigations.

2. The machine efficiency for Scheme V is significantly lower than Scheme III as well as the conventional scheme.

3. For Scheme III, the 75-μF capacitor case provides the best efficiency profile from 33% to 75% rated power output. From 75% to full rated power output, the 100-μF capacitor provides the most efficient operation of the generator.

The re-distribution of currents in the main and auxiliary windings, due to the capacitor, and therefore the re-distribution of the attendant copper losses together with similar trends in the rotor, is the primary reason for these three observations made from Figure 3.3. Further insight on these results can be gained by comparing Tables 2.1 and 2.2, which also shows that the auxiliary windings are under-utilized and the main windings are, sometimes, overloaded. These are the limitations of the desirable scheme III.

4. From Figure 3.4 it can be seen that Scheme III with the 75-μF capacitor exhibits the best power factor profile in the generator's operating range, though it is leading at a lower output range.

5. Scheme III with the 100-μF capacitor exhibited overcompensation of the reactive power demand by the generator.

6. Both Schemes III and V provide identical var compensation for a given value of fixed capacitor connected in series with each auxiliary winding.

7. As mentioned in Chapter 1, the uncompensated, conventional scheme exhibited a poor power factor profile varying from about 0.40 lagging at 25% output to 0.78 lagging at rated generation level.

Other pertinent observations that can be made are:

8. The voltage across the capacitor decreases as the generator output increases in the desirable Scheme III. The opposite trend was noticed for the undesirable Scheme V.

9. The generator could self-excite near 1,840 /min with the capacitor values tested, if isolated from the utility supply. Hence, suitable safety measures should be provided against this undesirable operation.

10. The introduction of the series capacitor in the auxiliary winding introduces additional harmonics into the generator current.

3.4 Recommendations

In the overall sense, it is recommended that wind farm operators implement Scheme III on a few generators of various sizes to determine whether it leads to better generator performance. Caution should be exercised in selecting the value of the fixed capacitor for a given size of machine. If the efficiency profile of a generator is to be further

improved, two fixed levels of var compensation with capacitors switched electronically in and out at the appropriate times, may be tried. Reference [9] provides detailed information on these investigations.

CHAPTER 4

ECONOMIC FEASIBILITY EVALUATION OF WIND TURBINE SYSTEMS

4.1 Introduction

Some of the predominant reasons for the accelerated development of renewable energy conversion systems are: First, the Public Utility Regulatory Policy Act of 1978 (PURPA), has the greatest influence on small power generation by providing utility interconnection facilities at 'avoided cost' to the power producer. Secondly, there are several tax incentives available to the power producer from the Federal and respective state governments. Thirdly, there is considerable improvement in the turbine and the WECS technology in the past decade [6]. The economic viability of these systems is usually evaluated by performing a suitable economic analysis prior to their purchase and installation by an entrepreneur. At the same time, the interconnecting utility is interested in investigating the economic impact of such systems on their system operation, particularly due to the excessive reactive power demand by scores of induction generators in a wind park.

This chapter summarizes the analysis for evaluating the payback period of a wind turbine system equipped with an induction generator. The analysis includes a general approach to the effects of different tariff rates, present worth value of money, income-taxes, various tax credits and inflation. In Section 4.2, the economic analysis from the

entrepreneur's point of view is presented [11]. Section 4.3 deals with the analysis from the utility's point of view [15].

4.2 Economic Analysis from Entrepreneur's Point of View

Cost Components

a) Capital cost on generator: In general, commercially-available NEMA Design B machines are used as induction generators. If C_C is the cost per kilowatt, and if the kW rating of the machine is known, then the capital cost of the generator C_{GEN} is given by

$$C_{GEN} = (C_C)(\text{kW Rating}) \tag{4.1}$$

b) Cost of turbine and installation: The cost of the WECS (excluding the generator) consists of the cost of the turbine, speed reduction gears, tower, wiring and installation. The land, transportation and miscellaneous cost components are application dependent and vary from place to place. This component of cost is referred as C_{INT}.

c) Maintenance cost: The cost of maintenance of the WECS depends mainly on the design of the system. Due to the lack of prolonged operating experience with any of the present machines, it is worth while to vary this component from 1% to 6% (CM) of the total installation cost [6].

d) Salvage value: It is assumed that the plant has zero salvage value at the end of its useful life.

e) Demand and energy cost components: Since each utility in the U.S adopts its own tariffs, an attempt is made to encompass all the cost components which appear in one or more of these tariffs. These are listed below in Table 4.1.

Table 4.1 Various Tariff components and cost Details

Tariff on	Legend	Unit Cost	Total Cost
Maximum demand	kW	C_{WD}	$C_{WDT} = (kW)(C_{WD})$
,,	kVA_S	C_{SD}	$C_{SDT} = (kVA_S)(C_{SD})$
Energy	kWh	C_W	$C_{WT} = (kWh)(C_W)$
,,	kVARh	C_Q	$C_{QT} = (kVARh)(C_Q)$
Reactive demand	kVAR	C_{QD}	$C_{QDT} = (kVAR)(C_{QD})$
Power factor penalty	$kVAR_S$	C_{WD}	$C_{PFP} = (kVAR_S)(C_{WD})$

The power factor penalty charge can be calculated as [2]:

$$kVAR_S = (PF1/PF2 - 1)(kW) \quad (4.2)$$

PF1 = specified compensated power factor by the utility

PF2 = machine uncompensated operating power factor

4.2.1 Cost Components

The cost compnents for the investment, and the economic returns are:

$$C_I = C_{GEN} + C_{INT} \quad (4.3)$$

$$C_R = C_{WT} - C_{QT} + C_{WDT} - C_{SDT} - C_{QDT} - C_{PFP} \quad (4.4)$$

The type of tariff selected will dictate which of the terms in eq. (4.4) occur in the analysis.

4.2.2 Application

The one-line diagram of a 50-kW WECS tied to a distribution system is shown in Fig.4.1. The figure also includes the electrical parameters of the components. The rating of the machine (specified in this example) as a motor is 75-hp. Its rating as an induction generator is specified to be 50-kW. However, the maxiumum monitored output [2] is only 40-kW and hence this value is used as the machine rating in all the calculations.

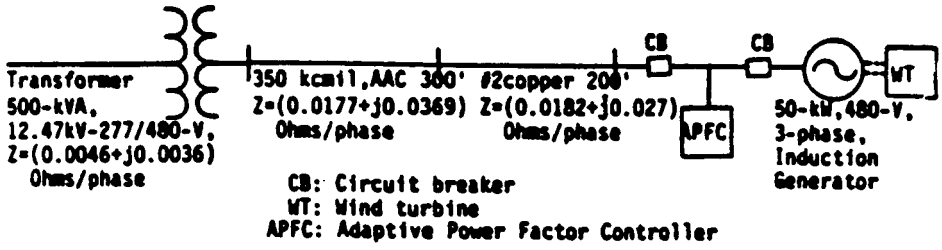

Figure 4.1: One Line Diagram of the System Used in the Example

The other details of the system information needed for the application are presented in Table 4.2. For simplicity it is assumed that the demand charges on max.kW, max.kVAR and max.kVA are all equal.

Table 4.2 Data for Economic Analysis [10]

Item	Legend	Value
Capital cost of APFC	C	$5,000
Real energy/year	kWh	82,000 kWh
Reactive energy/year	kVARh	93,500 KVARh
Max. kW monitored		40 kW
Desired power factor	PF1	0.95(lag)
Uncompensated power factor	PF2	0.60(lag)
kVA saved		24.6 kVA
Cost of released kVA	C	$12/kVA/year
Line resistance	R	0.0405 Ohms
Current before compensation	I	80 Amps
Current after compensation	I	51 Amps
Max.kVAR		40.3
Load factor	LF	0.4
Cost of real energy	C	$0.06/kWh
Cost of reactive energy		$0.00025/kVARh
Max. demand cost of kW, kVAR, kVA	C	$3.80/kW/month
Cost of generator/kW	C	$40/kW
Cost of installation	C	$950/kW
Cost of Generation	C_{GEN}	$1,200/kW
Cost of conservation	C_V	$0.002/kWh
Interconnection cost	C_{IC}	$1,200
Life period of generator	n	20 years
Interest rate	i	10%

Table 4.3 shows the various benefit components due to seven different tariffs:

Table 4.3 Calculated Annual Cost Benefits to the Wind farm Developer due to 50-kW WECS

Case	Tarrifs on	C_{WT} $	C_{QT} $	C_{WDT} $	C_{QDT} $	C_{SDT} $	C_{PFP} $	Total Benefits
I	kWh,kVARh,kW,&kVAR$_S$	4,920	(23)	1,824	-	-	(1,064)	5,657
II	kWh,kVARh,kW,& kVA	4,920	(23)	1,824	-	(1,122)	-	5,559
III	kWh,kVARh,kW,& kVAR	4,920	(23)	1,824	(1,837)	-	-	4,884
IV	kWh,kVARh,kW,kVA & kVAR	4,920	(23)	1,824	-	(1,122)	(1,064)	4,532
V	kWh,kVARh,& kW	4,920	(23)	1,824	-	-	-	6,721
VI	kWh,kVARh,kVA &kVAR$_S$	4,920	(23)	-	-	(1,122)	(1,064)	2,708
VII	kWh,& kVARh	4,920	(23)	-	-	-	-	4,897

(.) Implies a negative number

Table 4.4 presents the range of payback period calculated by four different methods for the seven cases identified in Table 4.3. This table shows that the payback period for case V is the shortest, when there are no penalty charges on the power factor, kVAR or kVA. The inclusion of taxes and tax credits makes the investment attractive.

Table 4.4 Calculated Payback Period in Years for the WECS

Case	Simple Method	Present Worth Method(PWM)	PWM with Income Tax & Tax Credits	PWM with taxes and Inflation
I	7.0	14.2	2.80	3.31
II	7.1	14.5	2.90	3.35
III	8.1	Above 20	3.28	3.62
IV	8.7	Above 20	3.41	3.78
V	5.9	9.2	2.79	2.90
VI	14.6	Above 20	5.00	7.00
VII	8.1	Above 20	3.28	3.62

4.3 Economic Analysis from Utility's Point-of-View [15]

As far as wind turbine systems are concerned, one of the primary concerns of a utility is the economic impact of interconnecting such systems to its network. The evaluation of economic feasibility due to the installation of a reactive compensation device, such as an Adaptive Power Factor Controller (APFC) mentioned at the beginning of this report, is summarized in this section. A simple methodology is presented which incorporates the adaptive nature of the device by including the daily load profile at the substation, and seasonal variations in load demand. The economic index is the break-even period in years. This methodology conforms to utility practice and EPRI guidelines documented in TAG [29]. The analysis is general and parametric in nature. Table 4.5 identifies the cost items entering into the analysis and the resulting benefit components, which represent the difference in various operating costs with and without APFC.

Table 4.5 Cost/Benefit Items of the Economic Analysis

Cost Components	Benefit Components
Capital cost of APFC, C1	Annual savings in energy loss, S1
Installation cost, C2	Savings in capacity loss, S2
Annual O&M cost for APFC, C3	Annual savings due to reactive power supplied, S3

4.3.1 Cost Components

The Levelized Revenue Requirement (LRR) of the two alternatives, namely, with and without APFC, should be equated to find the break-even period in years, which will enable the utility to make the proper economic decision.

$$LRR_c \text{ (with APFC)} = C_{1n} + C_{2n} + C_{3n} + C_{4n} + C_{5n} + C_{6n} \quad (4.5)$$

$$LRR_c \text{ (without APFC)} = C_{7n} + C_{8n} \quad (4.6)$$

The various components in equation (4.5) are:

(i) Annual capital cost of APFC in n^{th} year (C_{1n})

$$(C_{1n}) = (\text{kVAR rating}) (L_n) \quad (4.7)$$

where L_n = levelizing factor for n^{th} year as defined in the TAG. The value of n varies between 0 and N (useful lifetime of the APFC)

(ii) Annual installation cost of APFC in n^{th} year (C_{2n})

$$C_{2n} = (\text{actual installation cost of APFC, } C_2) (L_n) \quad (4.8)$$

(iii) Annual O&M cost of APFC in n^{th} year (C_{3n})

$$C_{3n} = (C_3) (P_{m,n}) \quad (4.9)$$

where C_3 = actual O&M cost of APFC/year

and $P_{m,n}$ = levelized carrying charge for n^{th} year with m years of tax recovery period.

(iv) Annual cost of energy loss in n^{th} year (with APFC)

$$C_{4n} = (kWh_c) (C_w) (1 + e_a) (1 + e_i) (P_{m,n}) \quad (4.10)$$

where

$$kWh_c = [(3) (R) (LF) (8,760) (10^{-3}) \sum_{j=1}^{s} \sum_{k=1}^{t} (I_{jk}^c)^2]/(s)(t)$$

R = Series resistance of the system shown in Figure 4.2.

LF = loss factor of the system

I^c_{jk} = line current after compensation

S = number of seasons in a year

t = number of discrete load points in daily demand profile

C_w = cost of real energy/kWh

e_i = p.u. inflation rate

e_a = p.u. escalation rate of the fuel

(v) Cost of capacity loss in n^{th} year (C_{5n})

$$C_{5n} = (kW_c)\ (C_{kW})(1 + e_i)\ (L_n) \tag{4.11}$$

where kW_c, capacity loss in year Z is given by

$$kW_c = [\ (3)\ (R) \sum_{j=1}^{s} \sum_{k=1}^{t} (I^c_{jk})^2\ ]/(s)\ (t)$$

C_{kW} = Cost of installed capacity/kW

It should be pointed out that C_5 is a one-time cost occuring at year Z where $0 \leq Z \leq n$.

(vi) Annual cost of reactive power supplied to the grid (C_{6n})

$$C_{6n} = (C_q)\ [\ \sum_{j=1}^{s} \sum_{k=1}^{t} (Q_{jk})/(s)(t)]\ (P_{m,n}) \tag{4.12}$$

where

C_q is the cost of reactive power/kVAR

Q_{jk} is the reactive demand before compensation.

The justification for including this last item stems from the need for a utility to recover the cost of the installation of reactive sources such as APFC or any other classical means. Some utilities are already charging industrial customers for poor power factor at the metering point.

The two cost components in equation (4.6) are:

(i) Annual energy loss in n^{th} year (without APFC) (C_{7n})

$$C_{7n} = (kWh_u)\ (C_w)\ (1 + e_a)\ (1 + e_i)\ (P_{m,n}) \qquad (4.13)$$

where

$$kWh_u = [(3)\ (R)\ (LF)\ (8{,}760)\ (10^{-3}) \sum_{j=1}^{s} \sum_{k=1}^{t} (I^u_{jk})^2/(s)(t)$$

I^u_{jk} = uncompensated line current

Other variables in equation (4.13) are already defined in equation (4.10).

(ii) Annual cost of capacity loss in n^{th} year

$$C_{8n} = (kW_u)\ (C_{kW})\ (1 + e_i)\ (L_n) \qquad (4.14)$$

where kW_u, capacity loss in year Z is given by

$$kW_u = (3)\ (R) \sum_{j=1}^{s} \sum_{k=1}^{t} (I^u_{jk})^2/(s)(t)$$

Now, the benefit components identified in Table 4.5 can be defined as:

Annual savings in energy loss, $S1 = C_{7n} - C_{4n}$

Savings in capital loss, $S2 = C_{8n} - C_{5n}$

Annual savings due to reactive power supplied, $S3 = C_{6n}$

4.3.2 Example System

The system used as an example of the method consists of a source, a transformer, and a line of variable length L miles supplying a cyclically varying load, such as wind farm, as shown in Figure 4.2. Though it is

cyclically varying load, such as wind farm, as shown in Figure 4.2. Though it is similar to Figure 4.1, it is of higher capacity, as viewed from a substation. The APFC is installed close to, or near, a major load point on the line where the uncompensated power factor is to be improved to unity.

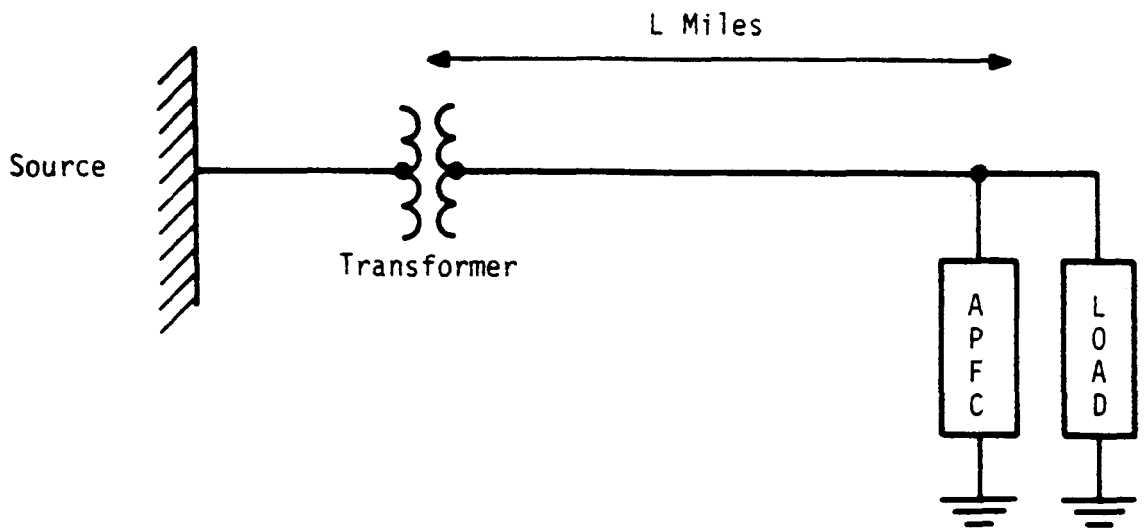

Figure 4-2 : One Line Diagram of the System

Table 4.6 lists the system and cost data. The load data used in the example are shown in Table 4.7, which includes the line power, reactive power with and without APFC. The results in the form of the levelized revenue requirements for the first 10 years are shown in Table 4.8 for the example under consideration. Finally, the calculated break-even period for different lengths of the distribution line and the various cost/kVAR of the APFC is presented in Table 4.9.

Table 4.6 Data for Economic Analysis of 2 MVAR APFC

Capital cost of APFC, C_1	\$(50 to 250)/kVAR
Cost of installation, C_2	\$10/kVAR
Incremental O&M cost on APFC, C_3	\$5/kVAR/year
Cost of reactive power, C_q	\$24/kVAR/year
Length of the line, L	L (1 to 5) miles
Line resistance	0.235 Ohms/mile
Transformer resistance	0.065 Ohms/mile
Loss factor, LF	0.4
Cost of real energy, C_W	\$0.035/kWh/month
Cost of generation capacity, C_{kW}	\$1,200/kW
Interest rate, i	10% per year
Real escalation of fuel cost, e_a	0.8% per year
Inflation rate, e_i	6% per year

Table 4.7 Load Data used in the Example

P_{jk}	Q_{jk}	I^U_{jk}	I^C_{jk}
1000.0	1600.0	87.4	46.3
1800.0	1700.0	114.6	83.3
2000.0	1800.0	124.6	92.6
2100.0	2000.0	134.3	97.2
1900.0	1700.0	118.0	88.0
1000.0	1600.0	87.4	46.3
2100.0	2000.0	134.3	97.2
2000.0	1800.0	124.6	92.6
1000.0	1600.0	87.4	46.3
1000.0	1700.0	91.3	46.3
1000.0	1700.0	91.3	46.3
2100.0	2000.0	134.3	97.2

Table 4.8 Levelized Cost Components on Year by Year Basis in Dollars (C_1 = \$150/kVAR, L = 4 miles)

Year	With APFC						Without APFC		
	APFC (C_{1n} +C_{2n})	O&M C_{3n}	Energy loss C_{4n}	Capacity loss C_{5n}	Reactive power C_{6n}	LRR_c	Energy loss C_{7n}	Capacity loss C_{8n}	LRR_u
1	59210	1910	5149	5212	45304	26177	11020	11154	22174
2	57660	1870	5317	5103	46781	23168	11379	10921	22300
	Break-even period = around 2 years								
3	55490	1820	5486	4966	48274	19489	11742	10629	22371
4	53630	1770	5658	4830	49780	16108	12109	10337	22445
5	51770	1730	5830	4721	51298	12753	12478	10103	22581
6	49910	1680	6004	4584	52826	9352	12850	9811	22661
7	48360	1640	6178	4475	54363	6290	13224	9578	22801
8	47120	1600	6354	4366	55908	3532	13599	9344	22943
9	45880	1570	6530	4284	57458	806	13976	9169	23145
10	44640	1540	6707	4202	59012	-1923	14354	8994	23348

LRR_c = Levelized revenue requirements for system with APFC

LRR_u = Levelized revenue requirements for system without APFC

Table 4.9 Calculated Break-Even Period for a 2 MVAR APFC Taking into Account Different Line Lengths

Cost of APFC per kVAR (\$)	Break-even Period (years)				
	L=5miles	L=4miles	L=3miles	L=2miles	L=1mile
50	1	1	1	1	1
100	1.0	1.2	1.3	1.4	1.5
150	2.0	2.2	3.0	4.0	4.5
200	6.3	7.1	8.0	9.0	9.5
250	10.5	10.8	11.7	13.0	14.2

CHAPTER 5

RELIABILITY EVALUATION

5.1 Introduction

To assure efficient and effective use of electric energy conversion, the wind turbine system equipped with induction generators must be designed to ensure reliable, and cost-effective operation. While these machines are intended to survive about 30 years in the normal industrial environment, can they have similar life span if they are exposed to continuously varying speed/load operation and hostile environmental conditions? There is hardly any established historical data available to confidently determine the reliability and life expectancy of these wind generators. Therefore, a methodology based on the fault tree technique was developed to determine the reliability indices of these generators, as well as the WECS. The results are summarized in this Chapter.

5.2 Induction Generator Reliability Analysis

Figure 4.1 shows the 50-kW test system, in which the induction generator is driven by a wind turbine. The output electrical power is deliverd from the generator stator terminals to a distribution network through two circuit-breakers on either side of the APFC and a step-up transformer. Suitable fuses, not shown in the figure, are installed in all three phases of the generator as a measure of overload protection. Functionally, the generator is expected to deliver maximum possible real power in the expected range of wind speed, while keeping the system

voltage within the allowable regulation. From the reliability point of view, such a generator can be modeled as 27 electro-mechanical components [9].

5.2.1 Failure Modes

The following undesirable modes of operation in the generator can be identified in accordance with IEEE standard STD-500 [30] and other references [31,32].

Mode A - Incipient Failure: Any imperfection in the generator can cause its incipient failure and this can lead to degraded or catastrophic failure if no corrective action is taken. Normal aging of the machine, excessive mechanical noise, vibration, overheating due to reduced cooling, or minor deviations in the output voltage due to increased voltage drop at the contacts are some of the causes leading to this mode of operation.

Mode B - Degraded operation: In this mode, the generator fails to perform within the expected specifications, such as reduced output from its terminals. This mode affects the energy produced by the generator and can manifest itself in one of the following three ways:

Sub-mode B1: One phase open
Sub-mode B2: Phase-to-phase short circuit
Sub-bode B3: One-phase-to ground fault

These three modes usually result due to abnormal operating conditions.

Mode C - Catastrophic failure: This mode implies that the generator totally fails to perform its intended function. A three-phase fault in the generator, a major mechanical component failure such as a

break or a crack in the shaft, or failure of the bearings are some of the causes leading to this mode.

5.2.2 Applications, Results and Conclusions

The fault methodology was applied to the 50-kW generator identified in Figure 4.1. The analysis assumed that component failure follows an exponential distribution. This is an established assumption based on experience for most of the engineering systems. The steps and procedure for this methodology is described in reference [9]. The results are summarized in Table 5.1 which shows the failure rates (λ) and the Mean Time to Failure (MTTF) = $1/\lambda$, for all the modes under consideration. The combined failure rate and the MTTF for the induction generator are given in row 7 of the table. The table also shows the corresponding values for standard induction motors and synchronous generators. Further, the reliability index of the generator, $R = \varepsilon^{-\lambda}$, which is a measure of its availability on a per unit basis, is given in Table 5.2 for each of the three modes under consideration, and the combined value in row 4 of this table.

The following conclusions can be made based on these results:

a) The calculated failure rate for the induction generator is higher (lower reliability index) than the corresponding value for a standard induction motor or synchronous generator as shown in Table 5.2.

Table 5.1 Failure Rates and the MTTF of 50-kW Induction Generator

Mode	Failure Rate(failure/year) (λ)		Mean-Time-to-Failure(years) ($1/\lambda$)	
	Range	Median Value	Range	Median Value
A	0.0695 - 0.0144	0.0293	14.39 - 69.26	34.04
B1	0.0322 - 0.0067	0.0115	31.02 - 148.96	86.60
B2	0.0286 - 0.0052	0.0118	34.88 - 191.69	84.43
B3	0.0293 - 0.0056	0.0119	34.15 - 180.14	83.75
B	0.0901 - 0.0175	0.0342	11.09 - 57.14	29.23
C	0.0743 - 0.0047	0.0312	13.46 - 212.76	32.05
Combined	0.2239 - 0.0366	0.0946	4.47 - 27.32	10.57
Induction motor{60}	0.0914 - 0.0061	0.0166	10.94 - 161.14	60.15
Synch. Generator	0.3628 - 0.0021	0.0394	2.75 - 475.48	25.36

Table 5.2 Reliability of Index of 50-kW Induction Generator

Mode	Reliability Index, R ($=\varepsilon^{-\lambda}$)	
	Range	Median Value
A	0.9328 - 0.9857	0.9712
B	0.9138 - 0.9827	0.9664
C	0.9284 - 0.9953	0.9693
Combined	0.7994 - 0.9641	0.9097
Std. Motor	0.9126 - 0.9939	0.9835
Syn. Gen	0.6957 - 0.9979	0.9613

The corresponding MTTF is also lower. This is to be expected since the wind generator operates in a more hostile environment, which was taken into consideration in selecting some of the component failure rates.

However, it is to be cautioned, that further validation of the analysis is required before placing confidence in these results. These can serve as a guide in improving the generator design for wind turbine applications.

b) Based on the results presented, the following critical components of the generator were identified. These were: bearings, phase windings, terminals, terminal board, slot insulation, and fan. Therefore, it is recommended that these components be given additional care in the design and/or maintenance stages.

5.3 Reliability Analysis of Wind Turbine Systems (or WECS)

The wind turbine system can be divided into six major components for evaluating its reliability. These are: (1) turbine, (2) brake, (3) gear box, (4) each circuit-breaker, (5) induction generator, and (6) APFC, some of which can be identified in Figure 4.1.

The hazard or failure rates required for conducting the investigation by the fault tree methodology are listed in Table 5.3. Since each component is more of a sub-system, it is reasonable to identify its failure rate based on the individual mode of failure identified in the previous section. This factor has been taken into consideration in listing the data in Table 5.3. In addition, an

Table 5.3 Failure Rates of WECS Components or sub-systems

Component or Sub-System	Failure Rate/10^6 Hours	
	Minimum - Maximum	Median Value
1(a,b,c)	0.115 - 2.700	1.175
2(a,b)	0.011 - 0.720	0.500
2(c)	0.010 - 0.700	0.400
3(a,b,c)	0.200 - 0.800	0.600
4(a,b)	0.320 - 0.900	0.700
4(c)	0.010 - 0.850	0.600
5(a)	0.014 - 0.069	0.0293
5(b)	0.017 - 0.090	0.0342
5(c)	0.004 - 0.074	0.0312
6(a,b,c)	0.620 - 0.900	0.770

(a) - failure rate for incipient failure
(b) - failure rate for degraded failure
(c) - failure rate for catastrophic failure

environmental stress factor of 1.4 was applied to all components to make the analysis more representative of outdoor conditions.

5.3.1 Application, Results and Conclusions

Tables 5.4 and 5.5 list the results obtained for the example system described in Figure 4.1. The calculated reliability index for the WECS was 0.9010 as listed in Table 5.5. The corresponding value provided by Southern California Edison Co. personnel based on a year's operation of their 50-kW system is 0.931. The theoretical result is conservative. The analysis needs further refinement to include the following additional environmental factors:

a) corrosion (in the coastal areas)

b) adverse weather (blowing sand in deserts)

c) cyclic loading conditions

The probability of shut down due to hazardous operation can be minimized by proper preventive maintenance practices, in which case it is necessary to include component repair time in the analysis.

Table 5.4 Calculated Failure Rates and the MTTF of WECS

	Failure Rate(Failure/year)		Mean-Time-To-Failure(years)	
Mode	Range	Median Value	Range	Median Value
A	0.0456 - 0.0058	0.0286	21.99 - 171.21	34.96
B	0.1082 - 0.0191	0.0424	9.21 - 52.41	23.55
C	0.2572 - 0.0032	0.0332	3.88 - 312.75	30.12
WECS	0.4110 - 0.0281	0.1042	2.43 - 35.57	9.59

Table 5.5 Reliability indices of WECS

Mode	Reliability Index, R	
	Range	Median Value
A	0.9555 - 0.9942	0.9718
B	0.8974 - 0.9810	0.9584
C	0.7734 - 0.9967	0.9673
WECS	0.6629 - 0.9722	0.9010

PART II

ADAPTIVE POWER FACTOR CONTROLLERS

CHAPTER 1

CONCEPT DEVELOPMENT, DESIGN AND DEMONSTRATION OF 7.5-kVAR ADAPTIVE POWER FACTOR CONTROLLER

1.1 Introduction

The goal of this part of the research was to design, build and test a device that adaptively compensates the reactive power of an induction generator. The device is called an Adaptive Power Factor Controller (APFC). To achieve adaptive compensation, the correct number of capacitors (fixed and switched) are used per phase to furnish enough reactive power to continuously correct the power factor in the desired range of generator operation [1,13].

This chapter presents the design, development and testing of a 7.5 kVAR APFC which incorporates the following features:

1. Adaptable to the changing demand of reactive power.
2. Avoids self-excitation and over-voltage problems.
3. Creates no transients during normal operation, or harmonic currents.
4. Modular to fit various sizes of generators.
5. Simple and inexpensive to build.
6. Fail-safe in operation.

The controller consists of two discrete groups of capacitors, fixed and switched, which furnish enough reactive power to an induction

generator throughout its desired operating range of speed. The number of switched capacitors is kept to a minimum to simplify the switching circuit, and yet provide adequate and varying reactive power compensation.

The controller presented in this report is also suitable in a number of other applications where an adaptive reactive power compensation is needed. Some of those worth mentioning are: process industries, industries using large induction motors, transmission lines, and distribution feeders. However, in this chapter only the application to induction generators is stressed.

1.2 Selection of Fixed and Switched Capacitors

An approximate model for a three-phase induction machine is shown in Figure 1.1. An approximate expression for the reactive power drawn by the machine can be obtained from this model

$$Q \approx V^2 \left(\frac{1}{X_m} + \frac{X_{eq}}{(R_{eq} + R_2 \frac{n}{n_s - n})^2 + X_{eq}^2} \right) \qquad (1.1)$$

where V is the line-to-line voltage, X_m is the magnetizing reactance, X_{eq} and R_{eq} are the lumped reactances and resistances of the stator and rotor windings respectively, R_2 is the rotor resistance referred to the stator, n_s and n are the synchronous speed and rotor speed respectively, and s is the per unit slip, which is negative for the generator mode of operation.

From equation (1.1), it is shown that the reactive power drawn by the machine for generator operation ($n > n_s$) is more than that for motor operation ($n < n_s$), for the same magnitude of slip. Also, the machine draws

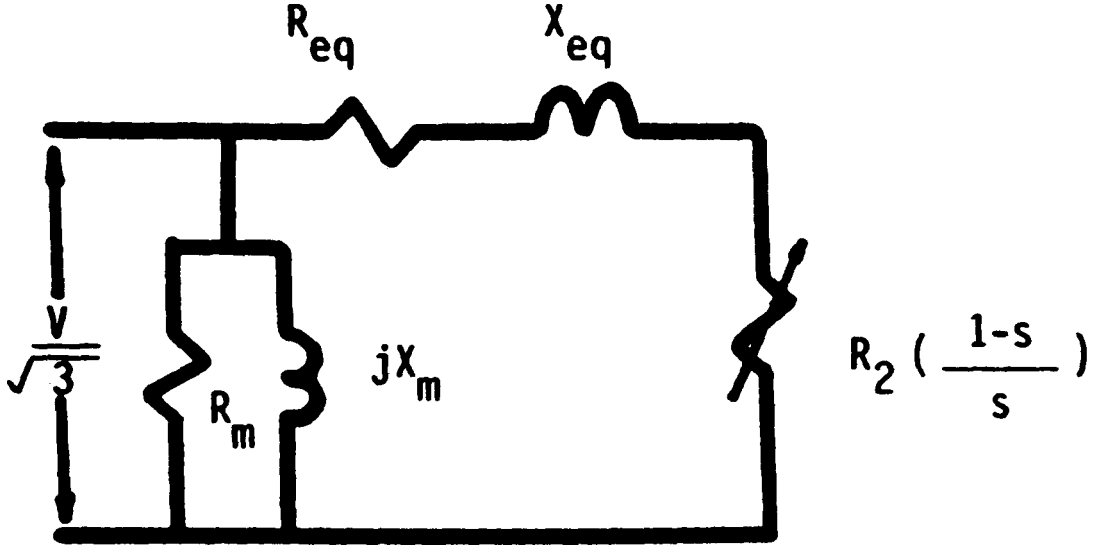

Figure 1.1: Approximate Model for a Three-Phase Induction Machine

minimum reactive power at synchronous speed ($n=n_s$). A typical reactive profile of an induction machine is shown in Figure 1.2 (p. 51).

The fixed capacitors provide all, or some of, the minimum demand of the reactive power (Q_{min}), and the switched capacitors continuously provide the additional demand of reactive power, which varies with the generator speed.

The fixed capacitors should be carefully selected to avoid self-excitation. Self-excitation is a phenomenon where the generator voltage builds up in an unregulated fashion when it operates without being connected to the power grid. The magnitude of the voltage depends on the speed of the generator and on the size of the capacitors connected to its terminals. Self-excitation poses safety problems to users, and maintenance personnel. A typical volt-speed characteristic of a self-excited induction generator is shown in Figure 1.3. For different sizes of fixed capacitors, the generator terminal voltage exceeds the rated value at different speeds. Increasing the value of the capacitance reduces the speed at which self-excitation occurs. The size of the fixed capacitor was selected to avoid self-excitation up to the maximum speed of the generator. This is because the speed of the induction generator may exceed the speed of the operating region due to gusts of wind (where induction generators are used on wind turbines), or similar external conditions.

To supply the maximum amount of switched VARs with the fewest number of capacitors, and still allow the maximum number of switching steps, the switched capacitors should be sized in a binary ratio of: 1,2,4,8, etc. (if 1 = 2 kVAR, then 2=4 kVAR and so on). For example, if the maximum

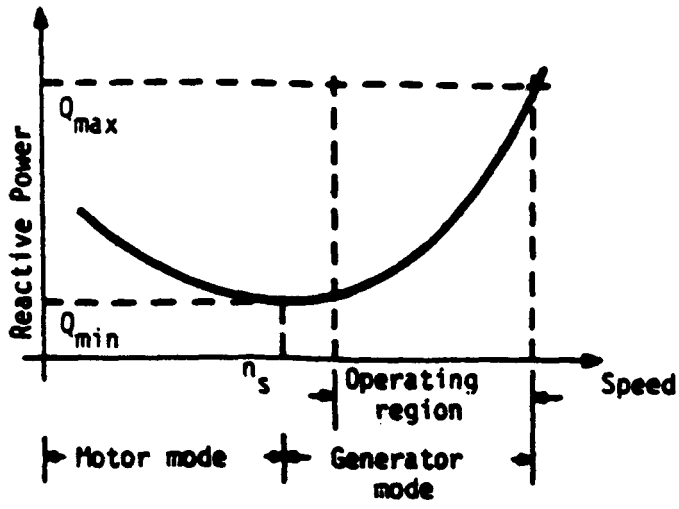

Figure 1.2: Typical Reactive Power Profile of an Induction Machine

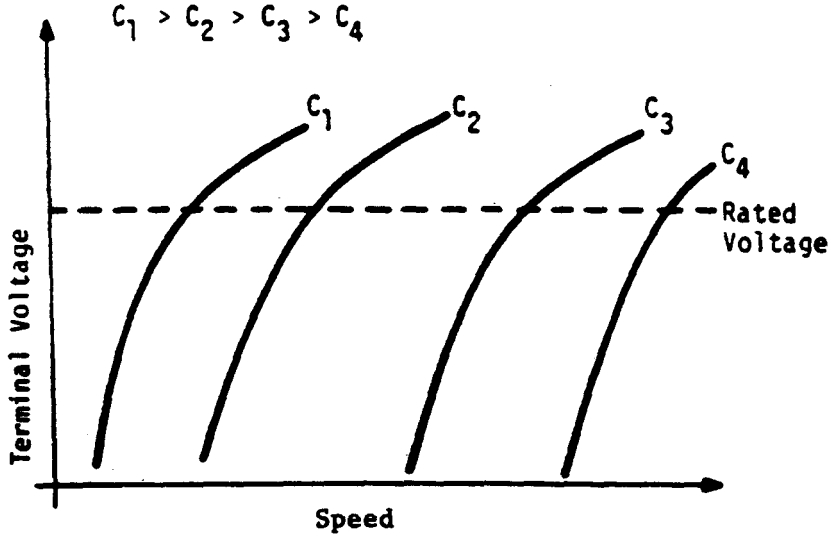

Figure 1.3: Typical Volt-Speed Characteristic of a Self-Excited Induction Machine

switched capacitance desired per phase (C_t) is known and the number of switched capacitors (n) is selected, the binary capacitor sizes should be $C_t/(2^n-1)$, $2C_t/(2^n-1)$, $4C_t/(2^n-1)$ and so on. In this case (2^n-1) different values of capacitance can be selected and switched by the adaptive scheme. For example, three switchable stages per phase lead to seven $(= 2^3-1)$ distinct steps of reactive power compensation (in addition to zero).

1.3 General Description of APFC Design

The APFC consists of four main circuits as shown in Figure 1.4. The Reactive Current Sensing Circuit measures the reactive current drawn by the generator in a single phase . This information is passed to the Decision Logic Circuit which is responsible for selecting the capacitor stages to be switched on. The Switching Circuit consists of the capacitors, power electronic switches and triggering mechanism for these switches. The Timing Circuit provides the correct waveforms for proper timing of each circuit. Three switched capacitor stages per phase are used in this design. They are sized in a binary ratio to provide seven equal compensation steps.

1.3.1 Reactive Current Sensing Circuit

The function of this circuit is to sense the load current in one phase. It then adjusts its magnitude to a desired level (the current signal is converted to a corresponding voltage signal and then amplified), and holds it at that value until the system phase voltage crosses the next zero point and is about to become negative. At this instant the line current is equal to the peak value of the reactive component [1-3]. This

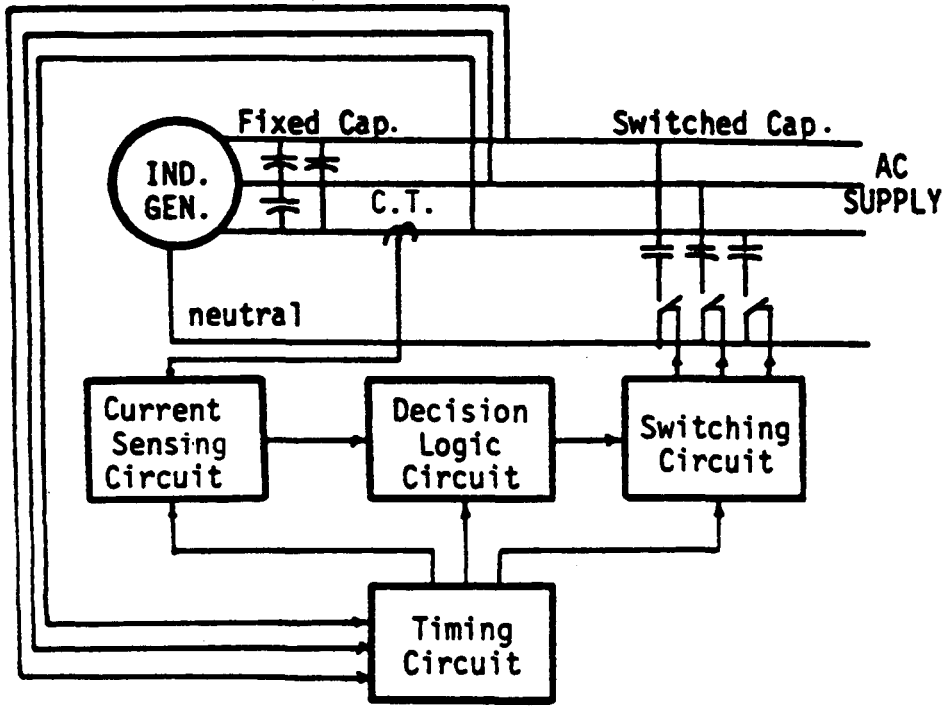

Figure 1.4: Block Diagram of 7.5 kVAR Adaptive Power Factor Controller

held value of voltage representing the line reactive current is then fed to a Decision Logic Circuit for determining the number of capacitors to be switched. Figure 1.5 shows the main components of the Reactive Current Sensing Circuit. The first component is the current transformer (C.T.) which senses the current in one phase. The current signal at the output of the C.T. is transformed into a voltage signal via R_1. The voltage signal is then amplified by the operational amplifier (UI) and fed to the sample and hold circuit (S & H). The S & H circuit holds this value of the current until the instant when the phase voltage is crossing zero and going negative.

1.3.2 Decision Logic Circuit

Figure 1.6 shows the components of the Decision Logic Circuit. The input to the Decision Logic Circuit is the output of the Reactive Current Sensing Circuit. This input is fed to seven comparators (U2a to U3c). The resistor ladder (R7-R14) is used to provide reference voltages to the comparators.

The priority encoder converts the output of the seven comparators into a three-bit code (A2, A1 and A0), one bit for each capacitor, i.e. A0 controls the smallest size capacitor, A1 controls the next larger size, and so on. Flip-flops are used to latch the priority encoder's output. The output of the latch triggers phase A capacitors first, then phase B and finally phase C for A-B-C sequence. For C-B-A sequence, the order of triggering would be reversed..

1.3.3 Switching Circuit

The Switching Circuit of one phase is shown in Figure 1.7. It consists of three capacitors; each of them is connected in series with a

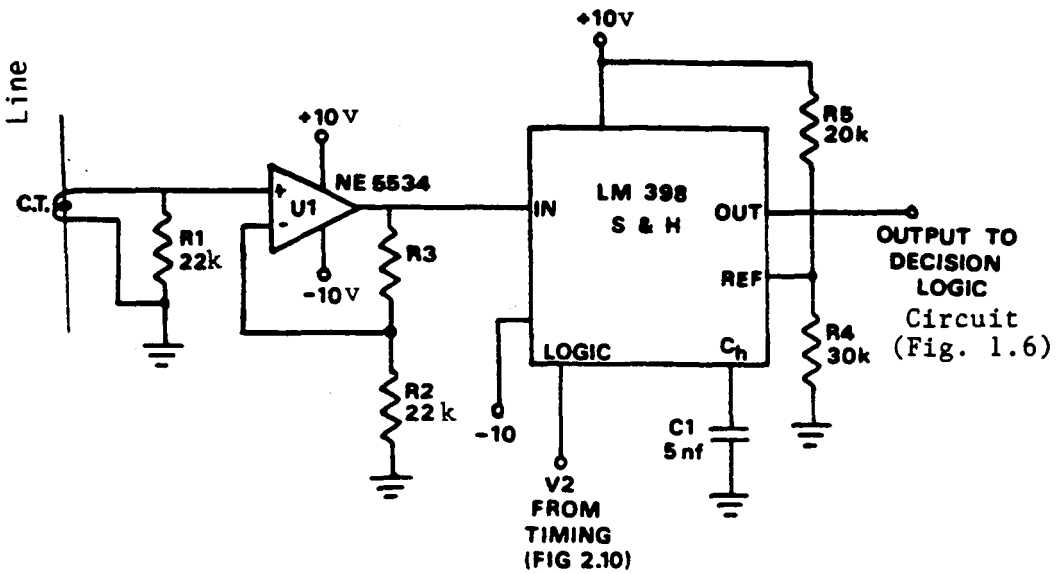

Figure 1.5: Reactive Current Sensing Circuit

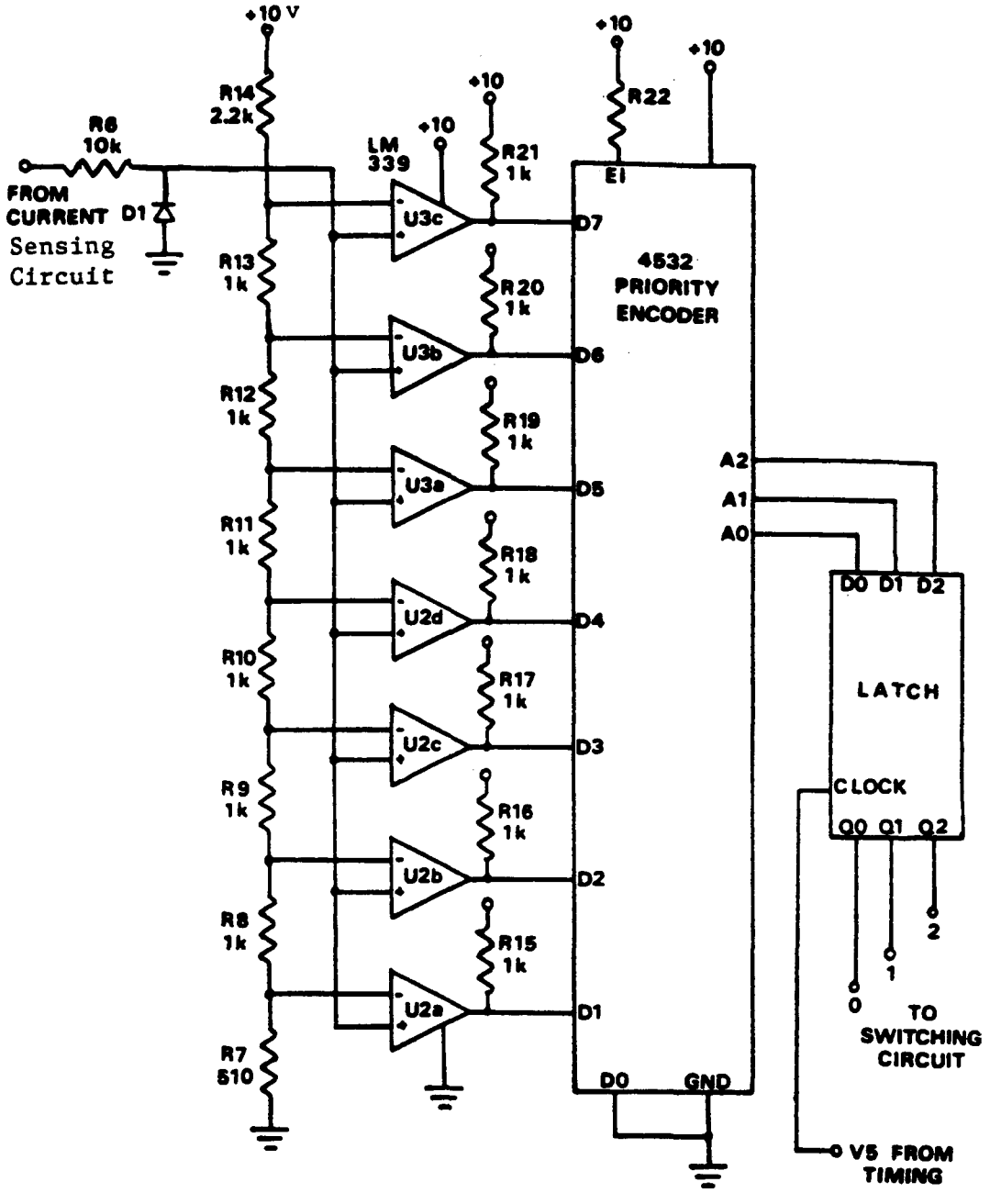

Figure 1.6: Decision Logic Circuit

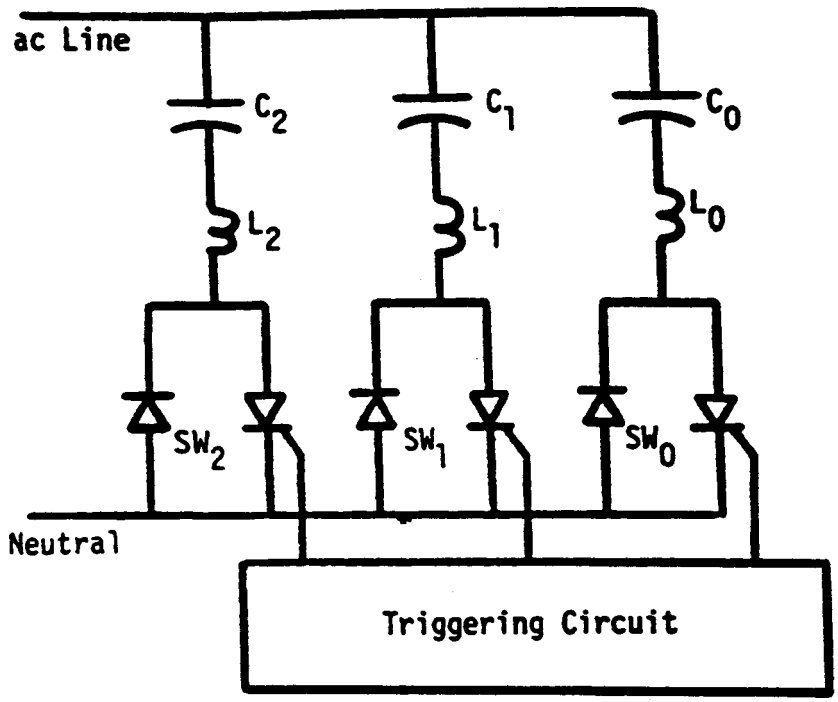

Figure 1.7: Switching Circuit

snubbing reactor (for di/dt protection) and an electronic switch. The electronic switch consists of a Silicon Controlled Rectifier (SCR) and a diode. The SCRs are triggered by the output of the Decision Logic Circuit. The timing signal is designed to ensure that the SCRs are triggered at the time when the voltage across each of them is zero so that transients can be eliminated.

During the negative half of the voltage cycle, all capacitors are charged negatively through the diodes. If no gate signal is applied on any SCR, no current will flow during the positive (or the negative) part of the cycle. The capacitors simply remain charged to the maximum negative voltage of the cycle. Once the capacitors have charged up through the diodes, the voltage across any SCR will be positive throughout the whole cycle, except at the negative peak of the phase voltage [1,13], when the voltage across the SCR is zero. To avoid large transient currents into the SCR, the SCR is turned on at the negative peak in the phase voltage. This is also the natural zero crossing of the capacitor current. In addition, small inductors, rated 100 microhenry, have been added in series with each of the capacitors to further protect the SCRs against excessive inrush current. This inrush current occurs when the voltage across the SCR is positive at the instant of triggering.

1.3.4 Timing Circuit

The Timing Circuit is shown in Figure 1.8. It supplies the rest of the circuits with correct timing signals to insure that the entire operation of the APFC is synchronized with the power line frequency. The

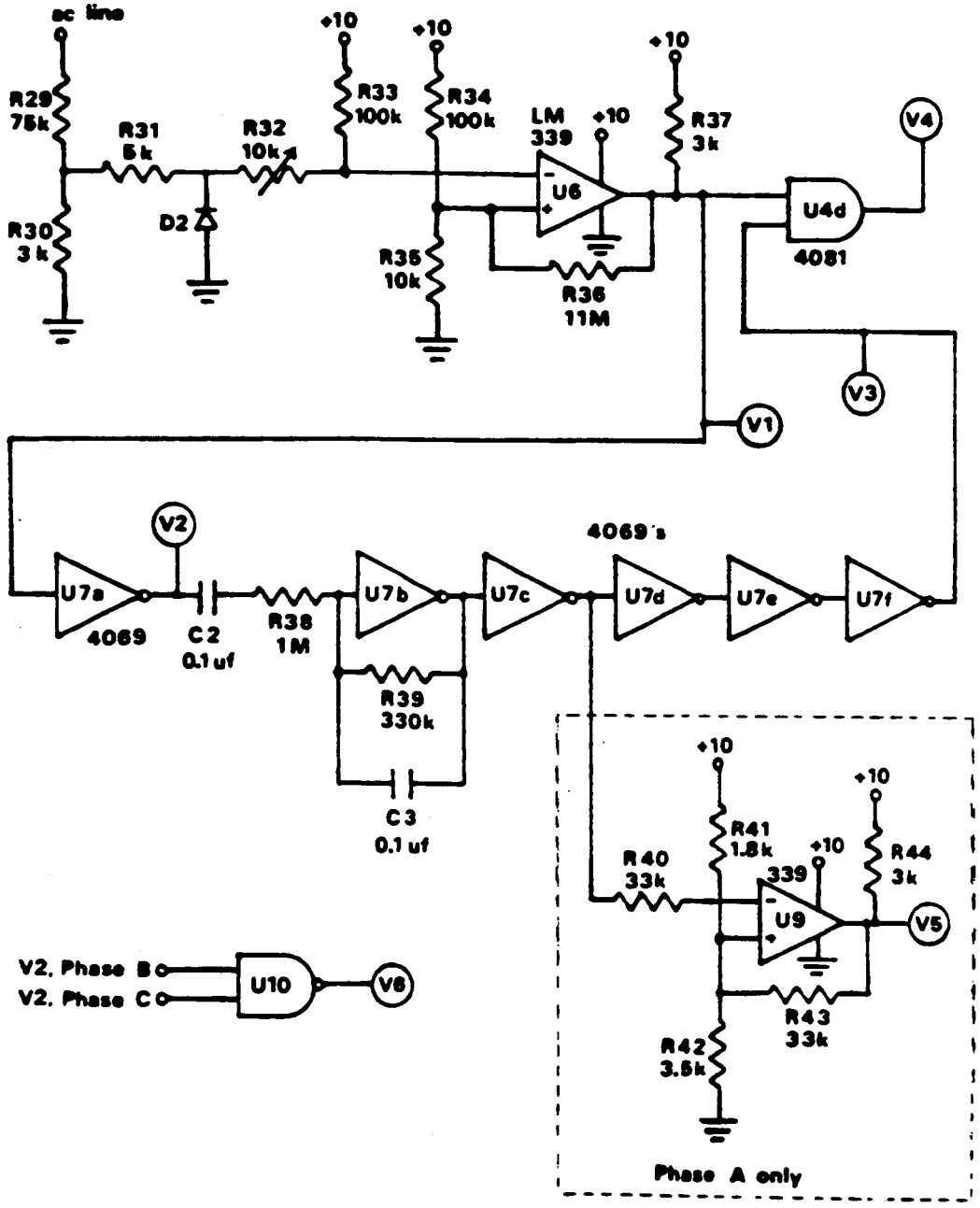

Figure 1.8: Timing Circuit

timing is very important to the system operation of the APFC. Incorrect timing could lead to incorrect compensation, or could trigger SCRs away from the zero-crossing, which could be destructive.

1.4 Laboratory Testing of 7.5-kVAR APFC

This section summarizes the test results of the APFC and examines the harmonic problems present during testing.

A 7.5-kVAR APFC was built in the Energy Systems Laboratory at the University of Washington . The device was tested on a 6.0-kW (7.5-hp motor rating) induction generator in the laboratory. The generator was driven by a dc motor to simulate variations of wind speed.

The reactive power profile of the test machine is shown in Figure 1.9 (a), and its power factor profile is shown in Figure 1.10 (a). These figures show that the power factor of the machine for motor operation is higher than that for generator operation. The generator power factor in the operating region ranged from 40% to 78% lagging, which is very poor.

The minimum reactive power needed by the machine is about 3.2-kVAR at a speed of 1795 r/min. To compensate this amount of VARs, about 60-μf capacitors per phase, connected in delta, (or an equivalent value connected in wye) were needed. However, the proper size of the capacitors was determined after a self-excitation test was made. The test was performed by running the generator unloaded with fixed capacitors connected to its terminals. The terminal voltage was observed at different speeds of rotation. As a result of this test, only 37.5-μf capacitor per phase connected in delta was found to be suitable for fixed

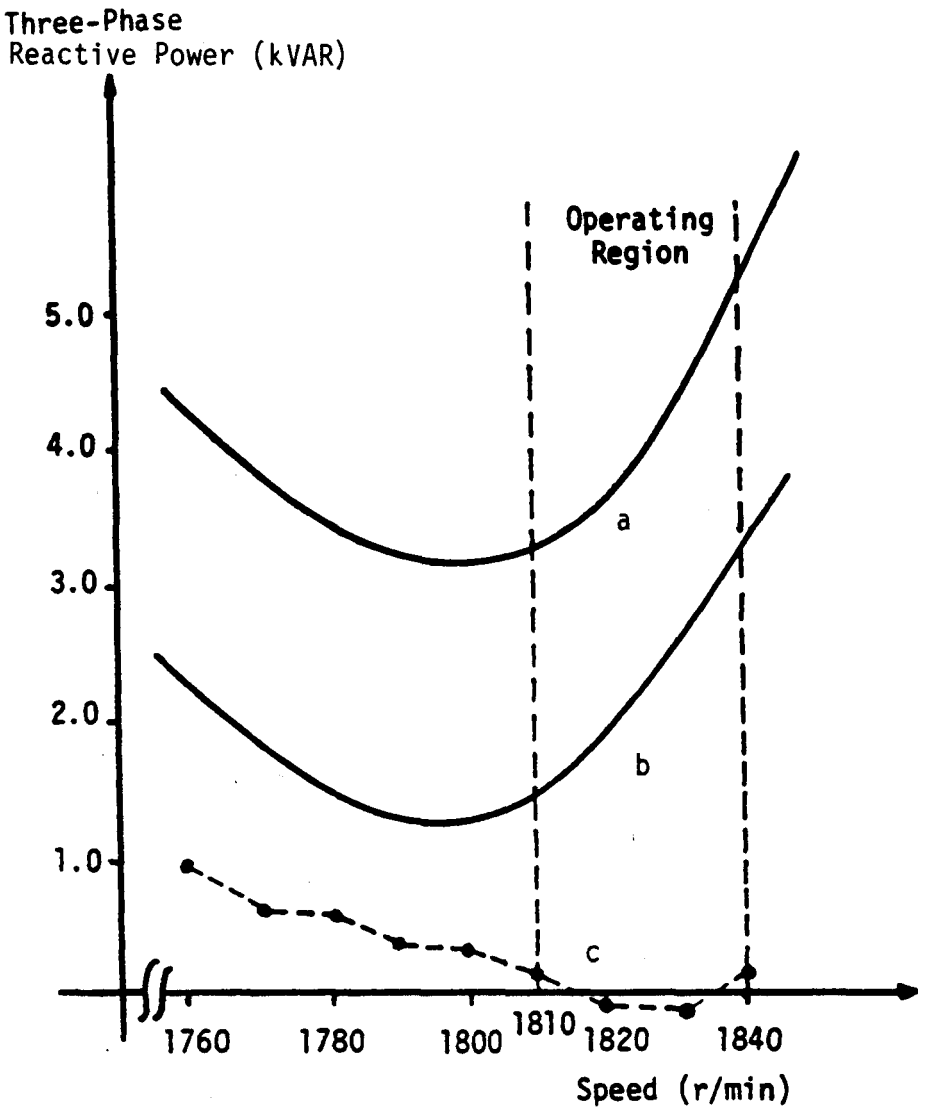

Figure 1.9: Reactive Power Profile of 6.0-kW Induction Generator

(a) Without Compensation
(b) With Fixed Compensation (37.5-μF per Phase Connected in Delta)
(c) With Fixed and Switched Compensation

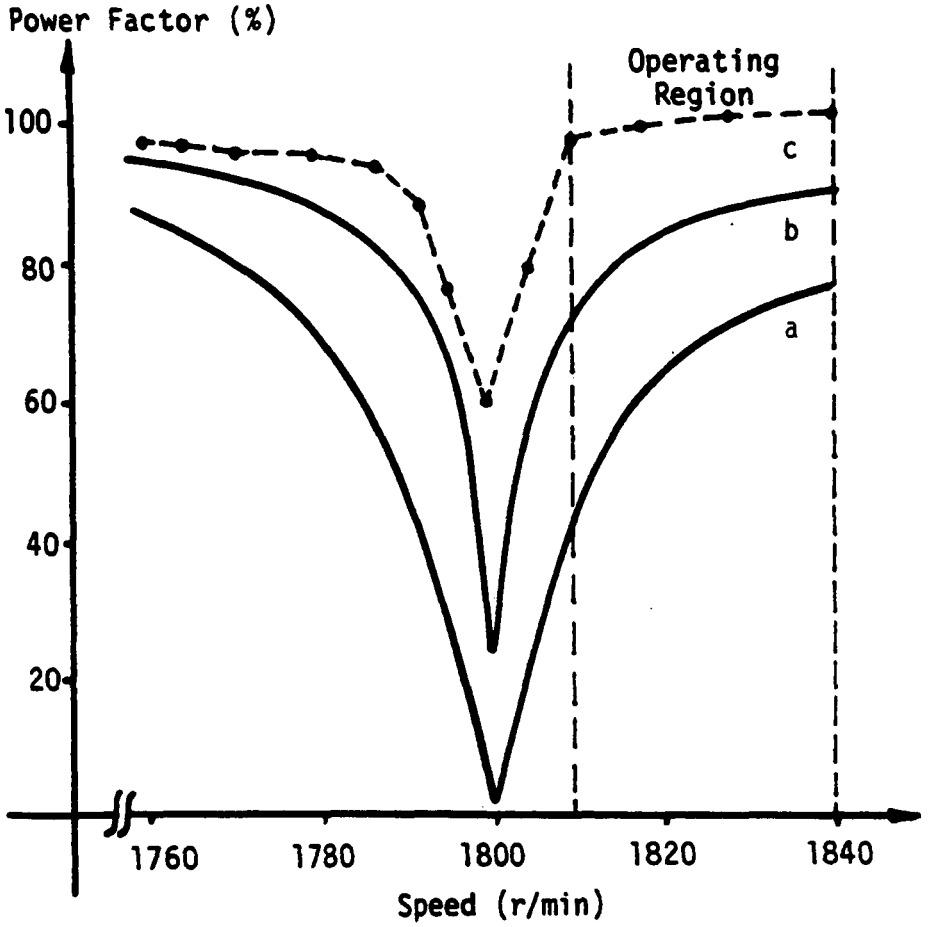

Figure 1.10: Power Factor Profile of 6.0-kW Induction Generator
(a) Without Compensation
(b) With Fixed Capacitors (37.5-μF per Phase Connected in Delta)
(c) With Fixed and Switched Capacitors

compensation since self-excitation occurs only at speeds higher than 1890 r/min, which is higher than the generator's full-load speed of 1840 r/min.

Figure 1.9 (b) shows the reactive power profile when 37.5-μf fixed capacitors were used, while Figure 1.10 (b) shows the corresponding power factor profile. With these fixed capacitors, the power factor improved to about 73% - 86% in the operating region of the generator.

As shown in Figure 1.9 (b), the maximum reactive power to be compensated, in addition to that provided by the fixed capacitors, is about 3.2-kVAR (which occurs at about 1840 r/min). This required a switchable capacitor scheme of about 175-μf per phase connected in wye. Three switchable capacitors per phase were selected in the following binary ratios: 25, 50 and 100-μf. This selection provided seven discrete values of reactive compensation: 0.456, 0.912, 1.368, 1.824, 2.280, 2.736 and 3.193-kVAR. The first two values, however, were used as long as the generator was energized.

The reactive power profile of the system with both fixed and switched schemes is shown in Figure 1.9 (c), and the corresponding power factor profile is shown in Figure 1.10 (c). It can be seen from these figures that the system with both fixed and switched capacitors provide the generator with almost all the needed reactive power. The power factor of the system is very close to unity in the operating region of the generator speed.

1.4.1 Waveform Analysis

Various waveforms illustrating the generator's phase voltage and line current at a speed of 1838 r/min, as seen from the feeder side, are

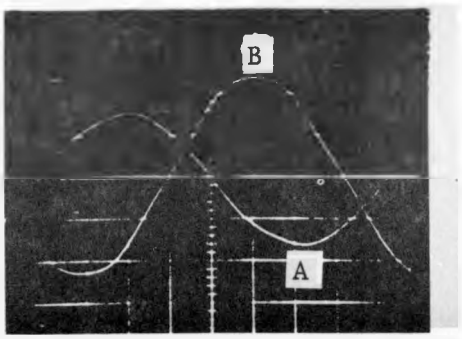

(a)

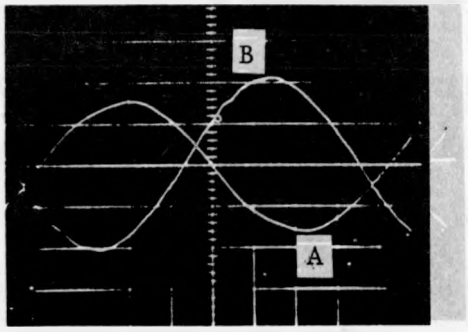

(b)

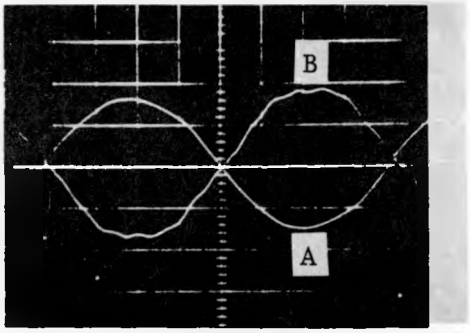

(c)

Figure 1.11: Generator Phase Voltage (A) and Line Current (B)

(a) Without Compensation
(b) With Fixed Capacitors (37.5-μF per Phase Connected in Delta)
(c) With Fixed and Switched Capacitors

shown in Figures 1.11 (a, b and c). Figure 1.11 (a) shows the generator voltage and current without capacitors. At the origin, as the voltage crosses zero, the current is positive, indicating that the generator draws reactive power as it delivers active power. The power factor in this case is about 73% lagging. With the fixed capacitors added, the calculated power factor as seen from the feeder side improved to about 86% lagging (see Figure 1.11 (b)). When both fixed and switched capacitors were used, the power factor reached almost unity as can be observed from Figure 1.11 (c).

1.4.2 Harmonic Analysis of Supply Voltage and Line Current

Figures 1.11 (a, b and c) show significant harmonic content in the line current. A spectrum analyzer was used to analyze the ac supply voltage in the laboratory. The result of this test is shown in Figure 1.12. The supply voltage was found to be contaminated with harmonics, with the third and fifth components dominating. The magnitudes of the harmonics shown in this supply voltage may not normally be a problem for most loads. However, shunt capacitors amplify the effect of the line current harmonics, since capacitive reactance decreases with increasing frequencies. Thus, supply voltages with a relatively low level of harmonics accentuate the corresponding harmonic components in the current.

In laboratory testing, the current harmonics did not have a large adverse effect on the operation of the controller. This is because the voltage harmonics observed in the laboratory added up to almost zero value at the zero crossing of the fundamental component of the voltage. Hence, the real component of the harmonic currents were also very small at this

point, and the sampled current at the zero crossing of the voltage still gave a good indication of the total reactive current.

1.4.3 Harmonics Generated by the APFC Switching

As mentioned earlier, the SCR of each capacitor is turned on at the negative peak of the corresponding phase voltage. This switching mechanism, together with the reverse connected diode, should not create additional harmonics in the line current. To verify this, the harmonic contents were recorded for two test cases:

Test Case 1: Normal operation where the switched capacitors were turned on by the Switching Circuit. The speed of the generator in this case was 1835 r/min.

Test Case 2: The test conditions were the same as in Test Case 1, except that the capacitors were directly connected to the lines (the SCR/diode pairs were shorted).

These two test cases should reveal any additional harmonics in the line current due to the switching of the SCRs. Figures 1.13 (a and b) show the harmonic content of the line current for Test Cases 1 and 2 respectively. A slight increase in some harmonics can be seen in Test Case 1 as compared with Test Case 2. The dominating harmonics (third, fifth and seventh) change very little, with the maximum increase being no more than 4 db for the seventh harmonic. The sixth and eighth harmonics increase by less than 10 db, but they can still be ignored, since they are at least 60 db below the fundamental. Thus, no additional harmonics are introduced due to the switching of SCRs of the APFC.

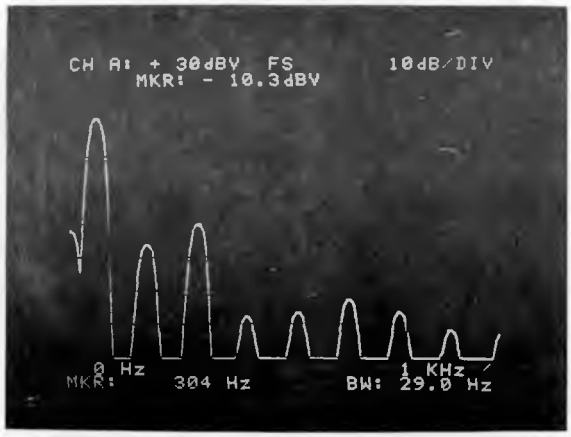

Figure 1.12: Harmonic Spectrum of the Supply Voltage

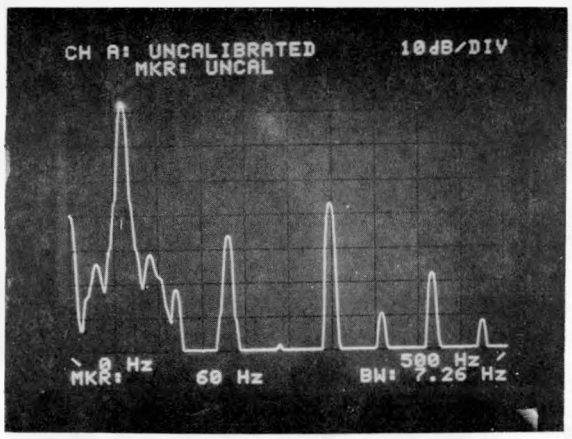

(a)

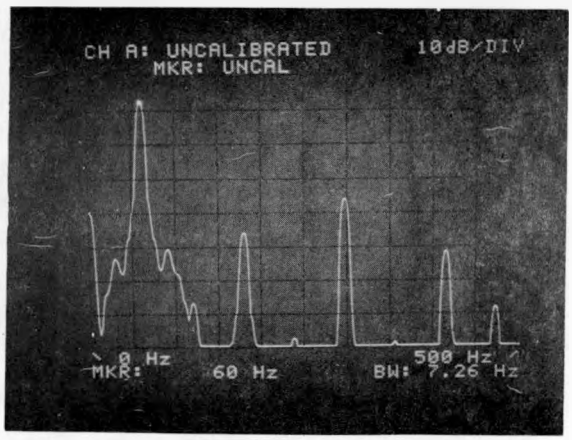

(b)

Figure 1.13: Harmonic Content of the Line Current

(a) When SCRs are in operation
(b) When SCRs are shorted

1.5 Disadvantages in the Design of the 7.5-kVAR APFC

Although the 7.5-kVAR APFC can function successfully in compensating the varying reactive power demand of an induction machine, the circuit design of the APFC possesses the following drawbacks which could limit its performance:

1. Only one phase of the reactive power current is sensed, and an equal amount of reactive power based on the sensed value is provided to each phase. This limits the APFC to performing effectively only in a balanced three-phase system.

2. There is no isolation between the electronic circuit and the power line. Any disturbance in the power line could transmit to the electronic circuit and result in the failure of the APFC's components.

3. The fixed capacitors are not controlled by the APFC. This could result in an over-voltage problem in case the inductive load is disconnected from the power line while the fixed capacitors are still switched on.

4. The switching of each capacitor is controlled by an SCR/diode pair. Since the switching of a diode cannot be externally controlled like an SCR, this might cause transients in the line current when the APFC is first turned on.

5. The circuit design is not compact. This increases the complexity and size of the circuit. For example, the Decision Logic Circuit (as shown in Figure 1.6) which is implemented by seven comparators,

an encoder and a latch, can be replaced by an analog-to-digital (A/D) converter.

CHAPTER 2

DESIGN AND FABRICATION OF THE 50-kVAR OPEN-LOOP APFC AND ITS TRANSIENT SIMULATION PERFORMANCE

2.1 Introduction

The Open-Loop Adaptive Power Factor Controller (OL-APFC) has the same basic features presented in Chapter 1. However, it has been improved to include the following modifications and additional features:

1. The reactive current of each phase can be sensed independently to provide appropriate reactive power compensation for unbalanced systems
2. The Decision Logic Circuit was re-designed to improve its reliability
3. The Triggering Circuit was re-designed to provide isolation from the power line and to reduce the effects of the electromagnetic interference
4. The Switching Circuit was modified to include the following features:
   a) The SCR/DIODE pairs were replaced by anti-parallel SCRs to prevent the transients due to the initial turning on of the APFC.
   b) Fixed capacitors can be switched to the power line via SCR pairs to prevent the transients due to the initial turning on of the APFC (the fixed capacitors were manually switched in the 7.5-kVAR APFC).

c) Four stages of switched capacitors were used per phase instead of three stages as in the 7.5 kVAR APFC. This was implemented to provide a smoother compensation.

5. The Timing Circuit was designed to synchronize with the power line frequency. This was done to eliminate false triggering and enhance the reliability of the device.
6. An Interlock Circuit was added to the design to eliminate the over-voltage or self-excitation problems that might exist due to the presence of the APFC capacitors.

2.2 General Description of OL-APFC

Figure 2.1 shows the following main functional blocks of the OL-APFC:

1) Reactive Current Sensing Circuit
2) Decision Logic Circuit
3) Triggering Circuits
4) Switching Circuits
5) Timing Circuit
6) Interlock Circuit

In addition to these blocks, current transformers, voltage transformers and protection circuits for solid-state switches are also shown. Two sets of capacitors were used per phase : fixed capacitors and switched capacitors. Their values are usually dictated by the reactive power profile of the load, such as the induction machine, a typical curve of which is shown in Figure 1.2. In the OL-APFC, the fixed capacitors were selected to compensate all the minimum reactive power demand of the generator. An Interlock Circuit was added to the

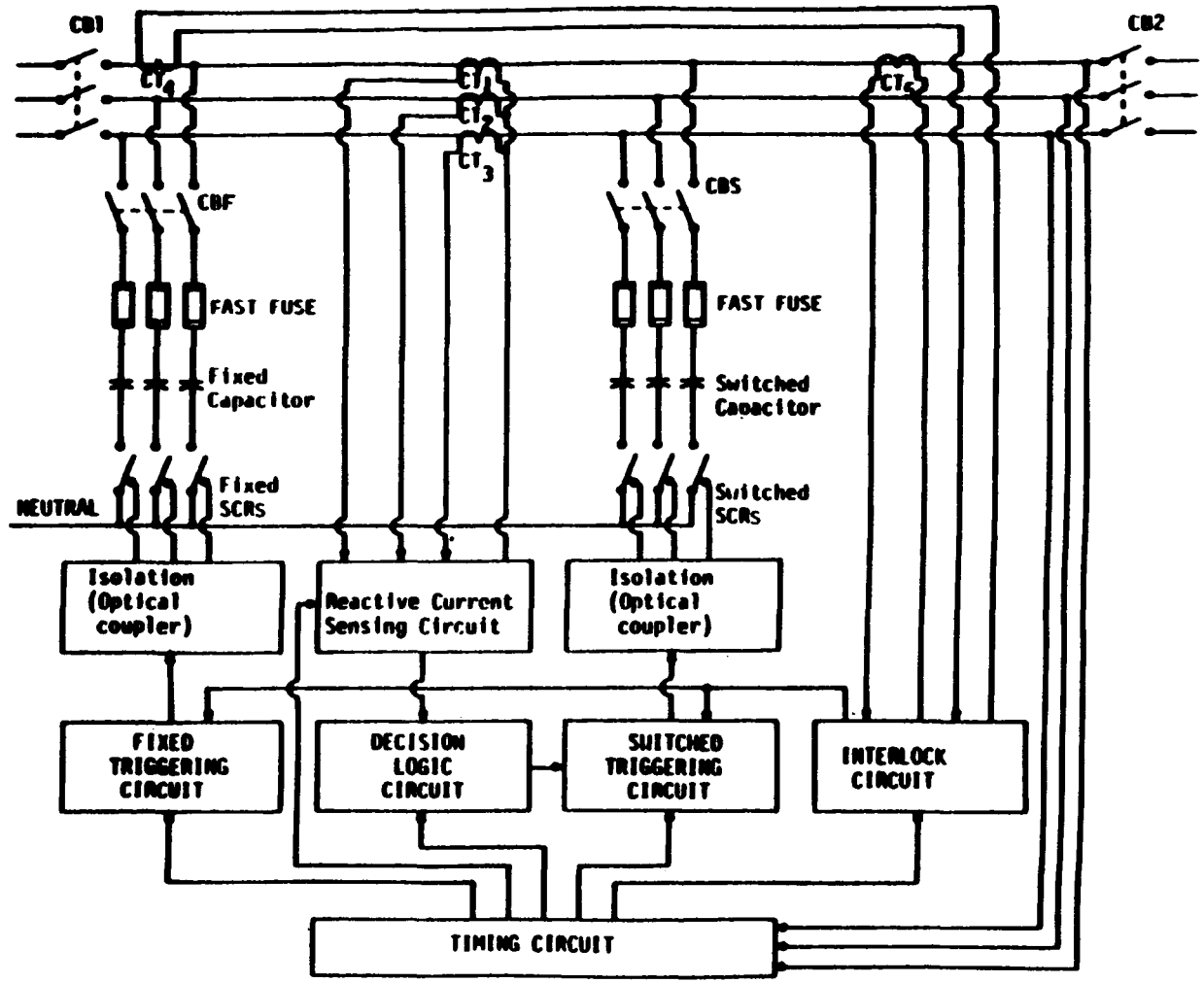

Figure 2.1: Functional Block Diagram of 50-kVAR OL-APFC

APFC to eliminate the self-excitation problem. The Interlock Circuit is described in detail in Section 2.2.6. Switched capacitors provide the remaining varying demand of reactive power. There are four switching stages per phase to yield the binary ratios of 1:2:4:8. This allows sixteen compensation steps per phase (including zero).

For clarity only one switched capacitor per phase is shown in Figure 2.1. Each of the six functional blocks are described in the following sections with suitable circuit diagrams.

2.2.1 Reactive Current Sensing Circuit

The line current in each phase, which contains the real and reactive components, is sensed by the current transformers CT_1,CT_2 or CT_3 as shown in Figure 2.1. The output of each current transformer is fed to the reactive current Sensing Circuit. In this circuit, the instantaneous current signal of each phase is locked at the instant the magnitude of the corresponding instantaneous phase voltage is zero and about to become negative. This locked value is proportional to the peak value of the reactive current. This independent phase sensing of the reactive current is a modification to the original design described in Chapter 1. It allows the capacitors of each phase to be switched independently which makes the device suitable for unbalanced power systems.

Figure 2.2 shows the main components of the reactive current Sensing Circuit. The line currents, which contain both real and reactive components are sensed via the current transformers (CTs). The current signals at the outputs of the CT's are transformed into a

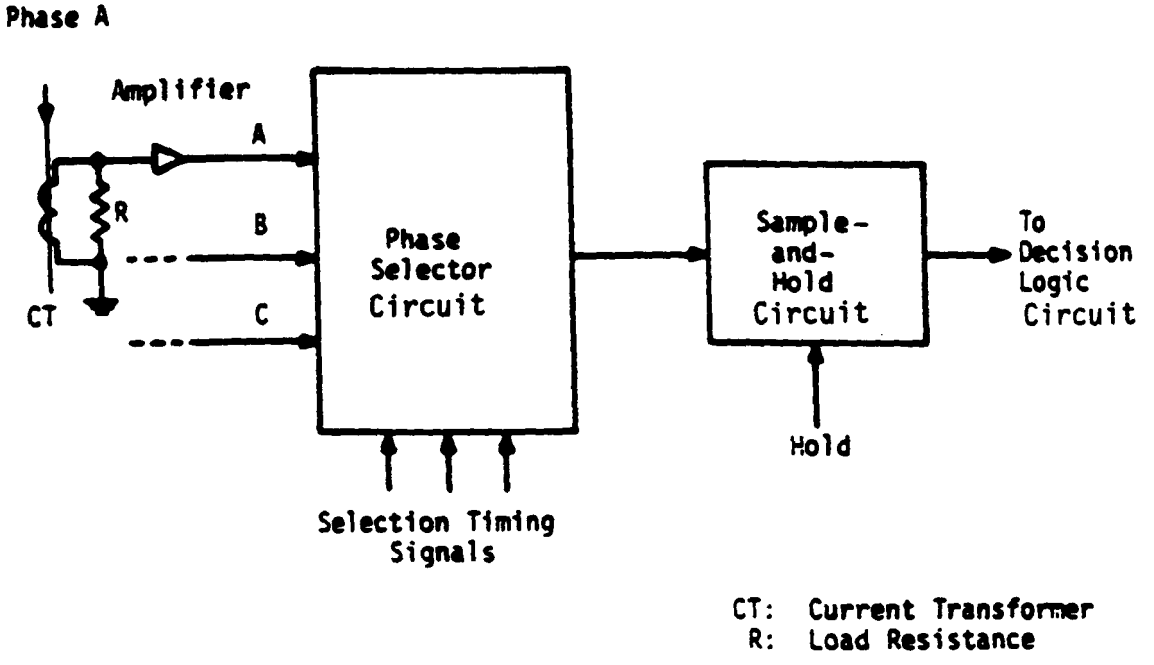

Figure 2.2: Reactive Current Sensing Circuit

voltage signal. An amplifier circuit in each phase amplifies the voltage signal to a satisfactory level, which is set a priori.

The amplified signals are selected once per cycle by using the proper selective timing signal; that is, phase A signal is selected for 1/3 of cycle time, phase B signal for the next 1/3 cycle and phase C signal for the remaining 1/3 cycle. The selection is illustrated in Figure 2.3. One cycle is divided equally into three time intervals denoted by t_1, t_2 and t_3 respectively. During the interval t_1, the selection timing of phase A is active, and the current waveform of this phase appears at the phase selector output. Similarly, the current waveform of phase B is available at the selector output during the time interval t_2, and that of phase C during t_3. The selected waveform will be captured at an appropriate time set by the timing signal.

During the time a current waveform is selected, the corresponding phase voltage is zero going negative. At this particular instant, the value of the line current is the same as the peak value of its reactive component. The sample-and-hold (S&H) is signaled to lock this value at its output. This output stays constant for 1/3 of a cycle as shown by Figure 2.3, and is fed to the Decision Logic Circuit which determines the amount of capacitance to be switched to provide the reactive compensation for that phase.

2.2.2 Decision Logic Circuit

The Decision Logic Circuit converts the magnitude of the reactive current per phase to a digital form of n bits for n switching stages. Figure 2.4 shows the main components of the Decision Logic Circuit. The

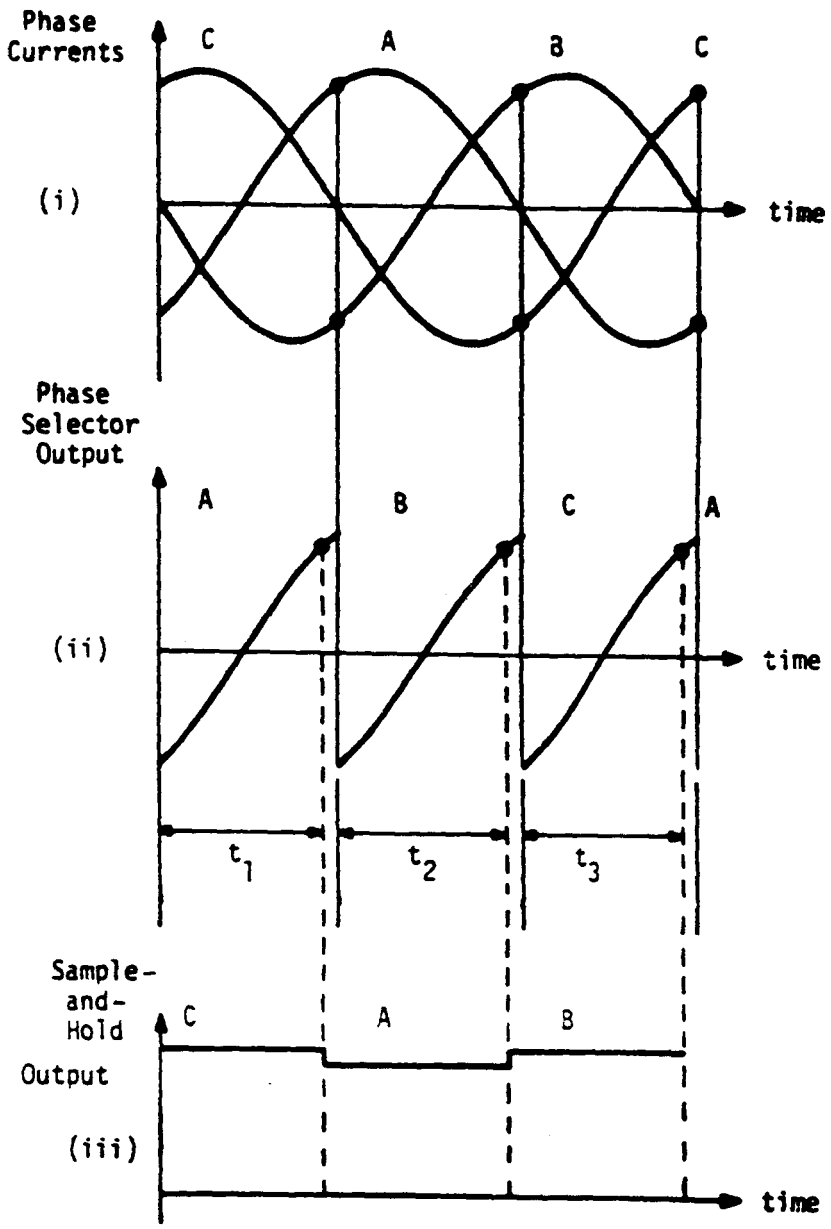

Figure 2.3: Waveforms for Reactive Current Sensing Circuit

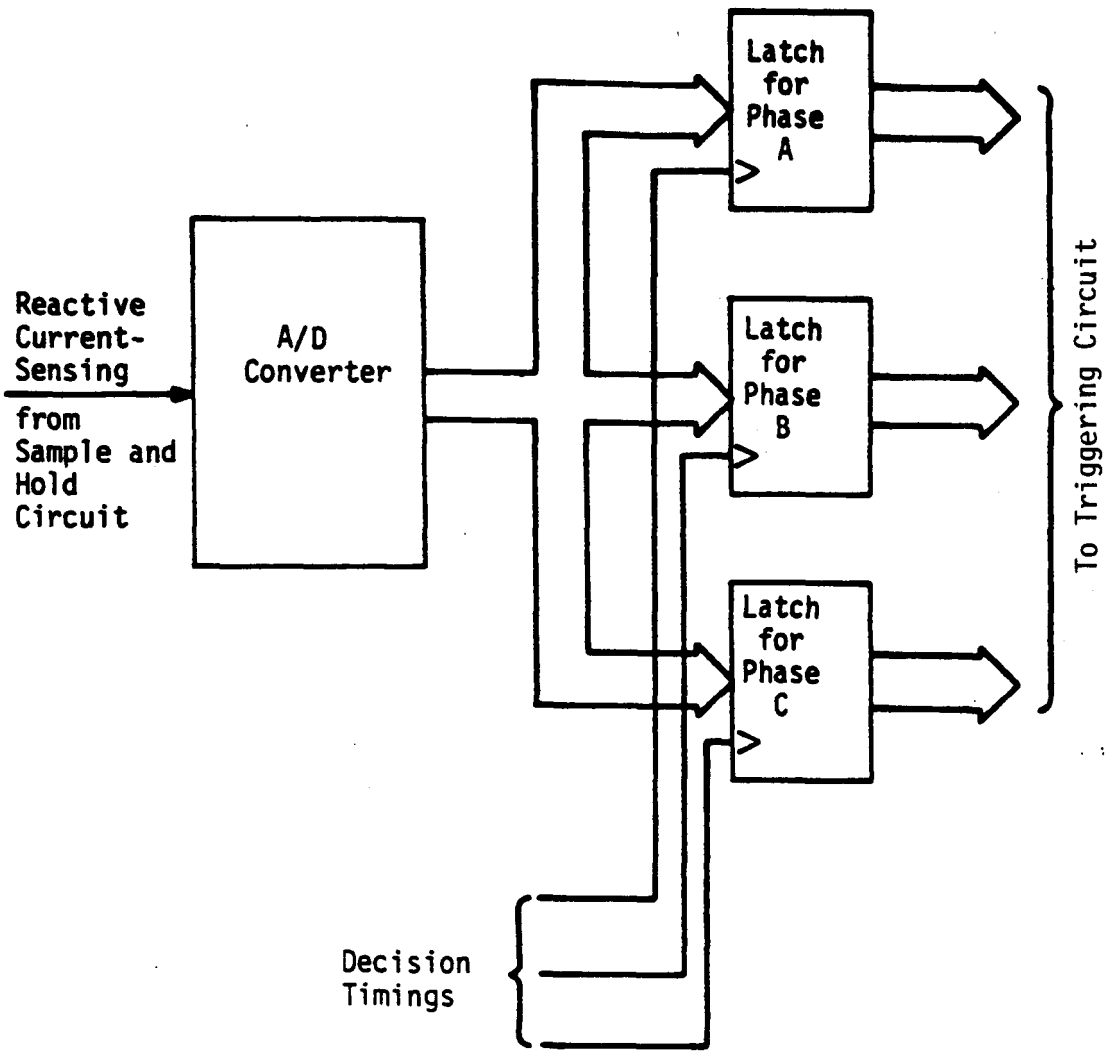

Figure 2.4: Block Diagram of Decision Logic Circuit

analog signal that represents the peak value of the reactive current is converted to a digital form by the analog-to-digital converter (A/D). There is a one-to-one correspondence between the (output) bits of the A/D and the number of switched capacitor stages for each phase. This means that the values of switched capacitors are chosen in the ratios of 1:2:4:8:, and that bit #1 of the A/D converter controls the smallest capacitor, bit #2 controls the next higher value and so on. Table 2.1 shows the output of the Decision Logic Circuit as a function of the reactive power demand.

The bits are available for each phase for 1/3 of a cycle and are stored for that phase by using an electronic latch. The output of the Decision Logic Circuit consists of 3 sets of binary code for the three phases, which control the switching mechanism of the OL-APFC by controlling the Triggering and, in turn, the Switching Circuits.

2.2.3 Triggering Circuit

The Triggering Circuit receives the four bits (commands) from the Decision Logic Circuit for each phase. Then it generates triggering signals to switch the SCRs. To eliminate the transients created by the switching of capacitors, each SCR is triggered at the instant when the voltage across it is zero or slightly negative.

The Triggering Circuit consists of a number of AND gates and optical couplers, as shown in Figure 2.5 where only one bit is shown. The command signals sent from the Decision Logic Circuit are allowed to pass through the AND gates when the switching timing signal is active at the zero voltage across the SCR. Optical couplers then translate these

Table 2.1: Decision Logic Output Signals as Function of Reactive Power Demand (Assumes the use of four switches per phase, Q_o is one unit of compensation.)

Q (reactive demand)	Decision Logic Signal Output			
	bit #4	bit #3	bit #2	bit#1
$0 < Q \leq .5\ Q_o$	0	0	0	0
$.5\ Q_o < Q \leq 1.5\ Q_o$	0	0	0	1
$1.5\ Q_o < Q \leq 2.5\ Q_o$	0	0	1	0
$2.5\ Q_o < Q \leq 3.5\ Q_o$	0	0	1	1
$3.5\ Q_o < Q \leq 4.5\ Q_o$	0	1	0	0
.	.	.	.	.
.	.	.	.	.
.	.	.	.	.
$7.5\ Q_o < Q \leq 8.5\ Q_o$	1	0	0	0
.	.	.	.	.
.	.	.	.	.
.	.	.	.	.
$14.5 Q_o < Q \leq Q_{max}$	1	1	1	1

commands into current signals which directly trigger the SCRs of the Switching Circuit. Figure 2.6 shows the triggering time of the SCRs; (a) is for the reverse SCR, and (b) is for the forward SCR. The triggering signal for the reverse SCR is only disabled by switching off the interlock signal.

2.2.4 Switching Circuit

The Switching Circuit switches the capacitors of each stage of each phase independently. Figure 2.7 shows the main components of one leg of the Switching Circuit in the OL-APFC. Each phase has a number of these switching capacitors sized in the binary ratios.

The OL-APFC is enabled by the interlock signal. The reverse SCRs are then triggered continuously and function as diodes. The reason for not using diodes here is to eliminate the initial transients due to the initial switching of the circuit breaker of the device, and to enhance the device's safety. When the circuit breaker is switched on, the reverse and forward SCRs will not allow any transient current to flow inside the capacitors due to the absence of their triggering signals.

When a particular capacitor is to be switched on, its forward SCR is turned on by the Triggering Circuit. To prevent harmonics and transients in the current, the SCR is triggered when the voltage across it is zero. The capacitor current then continuously flows for one cycle, with the first half of the cycle via the forward SCR, and the other half via the reverse SCR. When the cycle time expires, that capacitor is turned off unless its forward SCR is triggered again.

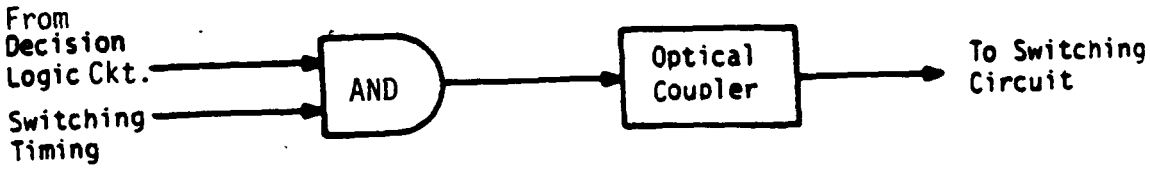

Figure 2.5: Triggering Circuit for One Bit

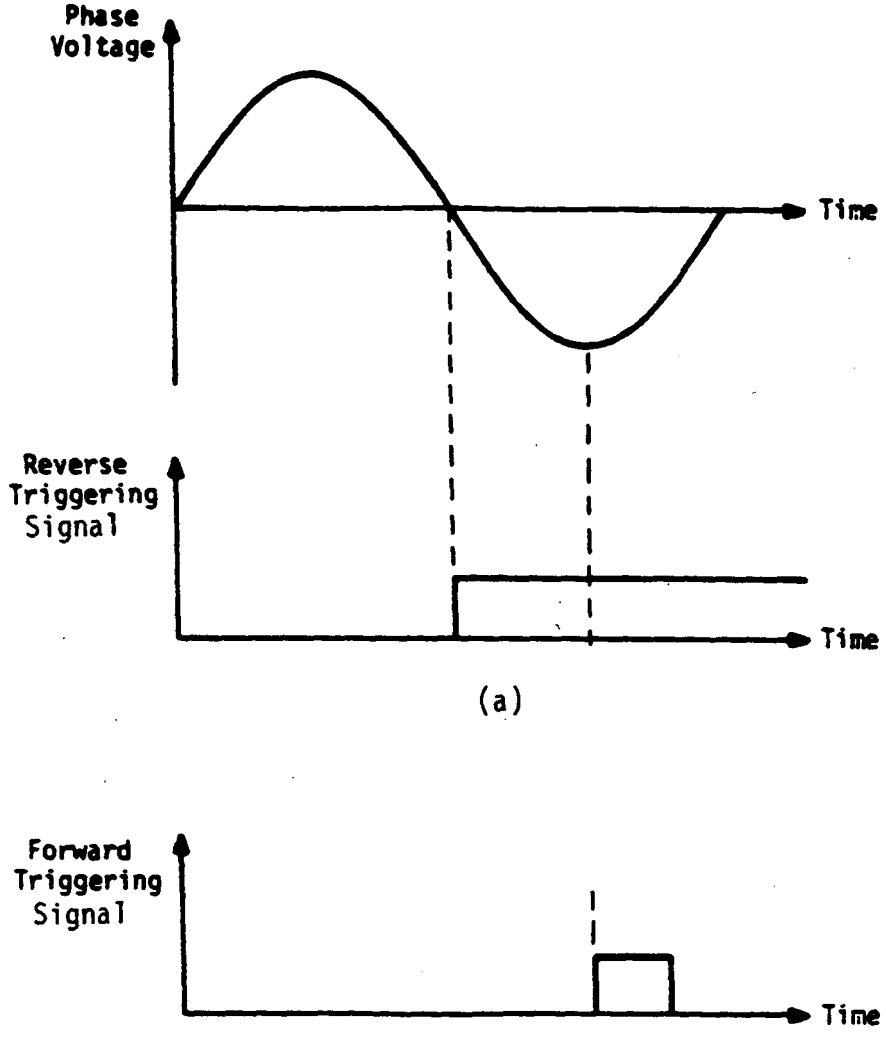

Figure 2.6: Triggering Scheme for SCRs
(a) Triggering for Reverse SCR
(b) Triggering for Forward SCR

In practice, it is impossible to trigger the forward SCR at exact points in time. Instead, this SCR is triggered during a time interval around the point where the voltage across it is zero. Therefore, Snubbing Circuits must be added as shown in Figure 2.8.

The Snubbing Circuits consist of the inductor L, to protect against excessive di/dt, and the R_s and C_s pair to prevent abrupt, excessive, dv/dt across each SCR. The resistor R_c connected in parallel with the capacitor is to discharge it slowly when the circuit is turned off.

2.2.5 Timing Circuit

The function of the timing circuit is to synchronize the operation of the entire OL-APFC circuit. The clock signals of the timing circuit are synchronized with the power line frequency to allow for the automatic adjustment of the timing signals whenever the line frequency shifts. Thus false triggering of SCRs can be eliminated even when the supply frequency varies.

The block diagram of the timing circuit is shown in Figure 2.9, and the timing waveforms are shown in Figure 2.10. As seen from Figure 2.9, there are four main sets of timing signals: The selection timing (one per phase) controls the phase selector of the reactive current Sensing Circuit. The sample timing (only one) controls the sampling and hold process. The decision timing (one per phase) signals the Decision Logic Circuit to send out commands to the Triggering Circuit. The switching timing (one per phase), controls the switching time of the SCRs.

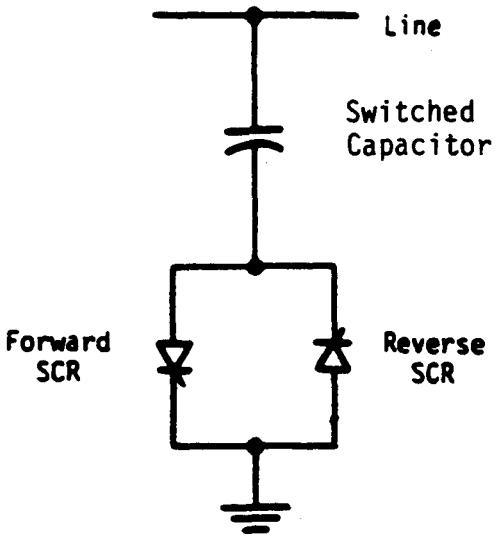

Figure 2.7: One Stage of the Switching Circuit

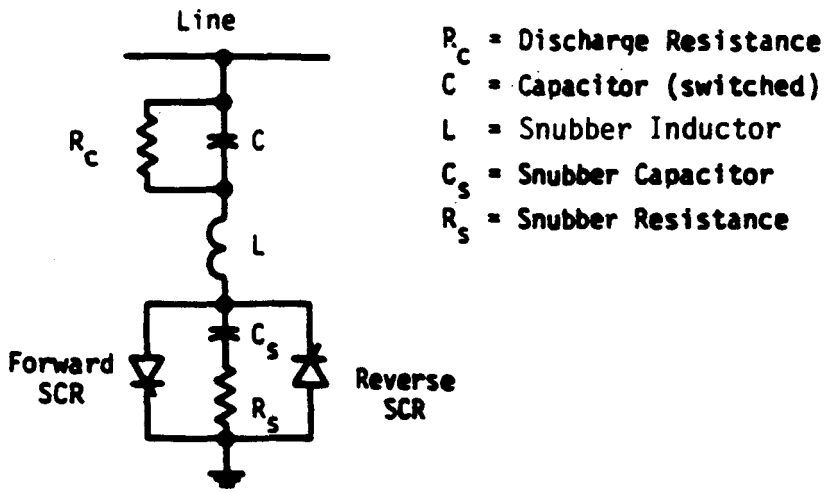

Figure 2.8: One Stage of the Switching Circuit with Snubbers and Discharge Resistor

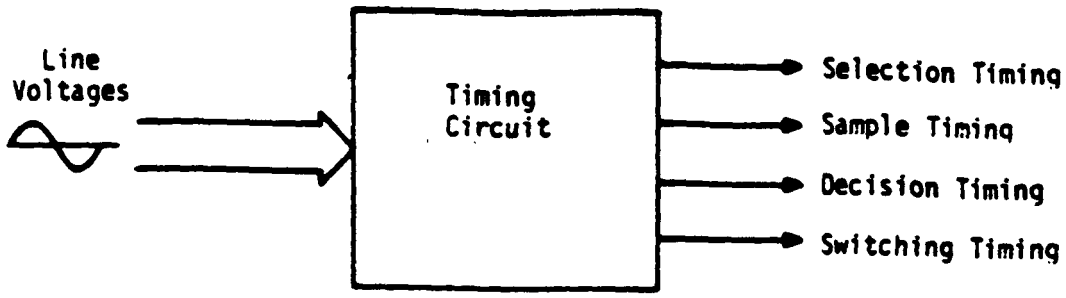

Figure 2.9: Block Diagram of Timing Circuit

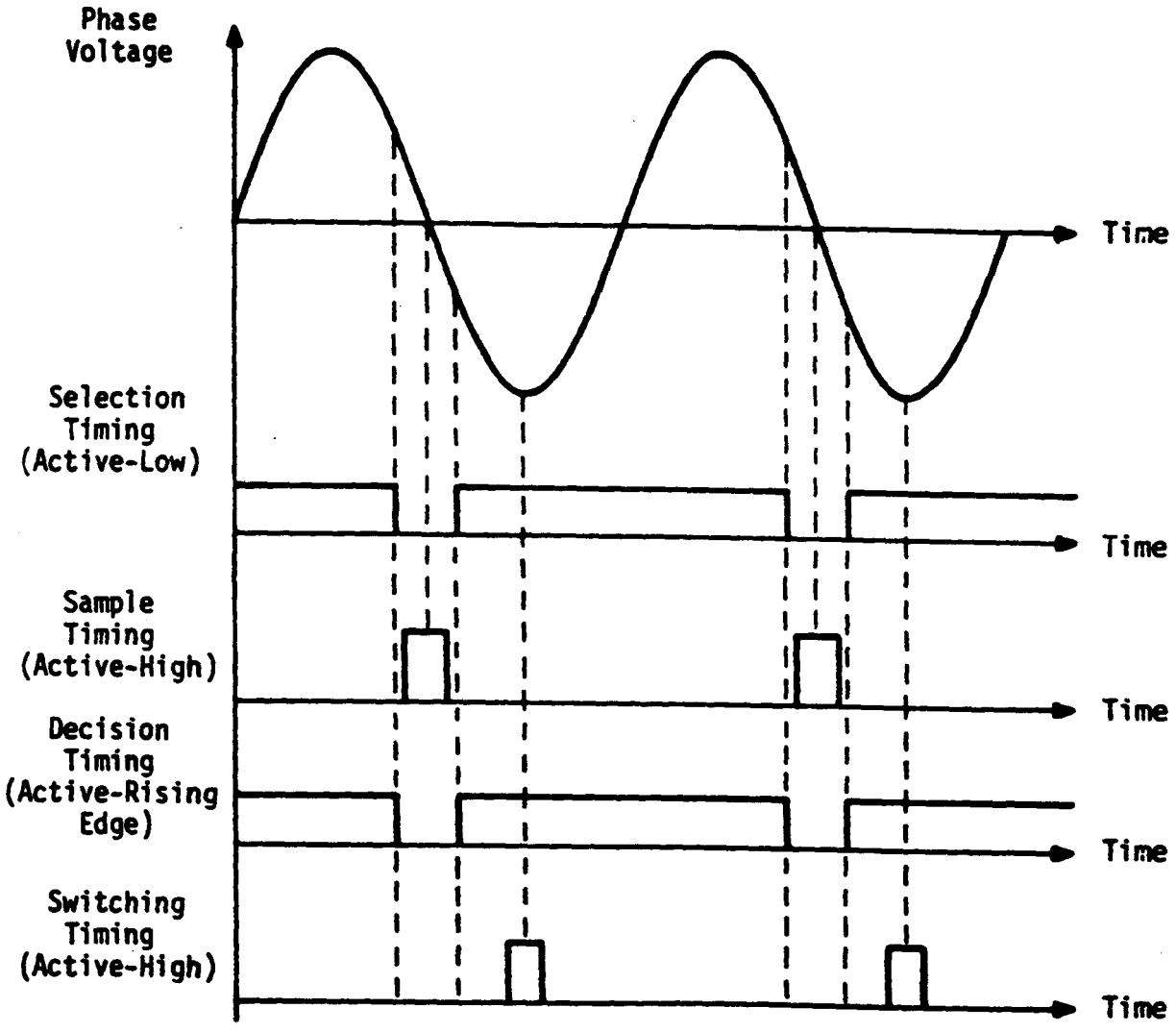

Figure 2.10: Main Timing Circuit Signals

The line voltages of the three phases, which are 120^{o} shifted from each other, are stepped down by two sets of transformer banks. The output waveforms of these transformers are used to generate the required timing signals through appropriate electronic circuits.

2.2.6 Interlock Circuit

The Interlock Circuit is another feature added to the original design described in Chapter 1. The main function of this circuit is to prevent self-excitation or overvoltage problems.

The circuit detects the line currents on both sides of the OL-APFC by means of the two current transformers CT_4 and CT_5 shown in Figure 2.1. When both CT_4 and CT_5 detect currents, the OL-APFC is enabled. When it is operating and the current signal from either CT_4 or CT_5 suddenly drops to zero (or a predetermined small value), the OL-APFC is disabled.

2.3 Transient Simulation and Analysis

Under normal operating conditions, each SCR is switched on at the instant when the voltage across it is zero. This is done to prevent transients in the power line and also to prevent damage to the components of the Switching Circuit.

The circuits of the OL-APFC consist of a large number of electronic components. The performance of the APFC depends on the operational status of all these components. If any one of them fails, the result of the failure might lead to one of two contingencies: 1) disabled triggering of SCRs, or 2) false triggering of SCRs. If the triggering of any SCR is disabled, the outcome is incorrect reactive

power compensation. It usually does not lead to any damage of the Switching Circuit components. On the other hand, when an SCR is triggered at the wrong instant, it might be switched on at some positive voltage across its terminals (anode-to-cathode). This could permanently short the SCR. If damaged, this SCR would result in a capacitor permanently connected to the power line, which might cause an over-voltage problem.

In this section, computer simulations of the Switching Circuit due to false triggering of SCRs are reported. The transient voltage and current waveform were studied, and the worst cases of false triggering were identified.

This study was made using the Electromagnetic Transient Program (EMTP) developed by BPA [33]. This program is proven to be a very powerful tool for transient and steady-state analysis of power systems. For brevity, only salient results are given in this section. For detailed analysis and results, refer to [17].

2.3.1 Analysis of Normal Operation

Figure 2.11 shows one leg of the Switching Circuit of the APFC. The source voltage is assumed to be 277-V line to ground. Figures 2.12 (a to c) show the simulated voltages and currents of the APFC during normal switching of the SCRs. Figure 2.12 (a) shows the phase voltage, Figure 2.12 (b) shows the voltage across the SCR pair and Figure 2.12 (c) shows the capacitor current. At the end of one cycle when the voltage across the SCR is zero going negative, the reverse SCR is switched on and stays on for a quarter of a cycle until the capacitor is

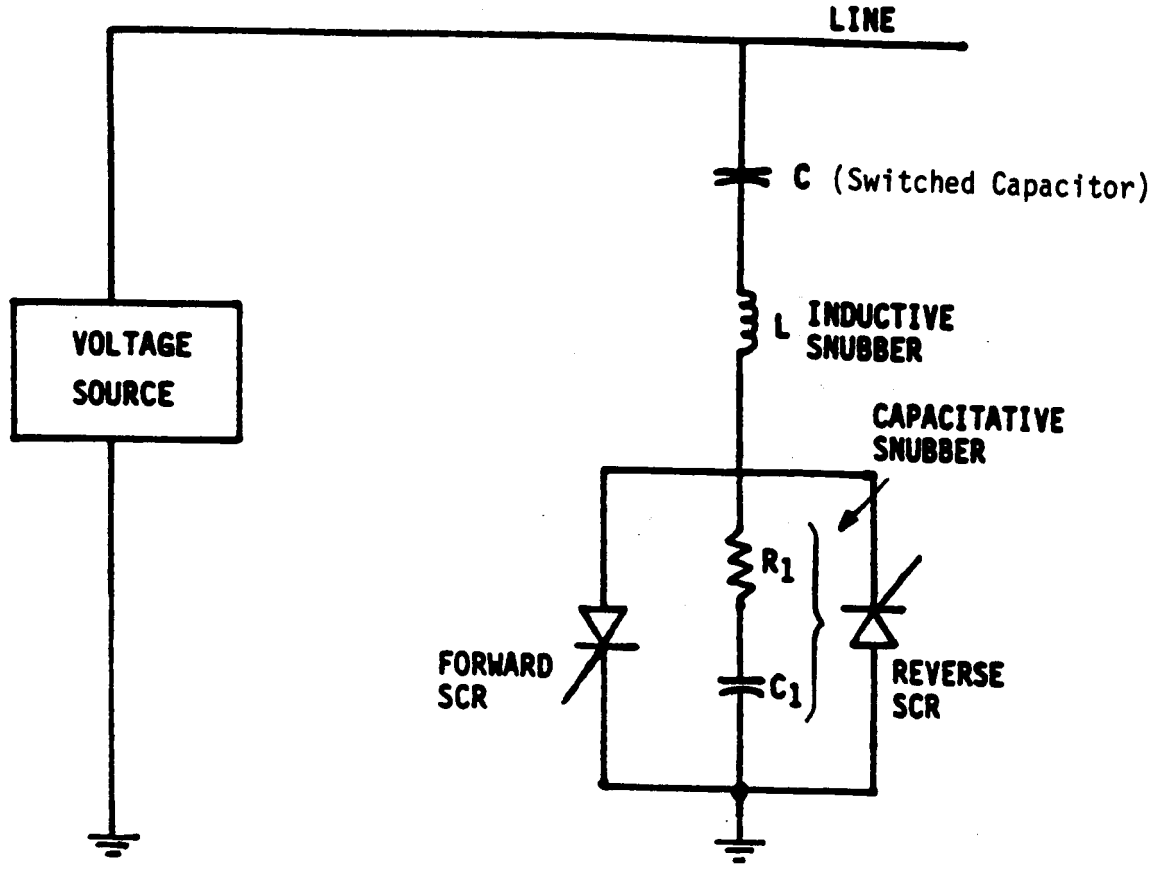

Figure 2.11: Test Circuit for the Transient Simulation

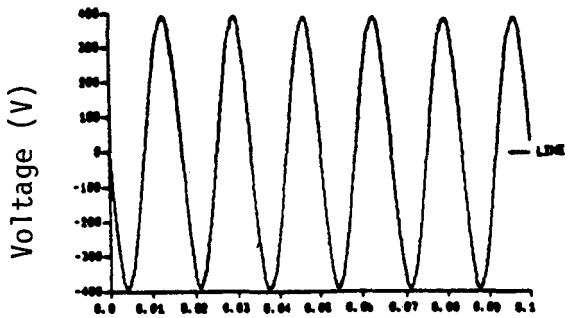

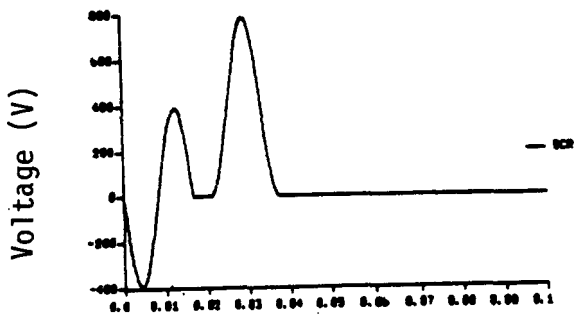

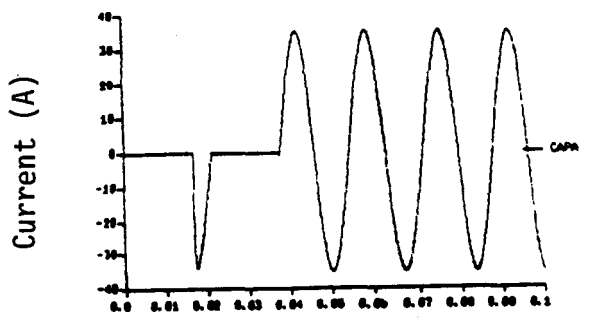

Figure 2.12: Normal Switching of the SCR

(a) Phase Voltage at the Point where the APFC is connected to the power supply
(b) Voltage Across the Back-to-Back SCR Pair
(c) Current through the capacitor

charged negatively. Once the capacitor is charged to the negative peak of phase voltage, the voltage across the SCR increases to double the phase voltage. The capacitors normally remain fully charged unless the forward SCR is triggered. The triggering signal switches on the forward SCR at zero voltage across it. Then the capacitor current continuously flows and the SCRs function as a back-to-back diode pair.

2.3.2 Effect of False Triggering of Reverse SCR

The reverse SCR is turned on at zero supply voltage or slightly negative voltage. It then receives a constant dc signal and acts as a diode. Should the reverse SCR be triggered at some positive voltage across it, transient currents will flow in the capacitor and will also propagate to the rest of the power system.

Figure 2.13 shows the voltages and currents of the Switching Circuit due to a 20^{o} (or 0.926 msec) delay in the triggering signal. The voltage source in this study is modeled by an induction generator equivalent circuit [13]. The three plots of Figure 2.13 (a to c) show the phase voltage, voltage across the SCR and the current through the capacitor respectively. Figures 2.13 (d to f) show the same results with the time scale expanded. The rate of rise of the voltage across the SCR, observed in Figure 2.13 (e), could permanently damage the SCR if it exceeds the device rating.

The worst case of false triggering of the reverse SCR occurs when the triggering signal is delayed by 90^{o} (or 4.16 msec). In this case the reverse SCR is triggered at maximum positive voltage across its terminals.

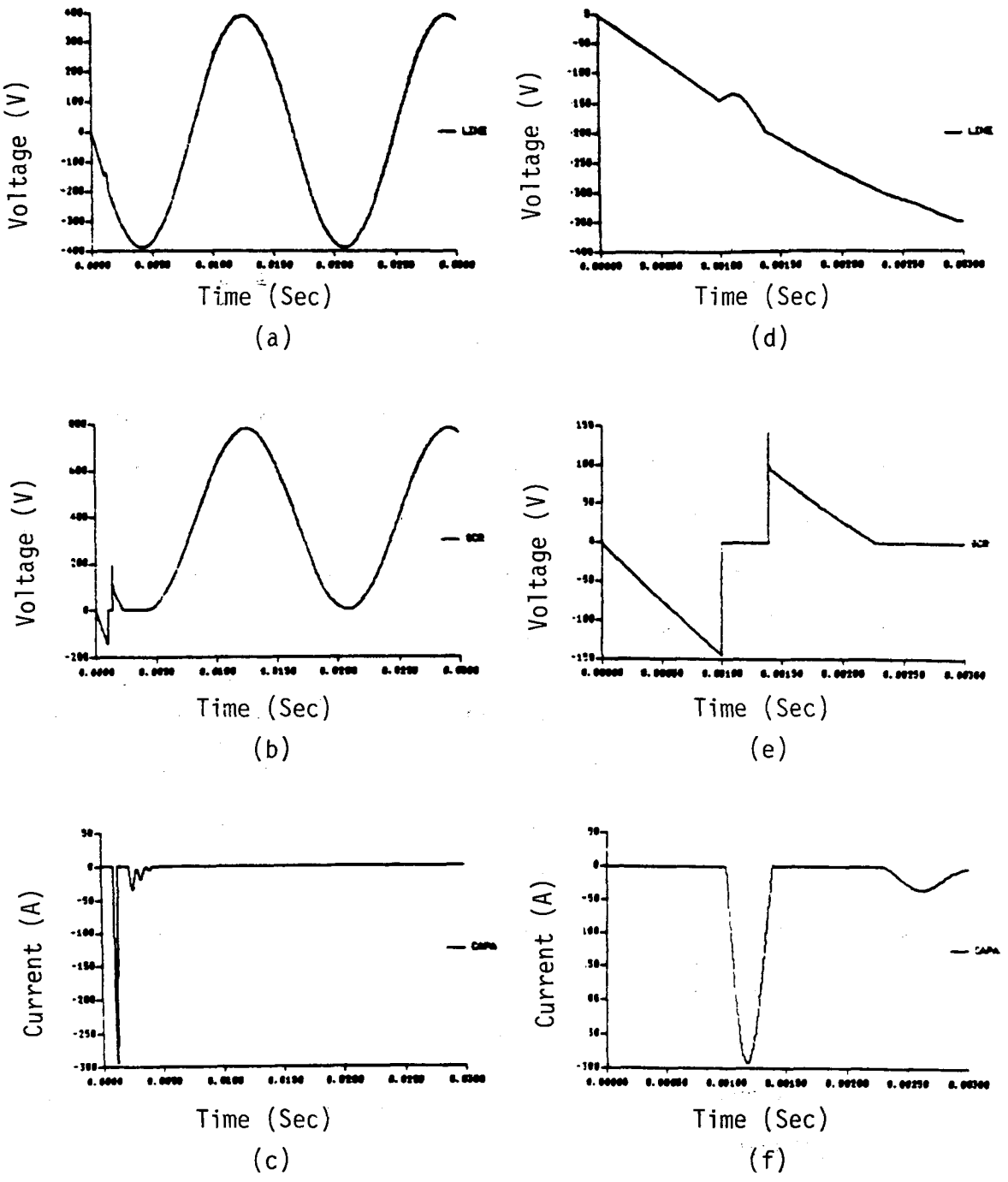

Figure 2.13: False Triggering of Reverse SCR with Time Delay = 20°

(a & d) Phase Voltage
(b & e) Voltage Across SCR
(c & f) Current Through Capacitor

2.3.3 Effect of False Triggering of Forward SCR

The reverse SCR keeps the capacitor charged to the negative peak voltage until the forward SCR is triggered. Once the capacitor has been charged by the reverse SCR, the voltage across the SCR pair will be a sinusoidal waveform with positive bias equal to the peak value of the phase voltage as shown in Figure 2.12 (b). The waveform shows that there is only one instant in each cycle that the voltage across the SCR becomes zero. Therefore, the triggering signal of the forward SCR has to be applied at this instant to prevent voltage or current transients.

Figure 2.14 shows the response of the Switching Circuit due to false triggering of the forward SCR. It is assumed in this case that the reverse SCR is turned on at the proper time and the capacitor is charged to the negative peak voltage. In this study, the triggering signal is delayed by about 80^{o}. The three plots of Figure 2.14 (a to c) show the phase voltage, voltage across the SCR and the current through the capacitor respectively. The same responses are also shown in Figures 2.14 (d to f) with the false triggering portion expanded. The dv/dt measured from Figure 2.14 (e) is approximately equal to 300 V/μs. This false triggering generates large current spikes, as shown in Figure 2.14 (c) and 2.14 (f).

The worst case for false triggering of the forward SCR occurs when the triggering signal is delayed by 180^{o}. In this case the forward SCR is switched when the voltage across its terminals is double the peak value. This is shown in Figures 2.15 (a to d). The dv/dt in this case is about 800 V/μs.

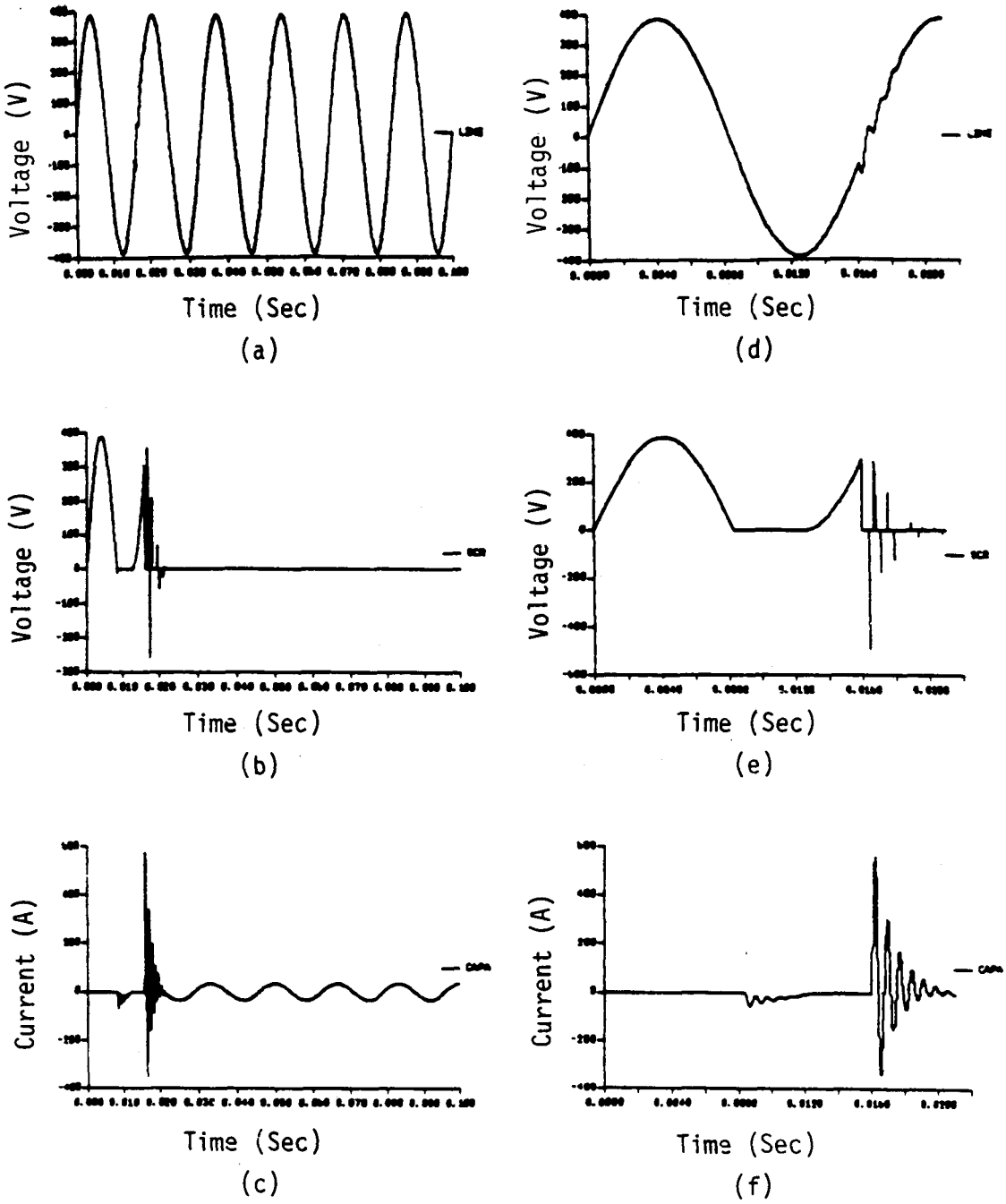

Figure 2.14: False Triggering of Forward SCR with Time Delay = 80°

(a & d) Phase Voltage
(b & e) Voltage Across SCR
(c & f) Current Flowing Through Capacitor

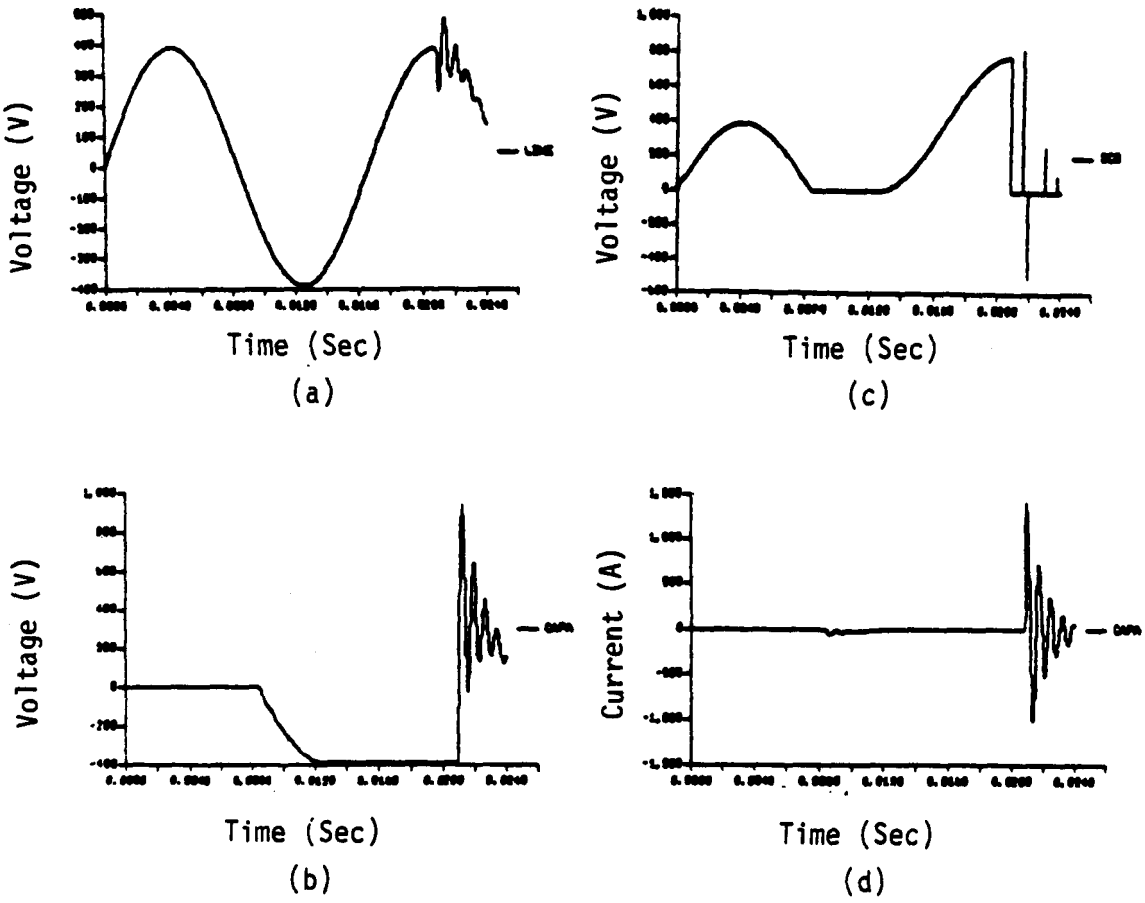

Figure 2.15: False Triggering of Forward SCR with Time Delay = 180°

(a) Line Voltage
(b) Voltage Across Capacitor
(c) Voltage Across SCR
(d) Current Through the Capacitor

CHAPTER 3

INSTALLATION AND FIELD TESTING OF 50-kVAR, OL-APFC AT SOUTHERN CALIFORNIA EDISON'S DEVERS SITE

3.1 Introduction

The 50-kVAR, OL-APFC was installed at Southern California Edison's Devers Test Site on March 22, 1985. The Installation and test results are given in detail in this section. A summary of these results are reported in reference [16].

Figure 3.1 shows the test system which includes both the induction generator and the 50-kVAR, OL-APFC. The generator is mounted vertically inside the tower. It is a standard 75 hp, NEMA class B, squirrel-cage induction motor used as a generator, with a power factor profile ranging from almost 0.30 lagging at 1/4 full load to about 0.70 lagging at full load.

Figure 3.2 shows a close-up view of the OL-APFC. This photograph also shows fast fuses to protect the SCRs, and transducers for sensing 18 variables of the system. These signals from the transducers are then fed to an IBM - PC/XT microcomputer, which acquires and processes the data. The computer is located in a trailer at about 300' from the wind turbine.

The 480-V three-phase supply to the generator is provided by a 12.47-kV/480-V distribution transformer near the trailer. The 12.47-kV primary distribution supply, in turn, is provided by a 115-kV/12.47-kV power transformer located in the substation near the site.

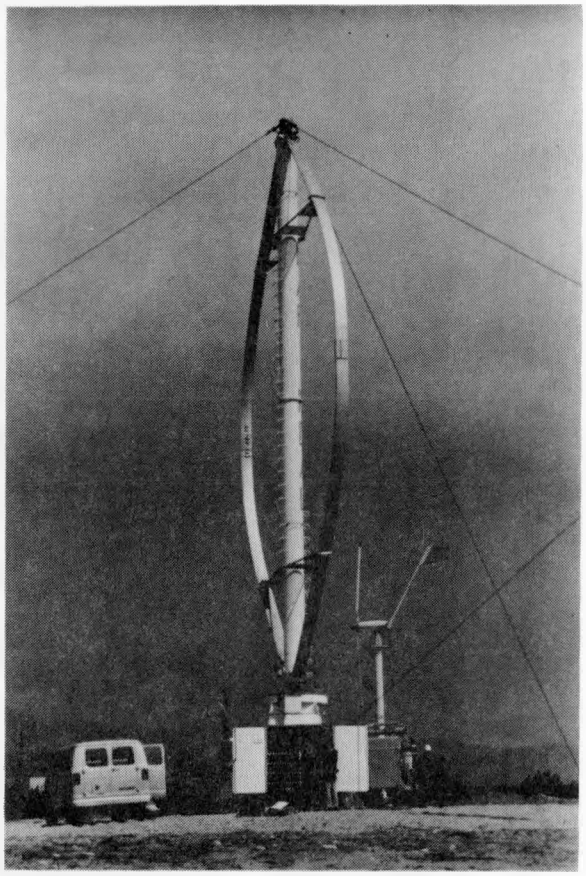

Figure 3.1: Complete Test System Showing Wind Turbine and APFC (Inside Cabinet)

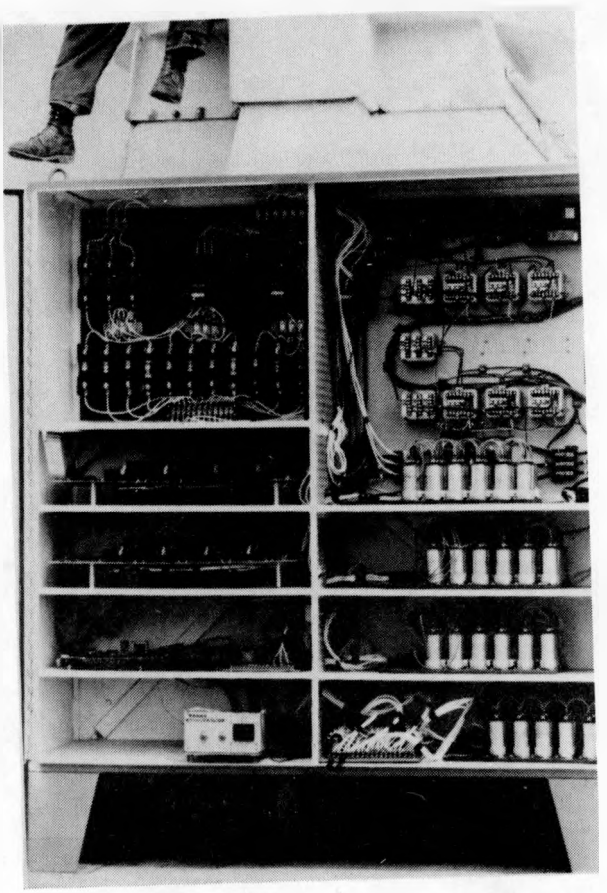

Figure 3.2: Closeup View of 50-kVAR. OL-APFC

Figure 3.3 shows the set-up of the test system which consists of the 50-kW induction generator, the OL-APFC and the 18 transducers. Current and reactive power transducers are connected on both sides of the OL-APFC - the generator side and the distribution system side. Voltage transducers are connected at the OL-APFC node. Real power transducers are connected on the generator side.

3.2 Steady-State Performance Test

Figures 3.4 to 3.6 show the steady-state performance results of the induction generator with the OL-APFC for 260 hours of operation. For brevity, only plots for phase "C" are presented in this report. The other two phases have similar plots. Each data point in these plots represent a 30-minute integrated average.

Figure 3.4 shows the real power generated by the induction machine. The magnitude of this real power depends on the wind speed. Figure 3.5 shows the reactive power measured on both sides of the OL-APFC; the reactive power drawn from the distribution system (Q_l), and the reactive power consumed by the induction generator (Q_g). The reactive power compensated by the OL-APFC is the difference between Q_g and Q_l. As can be seen from this plot, the OL-APFC compensates almost all the reactive power requirements of the induction generator. The variation in Q_l profile is due to the discrete switching of capacitors, and the 30-minute averaging of the signals. Figure 3.6 shows the current measured on both sides of the OL-APFC; the distribution line side, and the generator side. As expected, the magnitude of the distribution line current dropped to the magnitude of its real component. This reduction implies reduced losses in the distribution

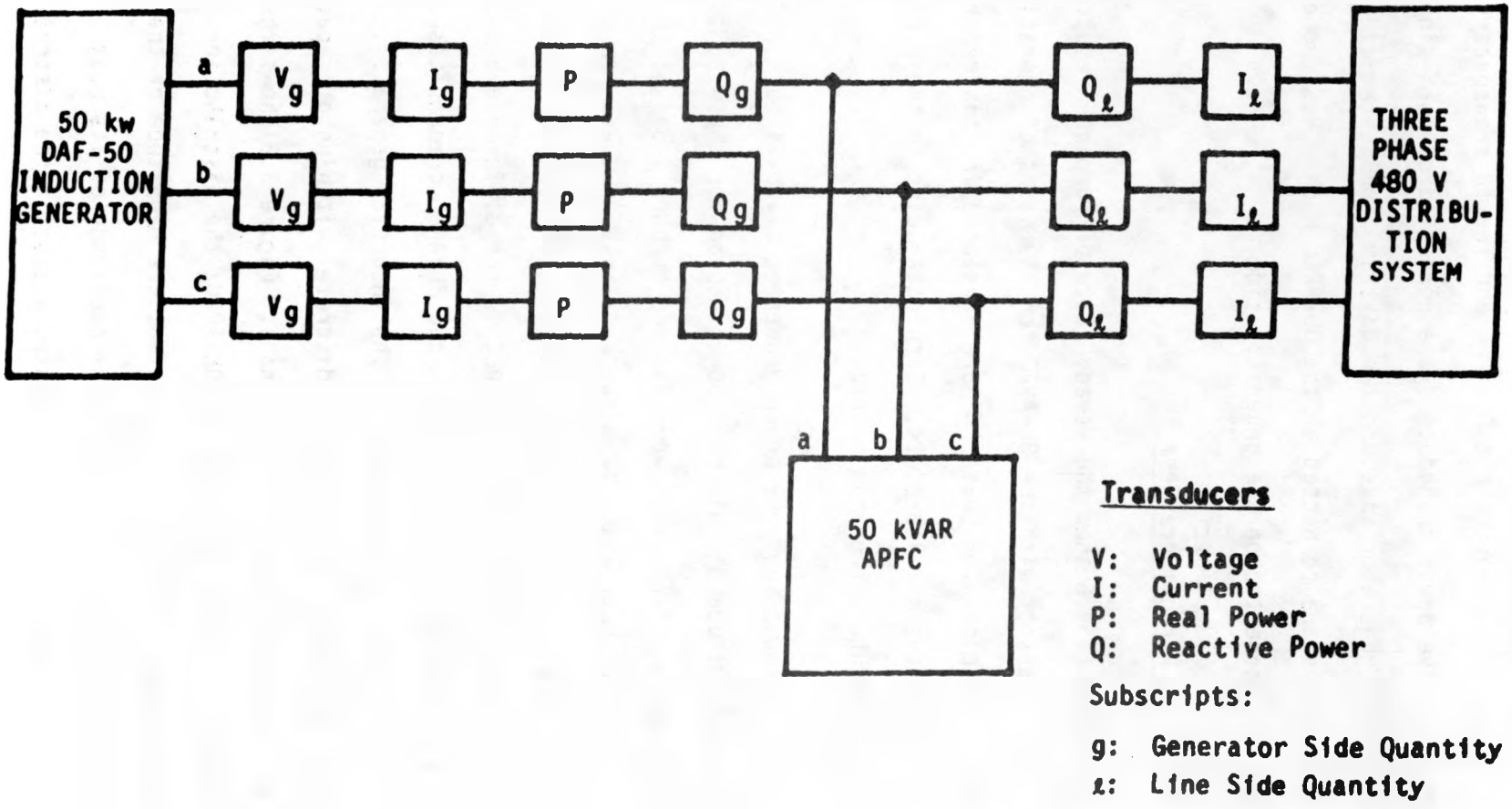

Figure 3.3: Complete Setup of Test System
Showing Location of Transducers

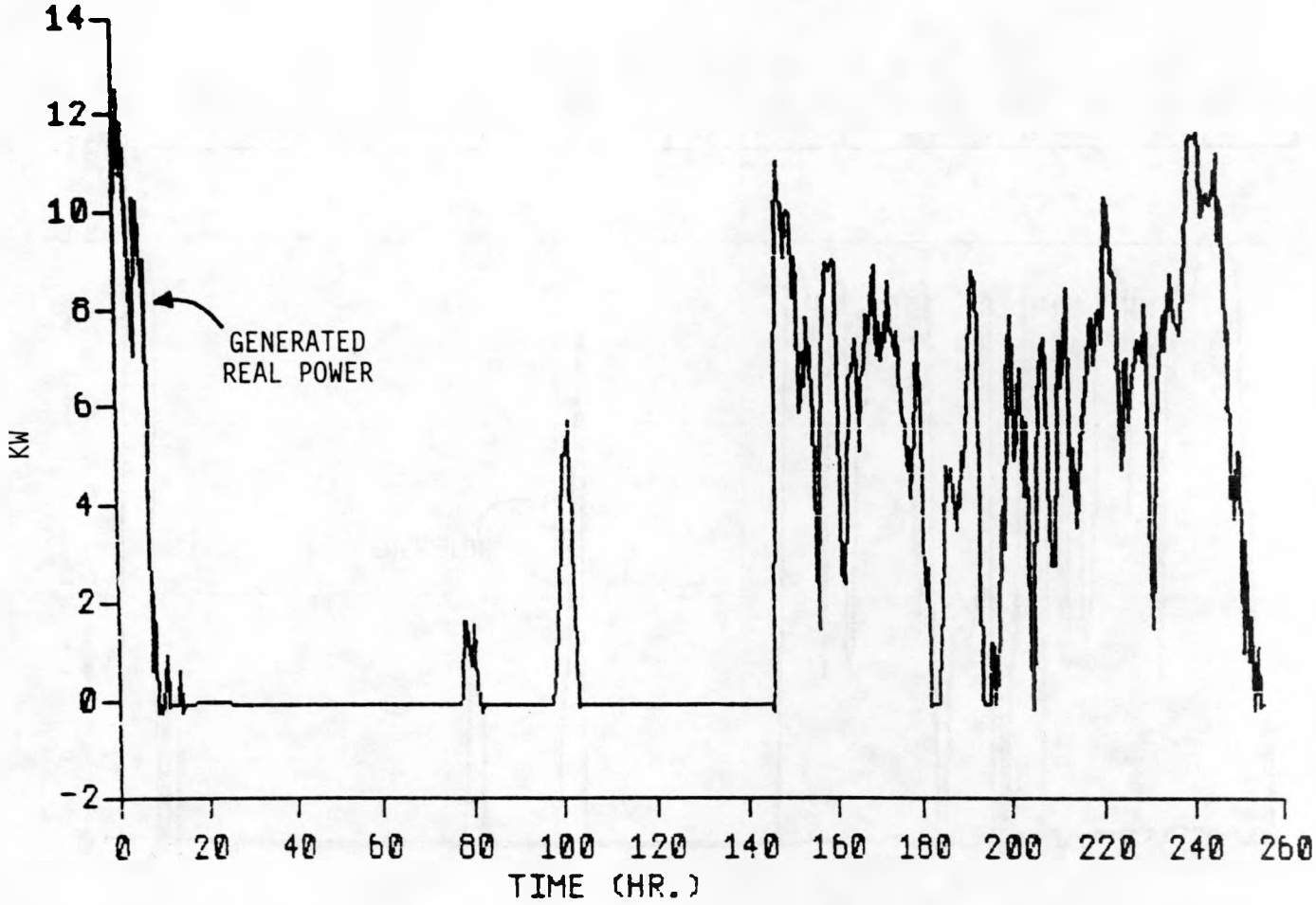

Figure 3.4: Steady-State Real Power Profile of Phase C (50-kVAR, OL-APFC)

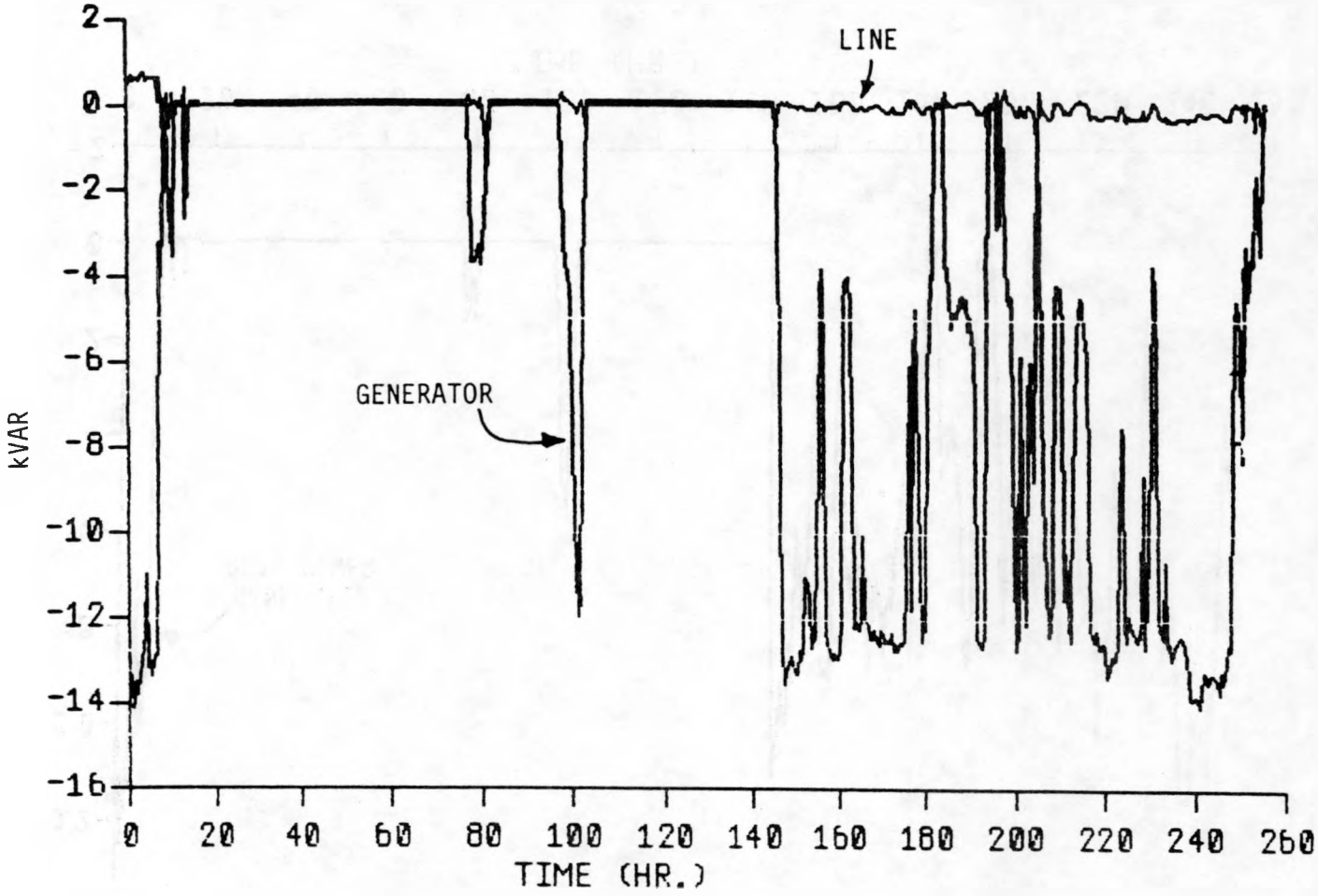

Figure 3.5: Steady-State Reactive Power Profile of Phase C (50-kVAR, OL-APFC)

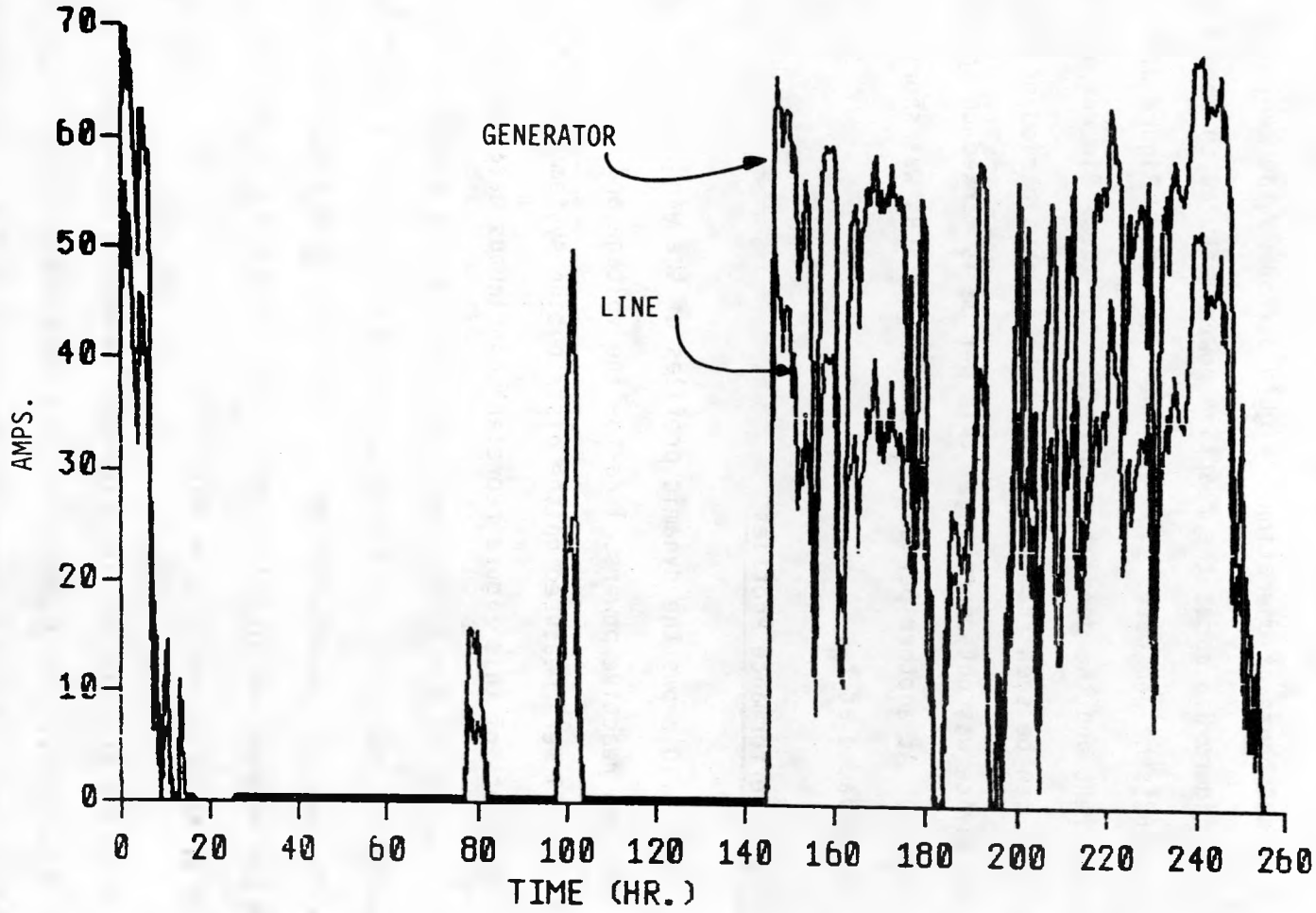

Figure 3.6: Steady-State Current Profile of Phase C (50-kVAR OL-APFC)

feeder or increase in the system capacity, and better voltage regulation of the system.

Figure 3.7 to 3.9 shows the cumulative data obtained from Devers for about 1,400 hours of operation. Figure 3.7 shows the real power generated. Figure 3.8 shows the reactive power measured on both sides of the OL-APFC; the generator side and the line side. Figure 3.9 shows the line current and the generator current. All these figures are for phase A. As can be seen from figure 3.8, there was a period of time where the device was not operating. This period is marked on the graph from t_1 to t_2. At another period, t_3, one of the SCRs was shorted, which was replaced at t_4.

3.3 Dynamic Performance Profiles

Figure 3.10 shows the dynamic profiles of the wind speed, three phase real and reactive powers, line-to-line voltage and current of phase "A". All were measured on the distribution system side of the OL-APFC. The plots of this figure represent continuous data acquisition (without averaging) for about 6 minutes. During this period the OL-APFC was turned off for about two minutes. The ability of the OL-APFC to reduce the reactive power and line current drawn from the distribution system can be observed in this figure. An improvement in voltage profile by about 3% can also be observed.

Figure 3.11 shows the instantaneous waveforms of the phase voltage and line currents. These waveforms were obtained with the aid of a digital scope. The figure shows the waveforms of the phase voltage and the capacitive current when the device is turned on at time t_{on}. The

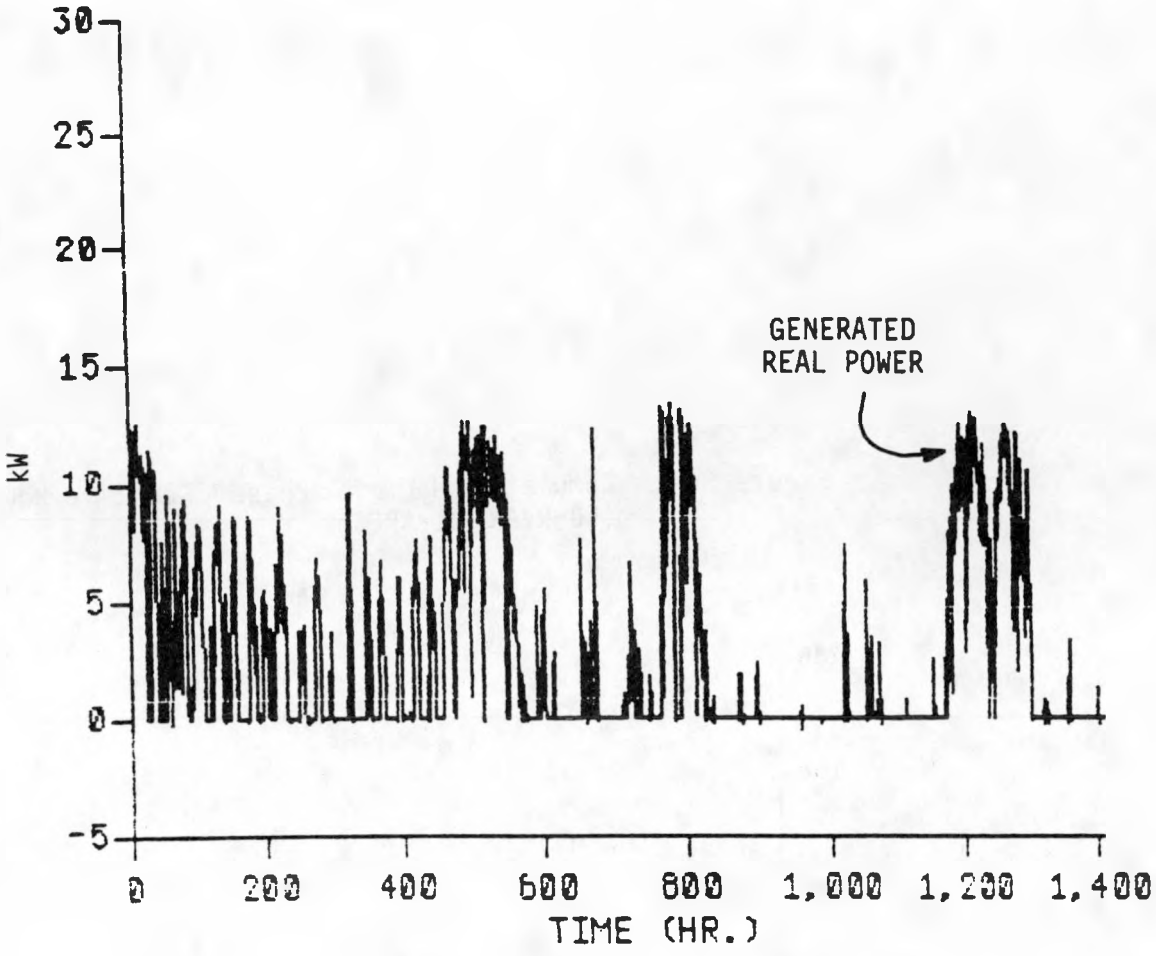

Figure 3.7: Cumulative Data of Phase A Real Power (50-kVAR, OL-APFC)

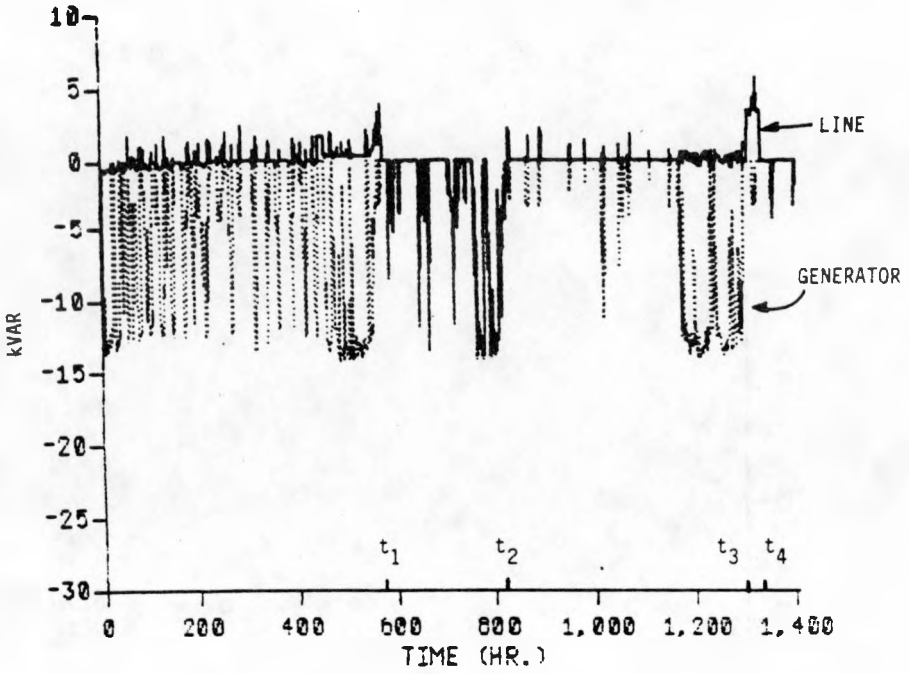

Figure 3.8: Cumulative Data for Phase A Reactive Power (50-kVAR, OL-APFC)

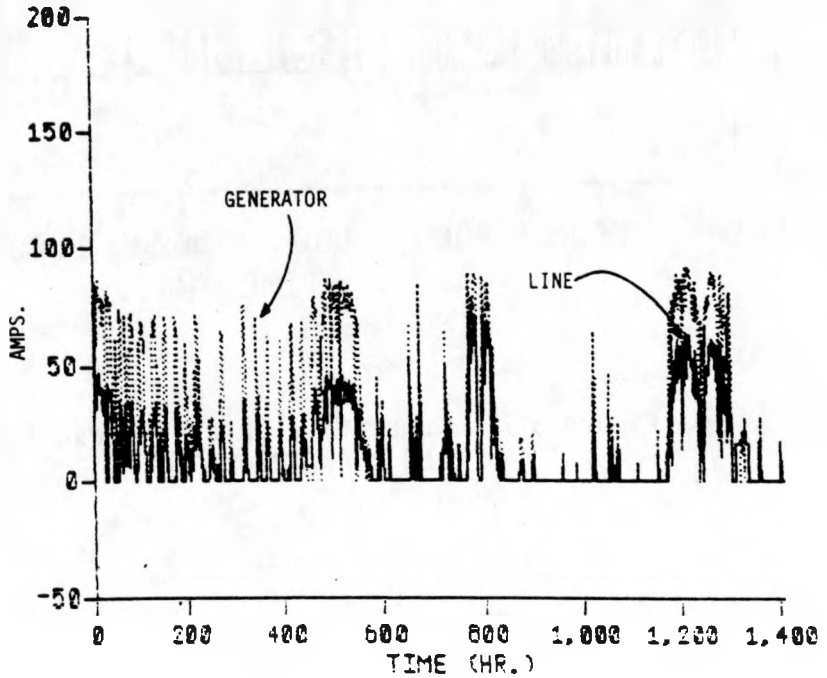

Figure 3.9: Cumulative Data for Phase A Current (50-kVAR, OL-APFC)

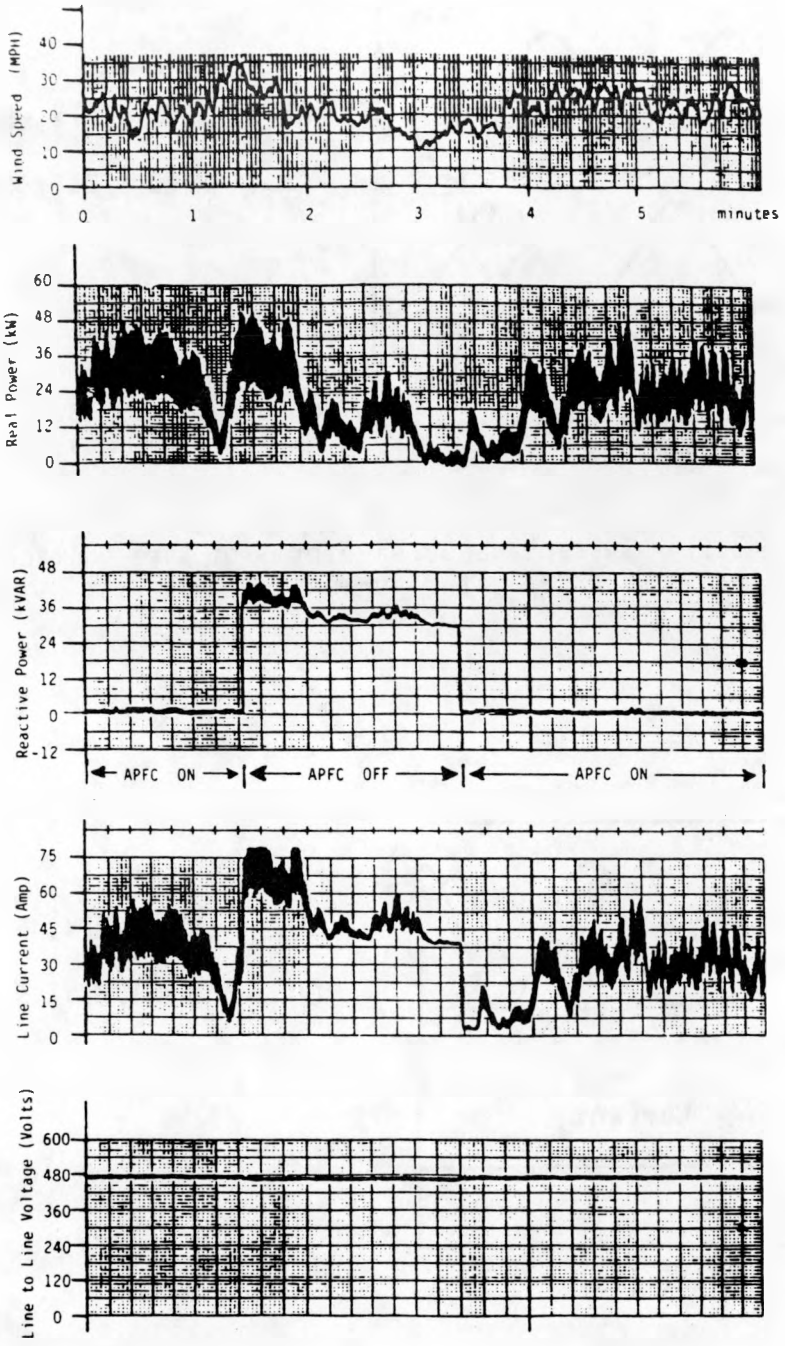

Figure 3.10: A Strip Chart Measurement Dynamic Profile

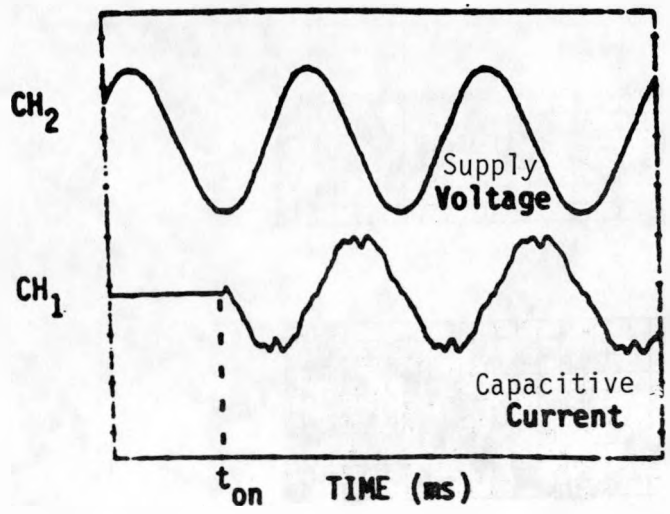

CH_1: 5.00 V/DIV, 5.00 ms/DIV

CH_2: 2.00 V/DIV, 5.00 ms/DIV

Figure 3.11: Instantaneous Waveforms of Line Voltage and Capacitor Current

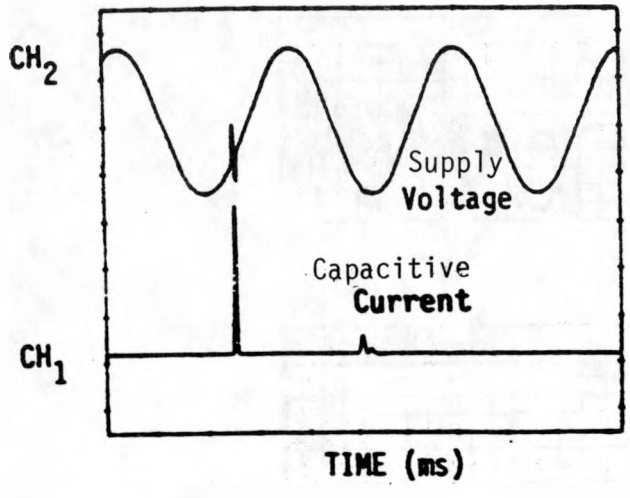

CH_1: 100m V/DIV, 5.00 ms/DIV

CH_2: 10.0 V/DIV, 5.00 ms/DIV

Figure 3.12: False Triggering of Reverse SCR

harmonics in line current are due to the presence of harmonics in the supply voltage as explained in Chapter 1. The figure shows no transients due to the switching of the capacitors. This is due to the fact that the SCRs are switched on at zero voltage across them.

To stress the importance of the timing of the SCR switching, two field tests were conducted: 1) wrong switching time (false triggering) for the reverse SCR and 2) false triggering for the forward SCR. The results of these two cases are shown in Figures 3.12 and 3.13. In Figure 3.12, the reverse SCR is switched on at positive voltage across it, and in Figure 3.13 the forward SCR is switched on at positive voltage across it. These types of false triggering create transients in both the voltage and current, and eventually will lead to permanent damage of the SCRs. Similar results were reported earlier in Section 2.3, (please refer to Figures 2.11 to 2.15) where the effects of false triggering were studied using computer simulation.

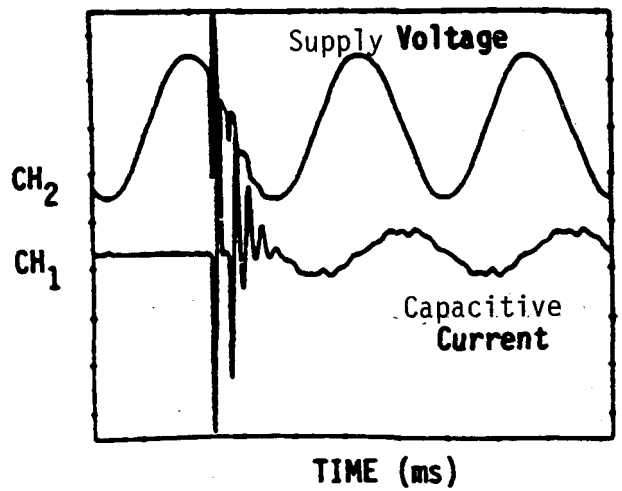

CH_1: 100m V/DIV, 5.00 ms/DIV

CH_2: 10.0 V/DIV, 5.00 ms/DIV

Figure 3.13: False Triggering of Forward SCR

CHAPTER 4

DEVELOPMENT AND DESIGN OF CLOSED-LOOP 300-kVAR APFC

4.1 Introduction

As explained in Chapters 1 and 2, the switched capacitors for reactive power compensation are determined by the load reactive current. To ensure that the correct number of capacitors are always switched in, the gain of the Reactive Current Sensing Circuit must be maintained constant. However, the parameters of most electronic components are likely to drift with temperature, which might cause the gain of the Sensing Circuit to drift, and result in erroneous compensation of reactive power.

Also, the malfunction of any SCR or fuse in the Switching Circuit is not sensed by the OL-APFC, and it is not accounted for in the Decision Logic Circuit. These malfunctions of the Switching Circuit result in a substantial over-compensation or under compensation of reactive power, as the case might be.

During field testing of the 50-kVAR, OL-APFC, the following two types of component failures occurred in the Switching Circuit due to a high-voltage transient in the power lines at Devers site:

1) A fast fuse opened due to an overcurrent problem created by a sudden overvoltage in the power lines, and resulted in a permanent open-circuit in the corresponding leg of the Switching Circuit. As a result, the capacitor of this leg failed to switch in when it was required to do so. This

type of failure leads to the under-compensation of reactive power.

2) By exceeding the di/dt rating due to the above mentioned disturbance, an SCR was permanently shorted, and resulted in a permanent connection of its capacitor to the power line. This type of failure results in over-compensation.

To improve the performance of the OL-APFC's operation, even when the parameters of the electronic components drift, or when the Switching Circuit's components fail, a closed-loop APFC (CL-APFC) with dual feedback loops was developed. The two loops are called:

1) Compensation Feedback Loop

2) Failure Feedback Loop

The compensation feedback loop is designed to sense the line reactive current, which is the vector sum of the load reactive current and the APFC current. The magnitude of the line reactive current is used to update the switching pattern of the capacitors by adding or subtracting capacitors from the previous pattern. This way, the line reactive current is continuously monitored, and corrected to almost zero. Hence, the effect of component parameter drift on the APFC compensation becomes negligible.

The failure feedback loop is designed to monitor the capacitor current and check its value against the input to the Triggering Circuit. These two values are matched at all times unless the Switching Circuit has a faulty component. If a component failure occurs, the failure feedback loop will adjust the reactive power to the next best value.

4.2 General Description of the Closed-Loop APFC

Figure 4.1 shows the block diagram of the CL-APFC which consists of nine main functional blocks:

1) Reactive Current Sensing and Encoding Circuit
2) Capacitor Current Sensing and Encoding Circuit
3) Summing Circuit
4) Failure Detection Circuit
5) Output Adjustment Circuit
6) Interlock Circuit
7) Fixed and Switched Triggering Circuits
8) Fixed and Adaptive Switching Circuits
9) Timing Circuit

In addition to these blocks, eight current transformers (CT_1 to CT_8) and four circuit breakers (CB_1 to CB_4) are employed.

The functions of the Switching Circuits, Triggering Circuits, Interlock Circuit and Timing Circuit are the same as those for the OL-APFC discussed in Chapter 2. The remaining functional blocks are briefly discussed below.

The details of the closed-loop APFC concept is shown in Figure 4.2. The Reactive Current Sensing and Encoding Circuit is used to measure the peak value of the line reactive current, and to encode this value into a binary code. The function of the Capacitor Current Sensing and Encoding Circuit is to sense the peak value of the capacitor current, and encode its peak value into a binary code. This binary code gives the magnitude of the capacitor current in units. The Summing

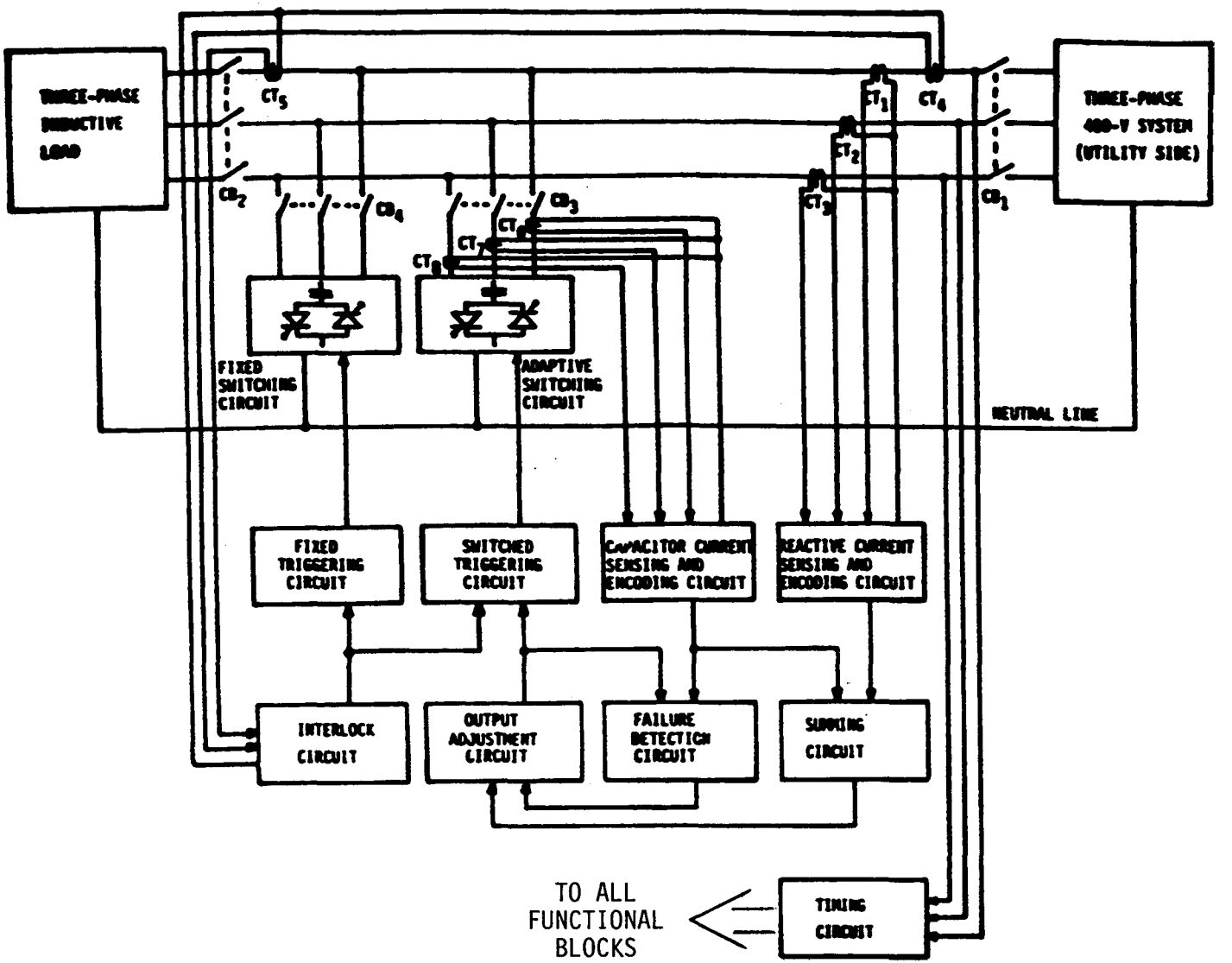

Figure 4.1: Functional Block Diagram of CL-APFC

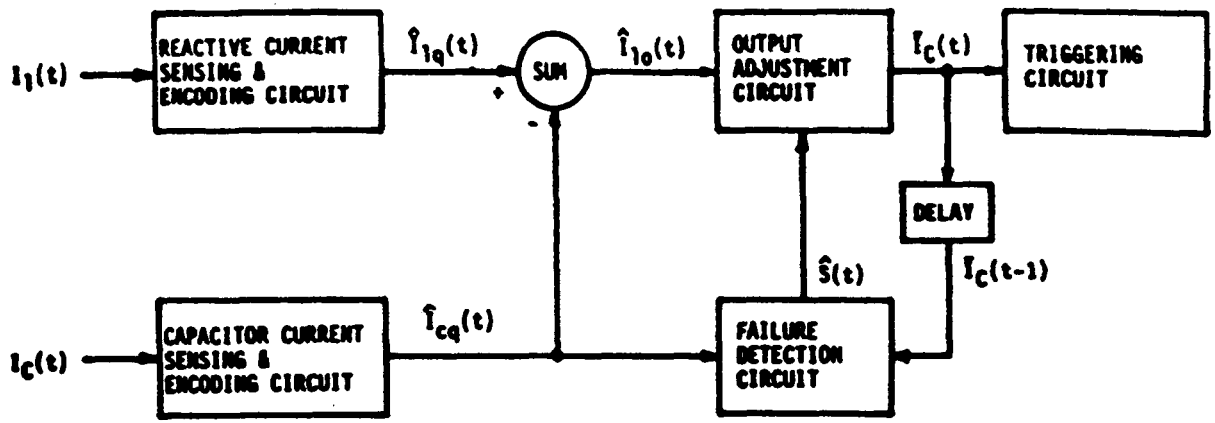

I: ANALOG SIGNAL
$\hat{I}$: DIGITAL CODE
$\bar{I}$: COMMAND CODE

Figure 4.2: Circuit for Closed-Loop Concept Description

Circuit is used to add the line reactive current code and the capacitor current code to generate another binary code. This binary code gives the magnitude of the load reactive current in units. The function of the Failure Detection Circuit is to detect failures of SCRs and fuses in the Switching Circuit. This is done by comparing the output of the Capacitor Current Sensing and Encoding Circuit and the Output Adjustment Circuit. An eight-bit status code is generated by this circuit which indicates the status of the Switching Circuit. There are two bits for each capacitor leg, which indicates either an open fuse or a shorted SCR. The purpose of the Output Adjustment Circuit is to adjust the output of the Summing Circuit to the next best value when a component in the Switching Circuit fails. A four-bit binary code is generated by this circuit. Each bit of this command will either switch on or switch off an SCR, i.e., one stage of capacitance.

4.3 Circuit Design of the Closed-loop APFC

Some of the circuits in the OL-APFC are utilized in the CL-APFC design. These circuits are:

1) Interlock Circuit,
2) Triggering Circuits,
3) Switching Circuits, and
4) Timing Circuit.

The design and operation of these circuits are discussed in Chapter 2. The details of the remaining circuits are given below:

4.3.1 Reactive Current Sensing and Encoding Circuit

The reactive Current Sensing and Encoding Circuit is designed to sense the peak value of the line reactive current of each phase, at the instant when the corresponding phase voltage is zero going negative. It also encodes this value into a five-bit line reactive current code ($\hat{I}_{lq1}$ to $\hat{I}_{lq5}$). This value is positive if the line current is lagging the phase voltage as shown in Figure 4.3 (a). In this case, the reactive power demand of the load is not fully compensated. The value of the line reactive current is negative if the line current is leading the phase voltage as shown in Figure 4.3 (b). In this case, the device is over compensating the reactive power demand. Table 4.1 shows the line reactive current code and its equivalent value in units.

Figure 4.4 shows the Reactive Current Sensing and Encoding Circuit. It consists of the Reactive Current Sensing Circuit and an A/D converter. The A/D converter (U_{59}) converts the line reactive current into a five-bit line reactive current code ($\hat{I}_{lq1}$ to $\hat{I}_{lq5}$). The AND gate (U_{60}) is used to generate a timing signal for the A/D converter.

4.3.2 Capacitor Current Sensing and Encoding Circuit

Figure 4.5 shows the basic components of the Capacitor Current Sensing and Encoding Circuit. It consists of the Reactive Current Sensing Circuit and an A/D converter. The A/D converter (U_{57}) is used to convert the capacitor current into a four-bit capacitor current code ($\hat{I}_{Cq1}$ to $\hat{I}_{Cq4}$).

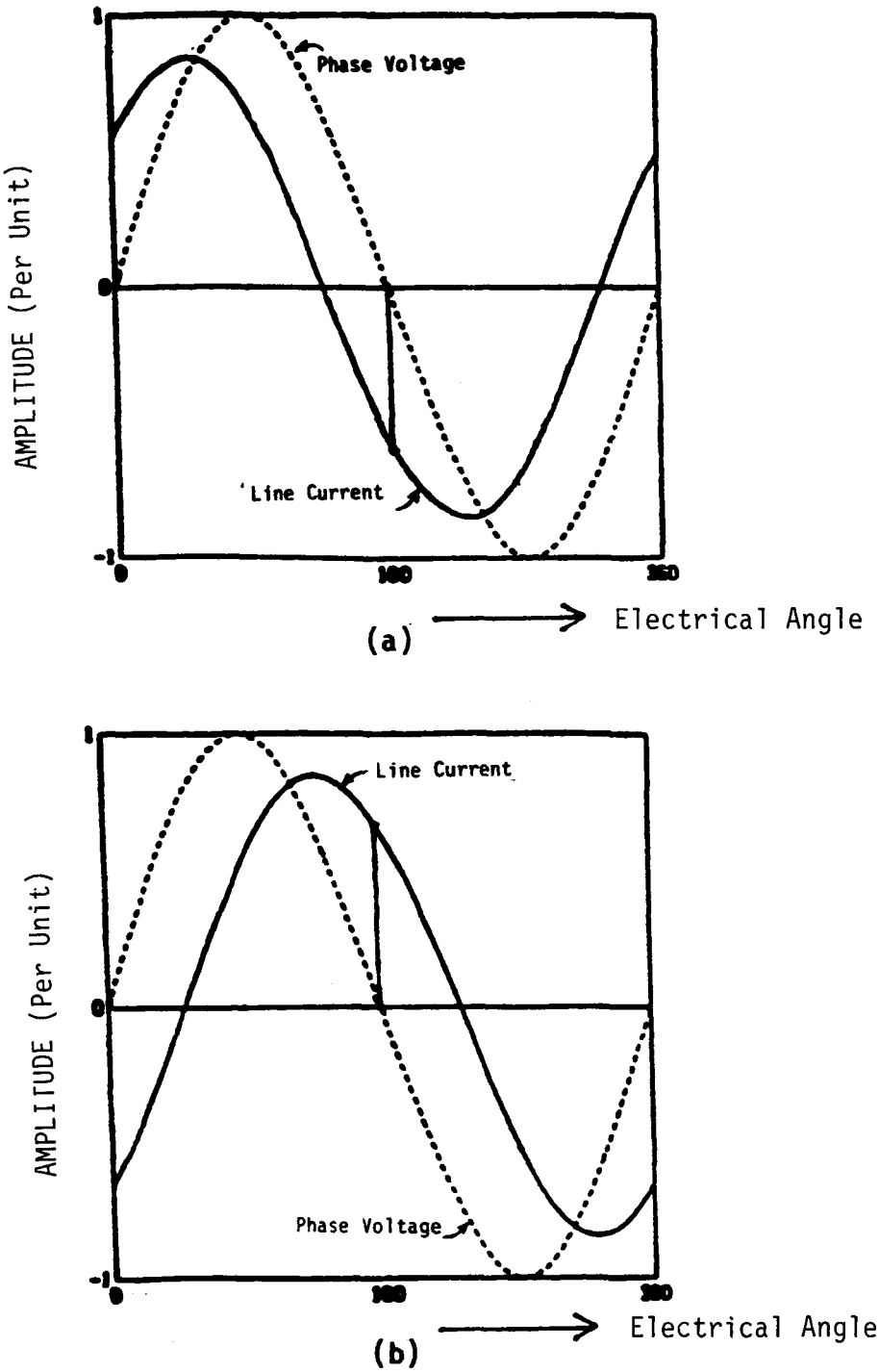

Figure 4.3: Line Current and Phase Voltage

(a) Line Current is Lagging with Respect to Phase Voltage

(b) Line Current is Leading with Respect to Phase Voltage

Table 4.1: Line Reactive Current Code

LINE REACTIVE CURRENT (UNITS)*	$\uparrow I_{1q}$				
	$\uparrow I_{1q5}$	$\uparrow I_{1q4}$	$\uparrow I_{1q3}$	$\uparrow I_{1q2}$	$\uparrow I_{1q1}$
+ 15	1	1	1	1	1
+ 14	1	1	1	1	0
+ 13	1	1	1	0	1
+ 12	1	1	1	0	0
+ 11	1	1	0	1	1
.	.	.	.	.	.
.	.	.	.	.	.
+ 2	1	0	0	1	0
+ 1	1	0	0	0	0
0	1	0	0	0	0
- 1	0	1	1	1	1
- 2	0	1	1	1	0
.	.	.	.	.	.
.	.	.	.	.	.
- 14	0	0	0	1	0
- 15	0	0	0	0	1

* POSITIVE SIGN MEANS LINE CURRENT IS LAGGING.
NEGATIVE SIGN MEANS LINE CURRENT IS LEADING.

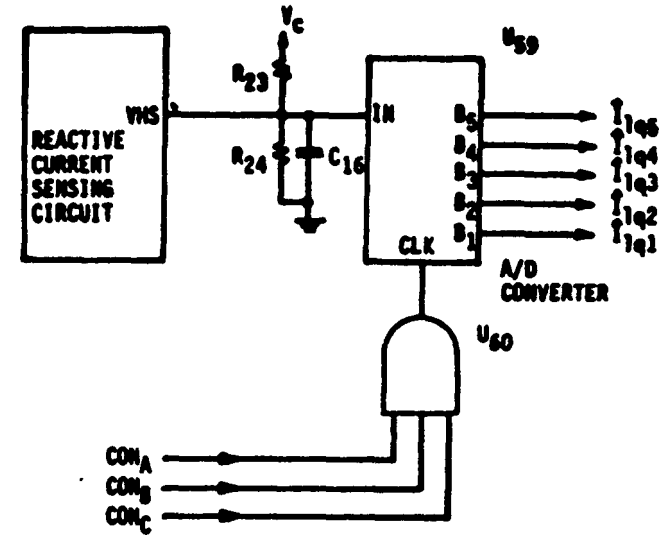

Figure 4.4: Reactive Current Sensing and Encoding Circuit

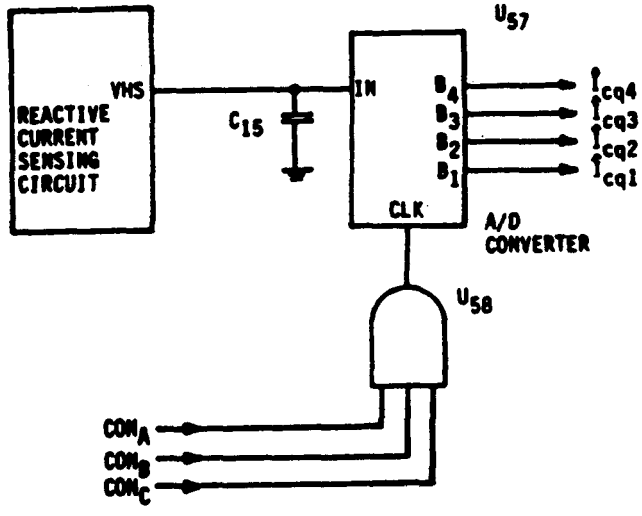

Figure 4.5: Capacitor Current Sensing and Encoding Circuit

4.3.3 Summing Circuit

The Summing Circuit is shown in Figure 4.6. It is an EPROM (Erasable Programmable Read Only Memory), and is used to add the line reactive current code and the capacitor current code to form the four-bit load reactive current code ($\hat{I}_{lo1}$ to $\hat{I}_{lo4}$). This load reactive current code gives the magnitude of the load reactive current in binary units.

4.3.4 Failure Detection Circuit

The Failure Detection Circuit is shown in Figure 4.7. It consists of a four-bit multiplexer and a four-bit comparator. The four-bit multiplexer uses three four-bit buffers (U_{65}, U_{66} and U_{67}). The multiplexer is used to multiplex the three phase capacitor current command into one four-bit command. This multiplexed command is then compared with the capacitor current code ($\hat{I}_{Cq1}$ to $\hat{I}_{Cq4}$) by the four-bit comparator (U_{68}) for one phase at a time. An eight-bit status code (SH_1 to SH_4, and OP_1 to OP_4) is then generated by U_{68} to indicate the status of each leg of the Switching Circuit. SH_i shows whether the SCR of BIT i in the Switching Circuit is shorted or operating normally. OP_i shows whether the fuse of BIT i is open or operating normally.

The operation of the comparator U_{68} is based on the fact that the values of the capacitor current code and the capacitor current command are equal to each other in normal operation (i.e., no component failure). Table 4.2 shows four cases for the inputs and outputs of the comparator for only one bit. In case 1 and case 4, $\hat{I}_{cqi}$ is equal to $\bar{I}_{ci}$, indicating that BIT i of the Switching Circuit is operating normally. In

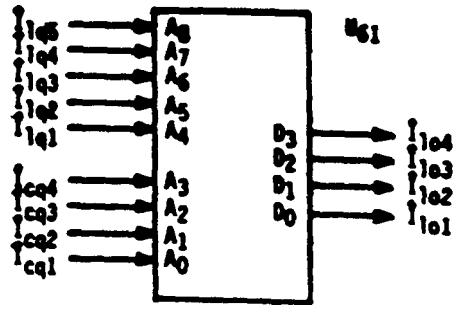

Figure 4.6: Summing Circuit

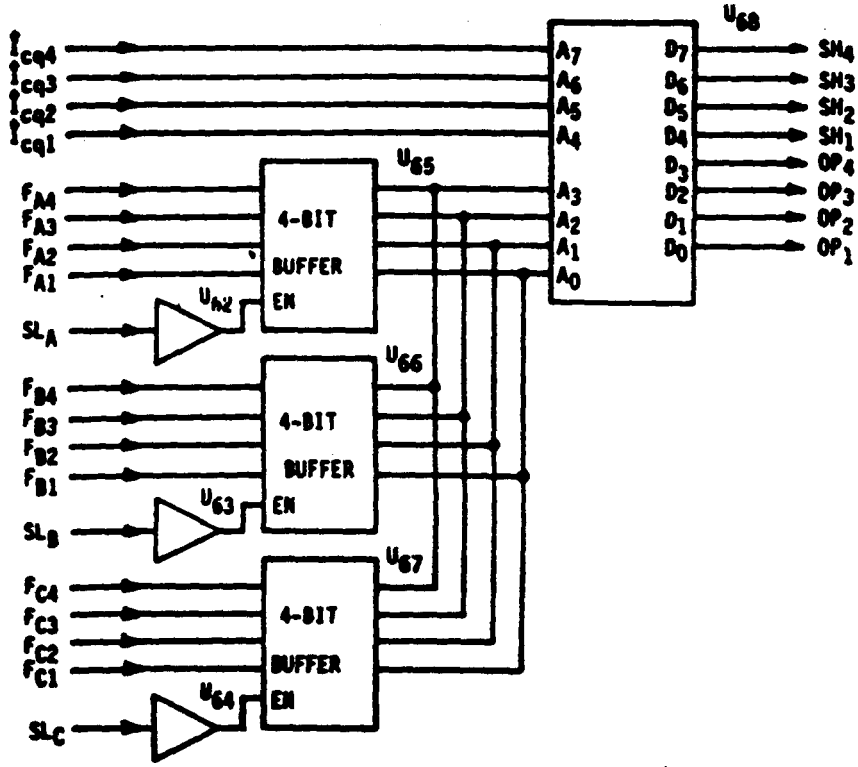

Figure 4.7: Failure Detection Circuit

Table 4.2: Failure Detection

CASE	$\hat{I}_{Ci}$	$\hat{I}_{cqi}$	SH_i	OP_i	STATUS
1	0	0	0	0	BIT i IS NORMAL
2	0	1	1	0	BIT i SCR IS SHORTED
3	1	0	0	1	BIT i FUSE IS OPEN
4	1	1	0	0	BIT i IS NORMAL

i = 1, 2, 3, 4

Table 4.3: Examples of Failure Detection

EXAMPLES	$\hat{I}_{cq4}$	$\hat{I}_{cq3}$	$\hat{I}_{cq2}$	$\hat{I}_{cq1}$	$\bar{I}_{C4}$	$\bar{I}_{C3}$	$\bar{I}_{C2}$	$\bar{I}_{C1}$	SH_4	SH_3	SH_2	SH_1	OP_4	OP_3	OP_2	OP_1	COMMENTS
1	0	1	0	1	0	1	0	1	0	0	0	0	0	0	0	0	ALL 4 BITS ARE NORMAL
2	0	1	0	1	0	1	0	0	0	0	0	1	0	0	0	0	BIT 1 SCR IS SHORTED
3	0	1	0	1	0	1	1	0	0	0	0	1	0	0	1	0	BIT 1 SCR IS SHORTED BIT 2 FUSE IS OPEN

case 2, $\hat{I}_{cqi}$ is "1" and $\bar{I}_{ci}$ is "0", indicating that the SCR of BIT i of the Switching Circuit is shorted. In case 3, $\hat{I}_{cqi}$ is "0" and $\bar{I}_{ci}$ is "1", indicating that the fuse of BIT i of the Switching Circuit is open. Three examples of the programming of all four bits of U_{68} are given in Table 4.3. In example 1, the Switching Circuit has no failure. In example 2, the SCR of BIT 1 is shorted. In example 3, the SCR of BIT 1 is shorted and the fuse of BIT 2 is open.

4.3.5 Output Adjustment Circuit

The load reactive current code and the status code are fed to the Output Adjustment Circuit, which in turn generates the capacitor current command ($\bar{I}_{c1}$ to $\bar{I}_{c4}$). The capacitor current command will be equal to the load reactive current code if the Switching Circuit is operating normally. However, if the Switching Circuit has component failures, the capacitor current command will be adjusted to the next best value.

For example, in normal operation, when the capacitor current command is 12 units, the capacitors of BIT 3 (4 units) and BIT 4 (8 units) should be switched in. Assume that the fuse of BIT 3 is open. The OL-APFC will provide 8 units of compensation. The deficit in this case is 4 units. On the other hand, the CL-APFC, due to the Adjustment Circuit, will provide 11 units of compensation by switching in the capacitors of BIT 1 (1 unit), BIT 2 (2 units) and BIT 4 (8 units). The deficit in this case is only one unit.

Other examples are shown in Figure 4.8. The figure shows the reactive current demand (in units) of the load and the reactive current of the OL-APFC and the CL-APFC (in units) for two cases - Case 1: When

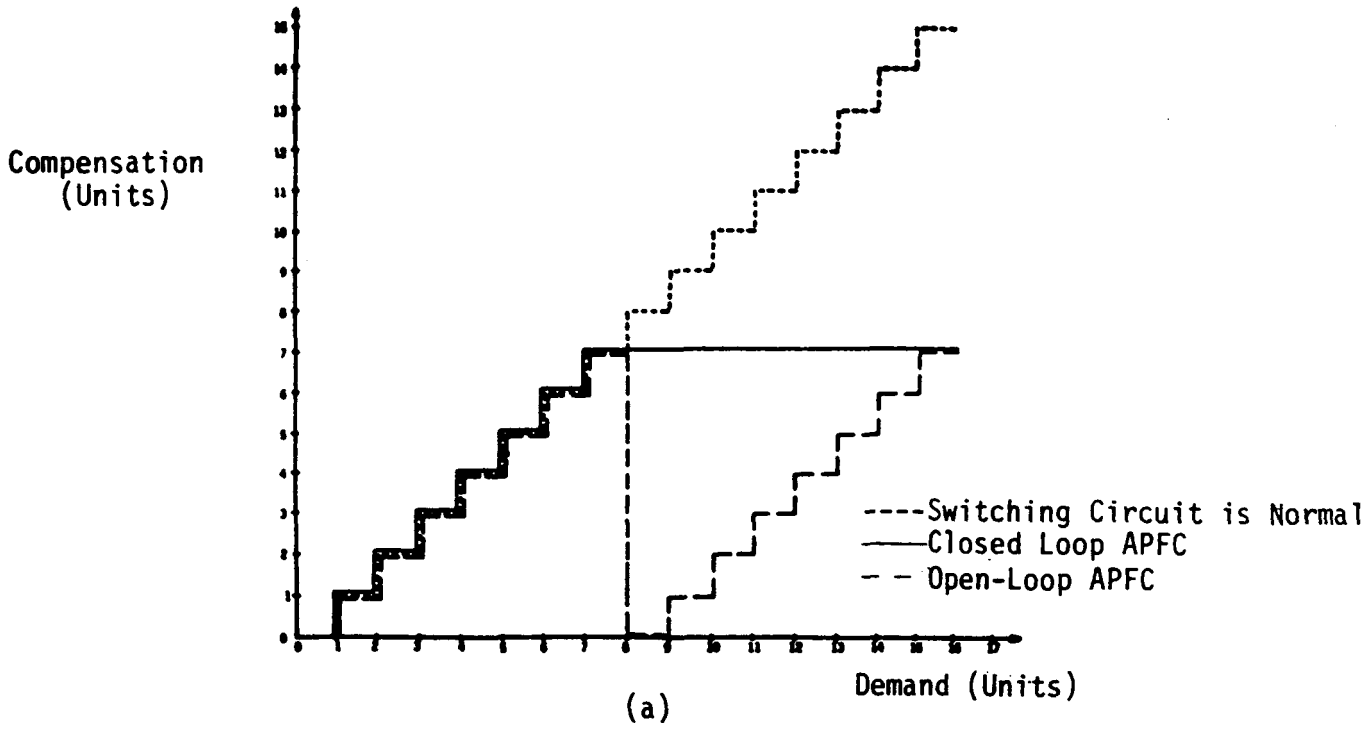

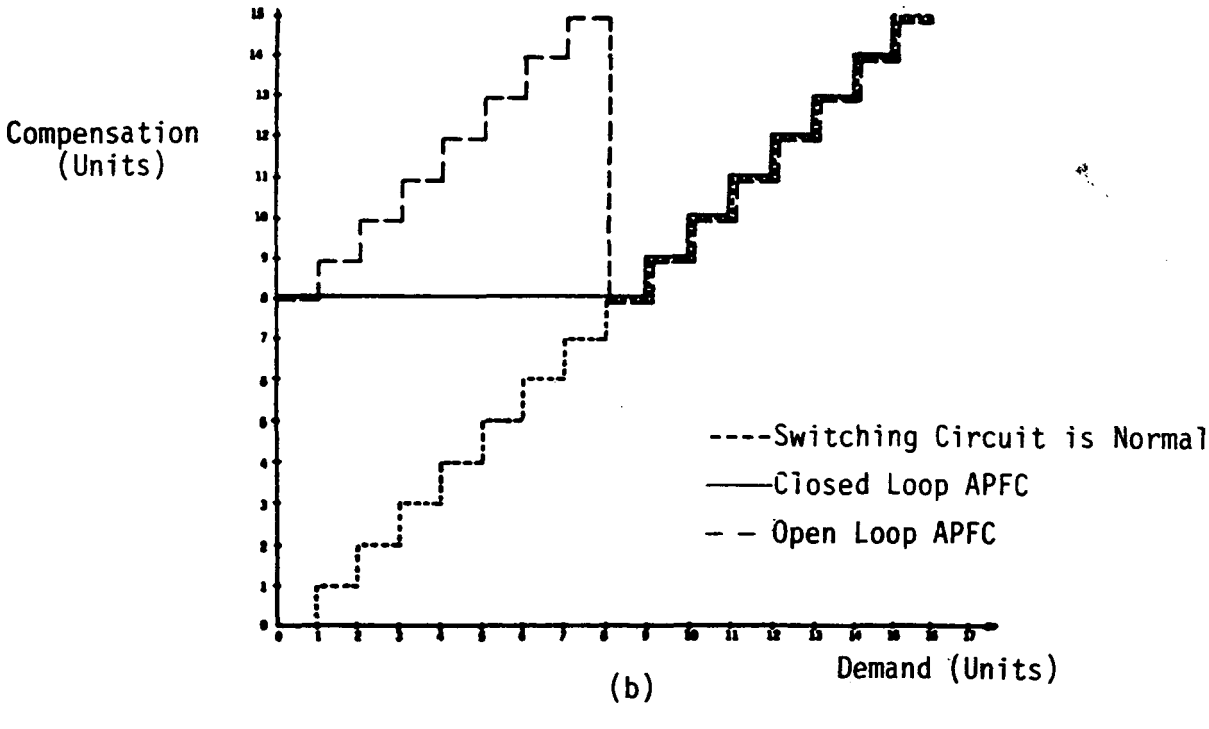

Figure 4.8: Relation of Reactive Current Demand and Compensation of the APFCs

(a) Fuse of Bit 4 is Open
(b) SCR of Bit 4 is Shorted

the fuse of BIT 4 is opened, and Case 2: When the SCR of BIT 4 is shorted.

Figure 4.8 (a) shows the case when the fuse of BIT 4 is open. Both, the CL-APFC and the OL-APFC provide correct reactive current compensation when the demand is 7 units or less. As seen in the figure, the CL-APFC provides 7 units of reactive current for any demand over 7 units. The OL-APFC provides no compensation for 8 units of demand, and 1 unit of reactive current for 9 units of demand and so on. The deficit for a demand greater than 9 units is always 8 units for the OL-APFC.

Figure 4.8 (b) shows the case when the SCR of BIT 4 is shorted. Both, the CL-APFC and the OL-APFC provide correct reactive current compensation when the demand is 8 units or more. As seen in the figure, the CL-APFC provides 8 units of reactive current for any demand less than 8 units. The OL-APFC provides 8 units of over compensation for any demand under 8 units, i.e., 15 units of reactive current for the demand of 7 units and so on.

CHAPTER 5

INSTALLATION AND TESTING OF 300-KVAR CLOSED-LOOP APFC AT OAK CREEK ENERGY SYSTEMS WIND PARK TEHACHAPI, CALIFORNIA

5.1 Introduction

The three-phase, 300-KVAR, 480-V closed-loop APFC discussed in Chapter 4 was built in the Energy Laboratory at the University of Washington's Department of Electrical Engineering. The device was intended to adaptively compensate the reactive power demand of a group of seven induction-generator wind-turbines at the Oak Creek energy systems wind park near Tehachapi, California. Each wind turbine is rated at 65-kW. Since a fixed capacitor bank of 90 kVAR had already been installed for these induction generators, only four stages of switched capacitors per phase were needed to provide 7, 14, 28 and 56 kVARs respectively.

The APFC was designed to operate in either closed-loop mode or open-loop mode. In the closed-loop mode, two sets of current transformers are used to sense the line current and the capacitor current respectively.

Two types of tests were conducted for the 300-kVAR APFC: laboratory testing and field testing. The APFC was tested in the Energy Laboratory before it was transported to the field testing site. The laboratory testing was conducted for a reduced loading condition since the current supply capability in the laboratory is less than the full

load requirements of the APFC. After successful laboratory testing, the APFC was transported to Oak Creek Wind Farm at Tehachapi, California on May 19, 1986. Full load testing was then conducted.

5.2 Site Test of the 300 kVAR APFC

The test site at Tehachapi is shown in Figure 5.1. Some of the horizontal axis wind machines are shown in the background. It also shows the trailer in which the device is housed, and a distribution transformer adjacent to the trailer. The seven induction generators are connected to this transformer at 480-V. The primary side of the transformer is connected to the utility feeder at 12.47-kV.

The photographs shown in Figure 5.2 to 5.5 were taken inside the trailer. Figure 5.2 shows the NEMA enclosure which contains the electronic circuit. Figure 5.3 shows the SCR modules of phases A and B. Figure 5.4 shows the capacitor modules and the snubbing inductor of phase A. Figure 5.5 shows the transducers and the IBM-PC/XT microcomputer-based data acquisition system for monitoring 18 electrical variables of the 7-generator cluster.

At the site, the waveform of the phase voltage was found to be contaminated with harmonics, as shown in Figure 5.6, especially when the induction generators were operating at low wind speeds. These voltage harmonics produce harmonics in the capacitor current and consequently in the line current. Under these circumstances, the accuracy of sensing the capacitor current at the zero crossing of the phase voltage is found to be very poor. The APFC was then set to the open-loop mode, where it is less sensitive to the voltage harmonics.

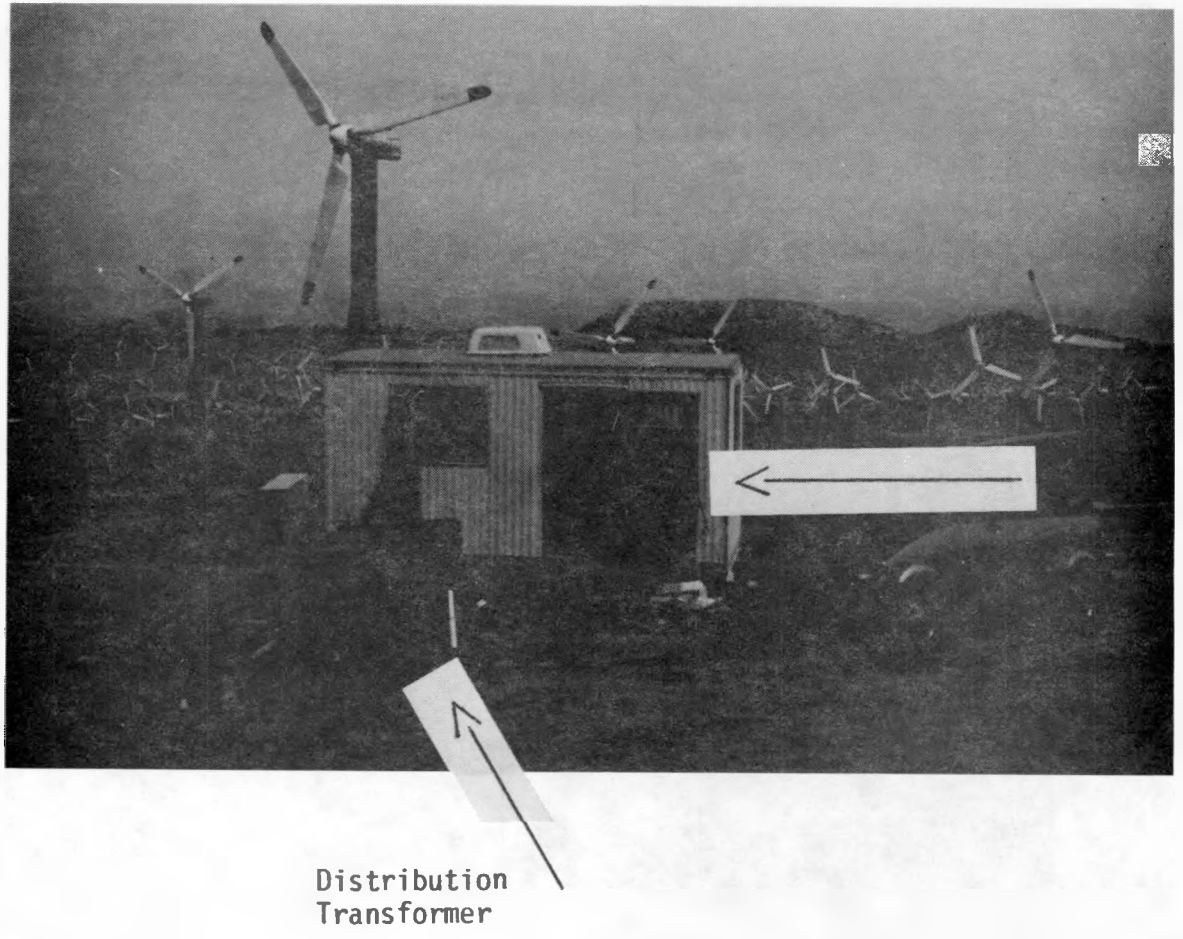

Figure 5.1: Photograph of 300-kVAR APFC at Tehachapi Site
(APFC inside trailer)

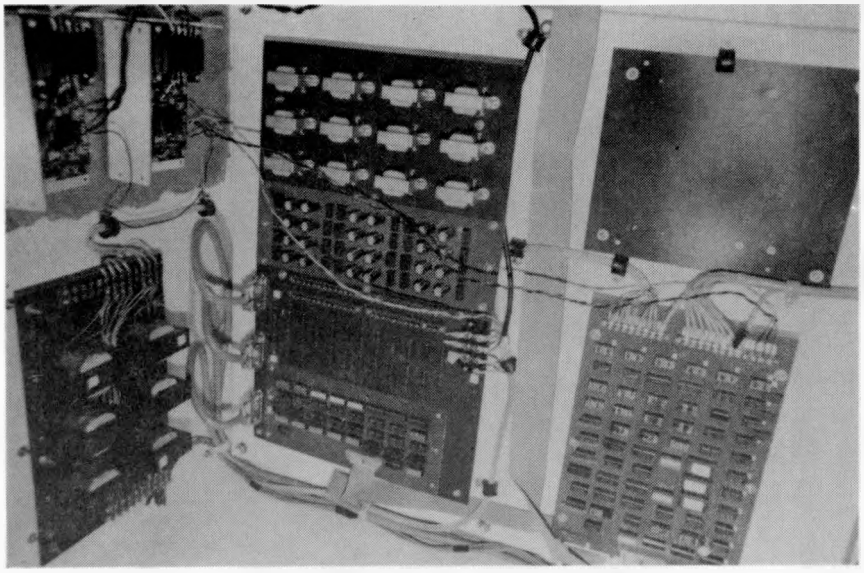

Figure 5.2: Photograph of Electronic Circuit Module of the 300-kVAR APFC

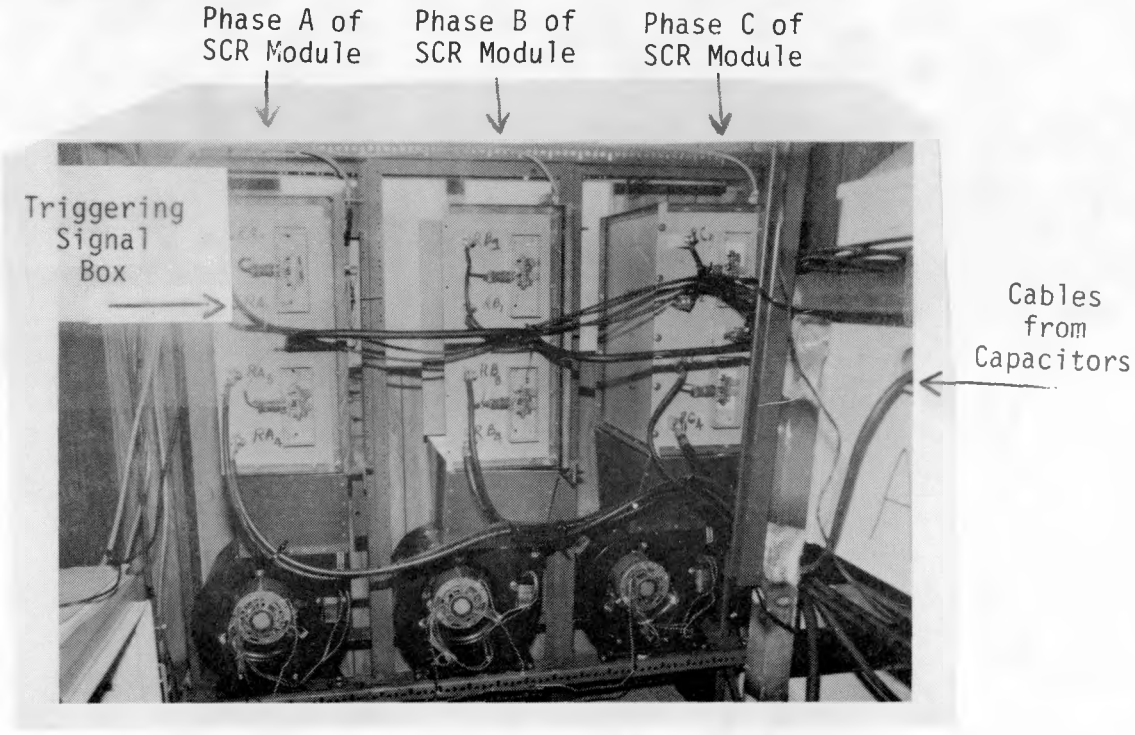

Figure 5.3: Photograph of SCR Module of the 300-kVAR APFC

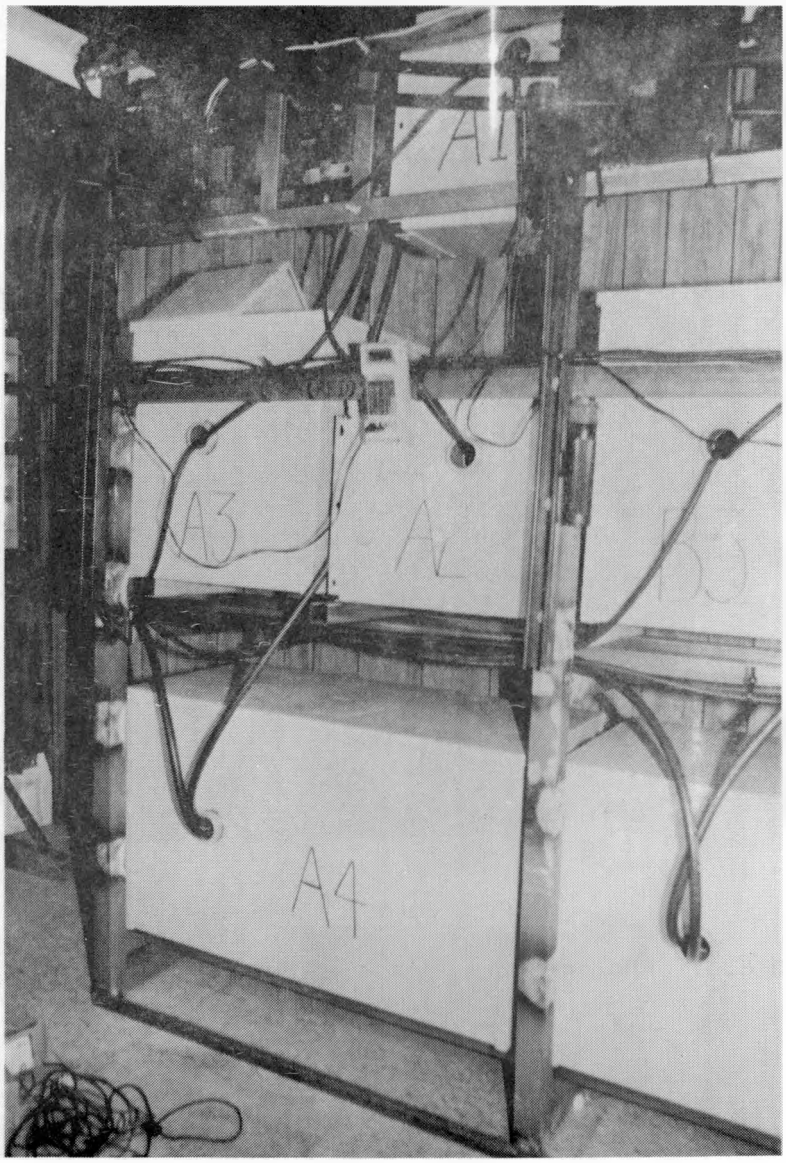

Figure 5.4: Photograph of Capacitor Module and Snubbing Inductor of the 300-kVAR APFC

Figure 5.5: Photograph of Transducers and Data Acquisition System of the 300-kVAR, APFC

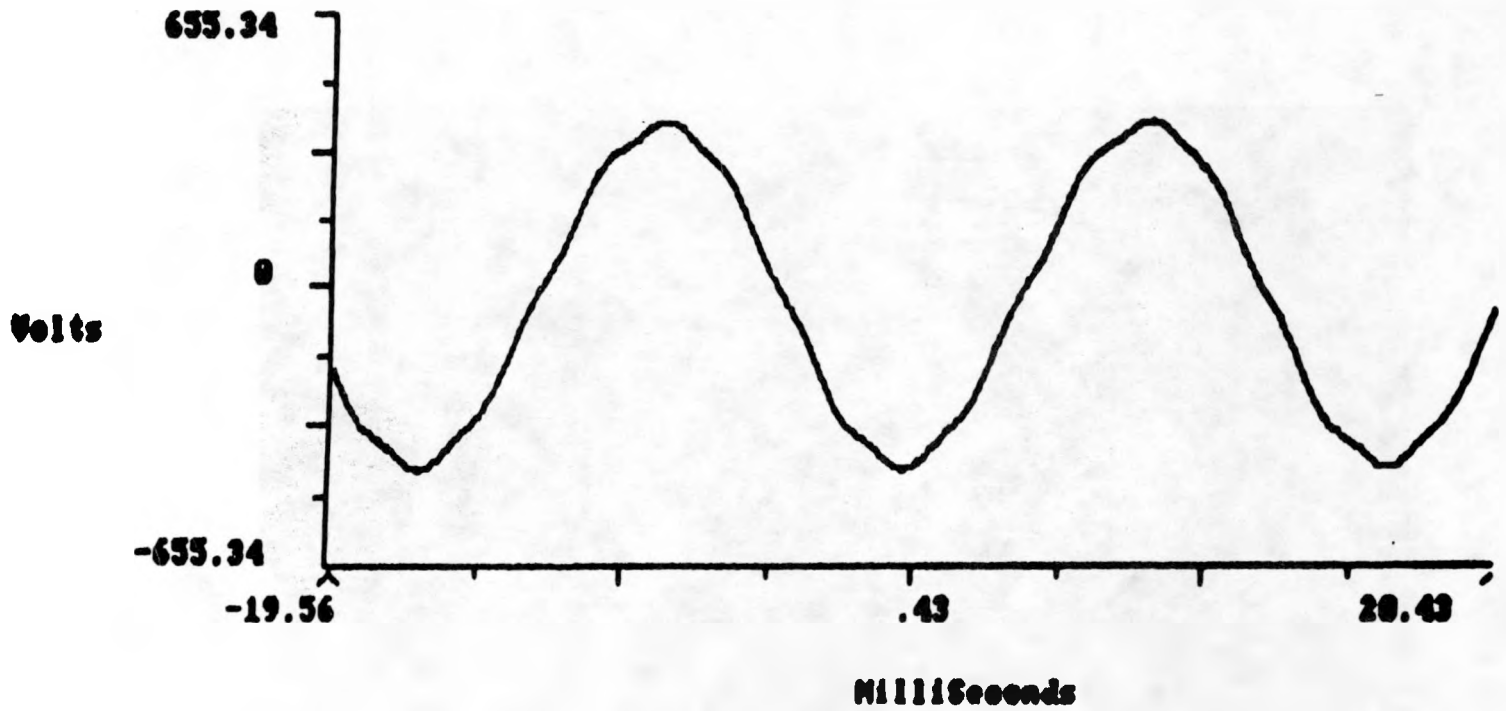

Figure 5.6: Waveform of Phase Voltage Showing Harmonics Contamination

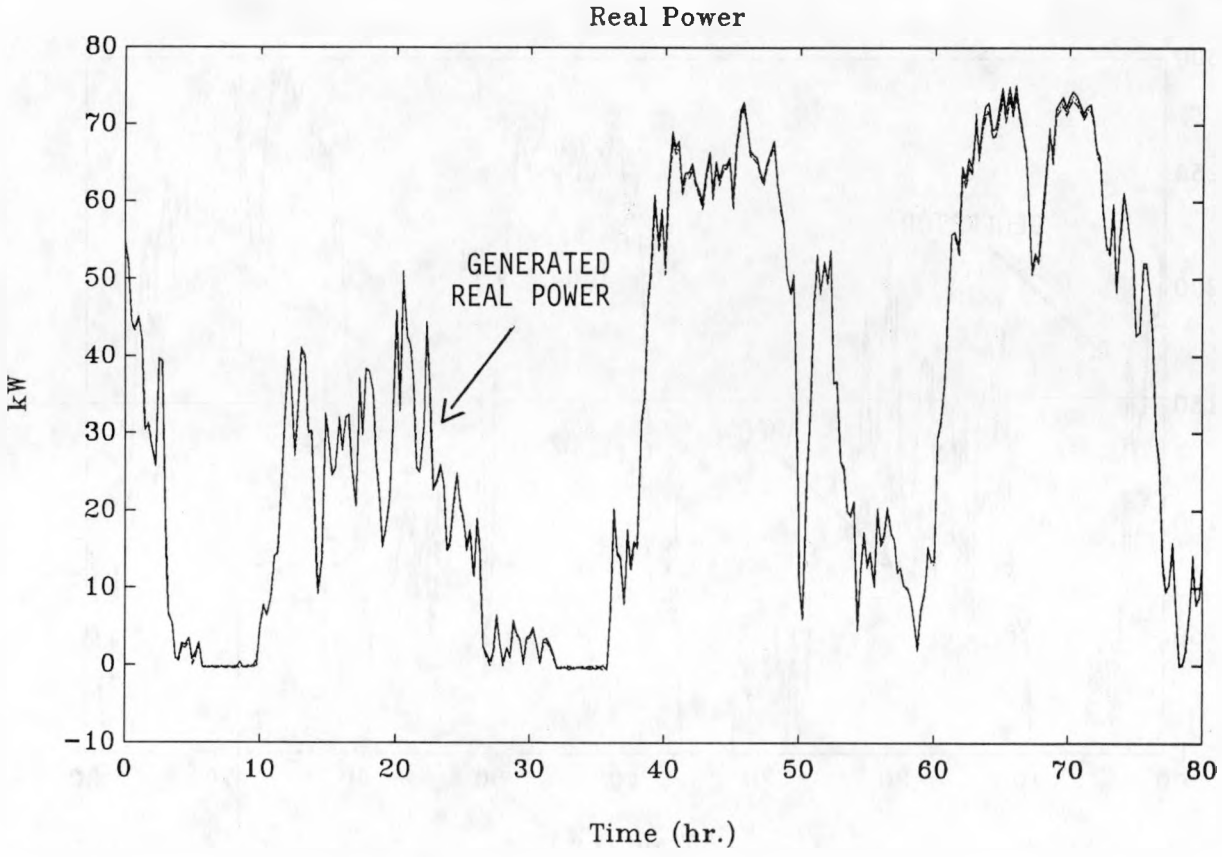

Figure 5.7: Steady-State Real Power Profile (300-kVAR APFC)

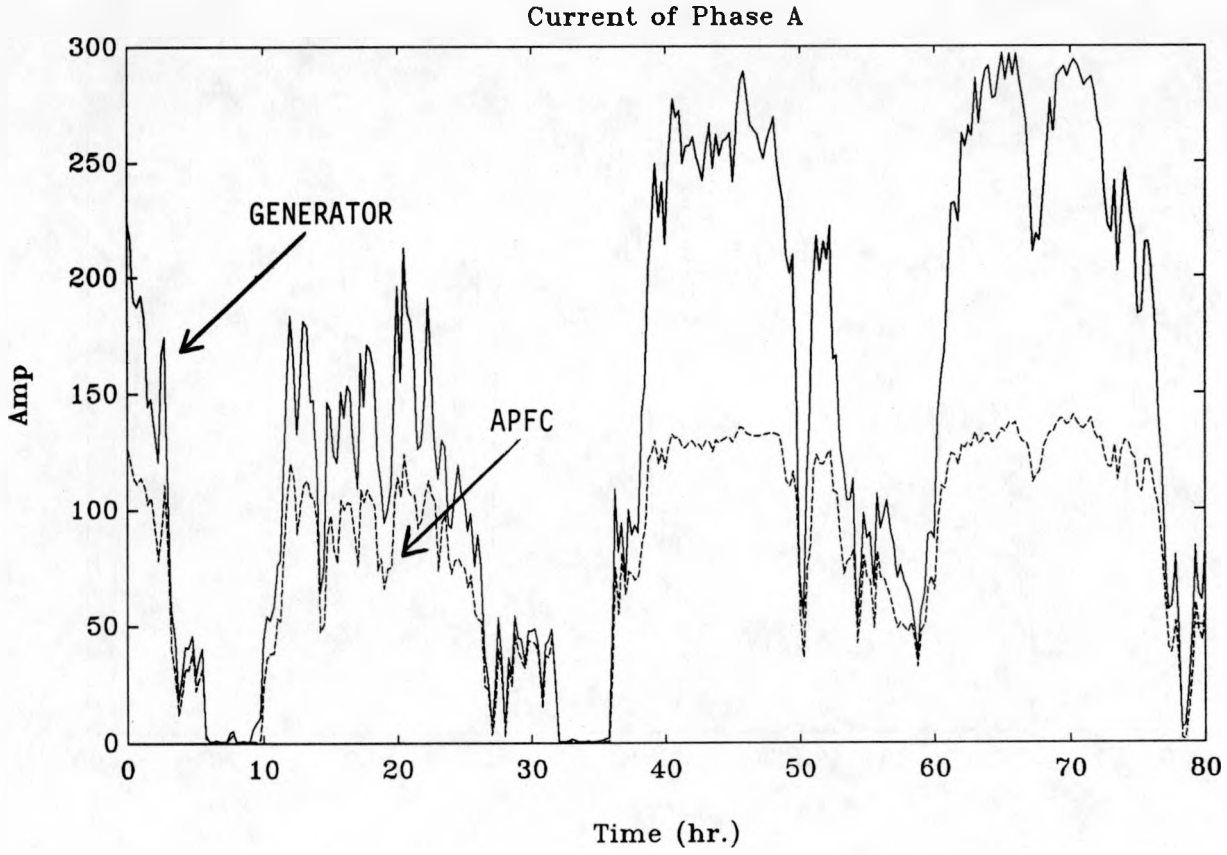

Figure 5.8: Steady-State Current Profile (300-kVAR APFC)

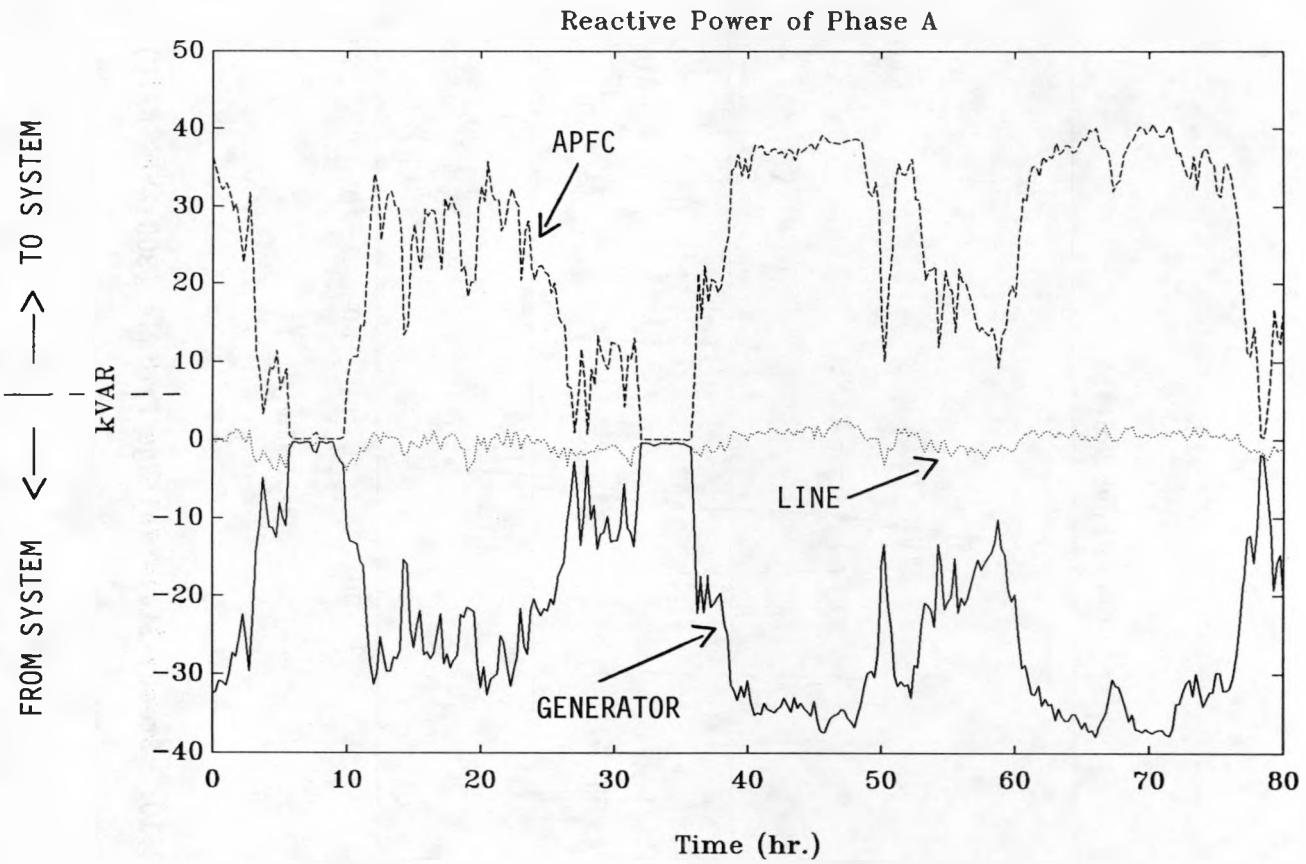

Figure 5.9: Steady-State Reactive Power Profile (300-kVAR APFC)

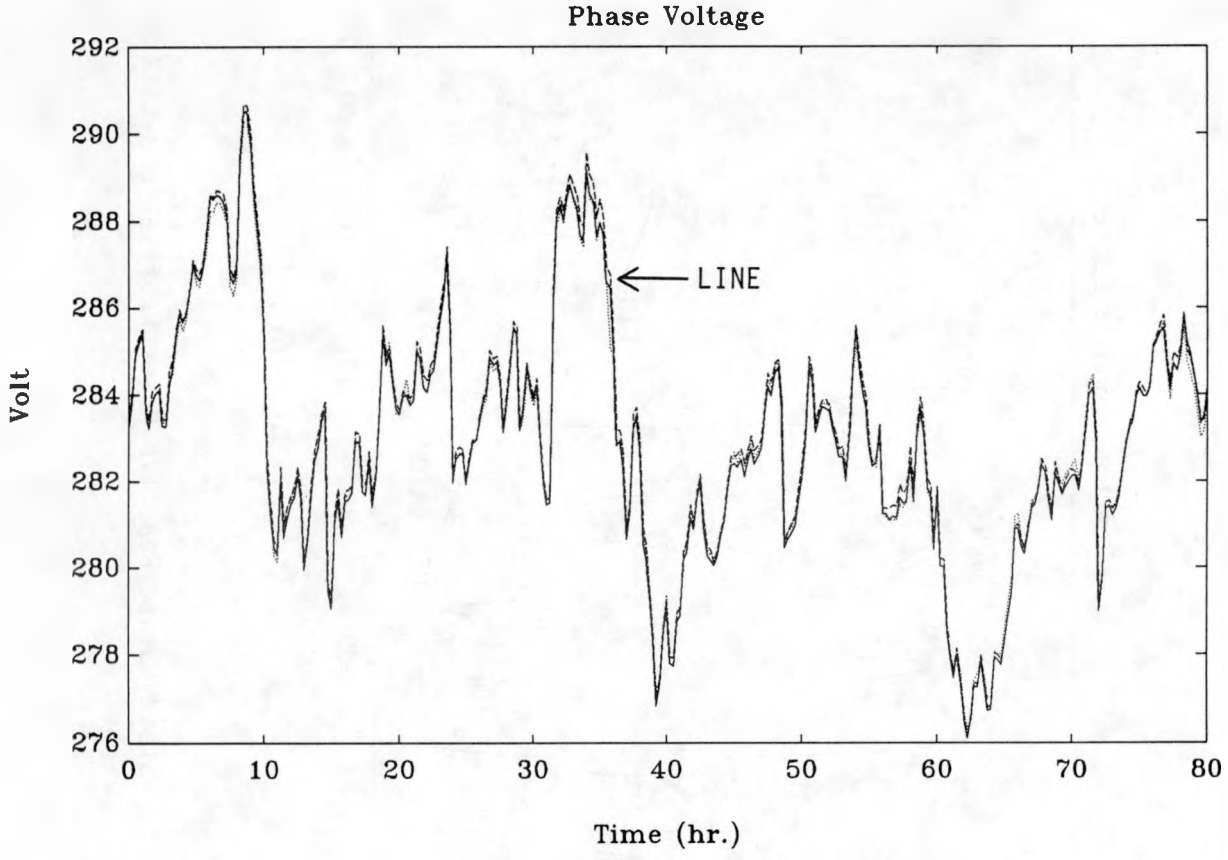

Figure 5.10: Steady-State Voltage Profile (300-kVAR APFC)

Figures 5.7 to 5.10 show the results obtained at the site with the APFC operating in the open-loop control mode. The results of phases A, B and C are very similar to one another. For brevity, only the plots of phase A are presented. Each data point in these plots represents a 15-minute average of the collected data gathered by the data acquisition system.

Figure 5.7 shows the real power generated by the seven induction generators. Figure 5.8 shows the currents measured on the generator side and the APFC side. The dashed line represents the current on the APFC side and the solid line represents the current on the generator side. The current on the generator side has both real and reactive component, whereas the APFC current is mainly capacitive.

Figure 5.9 shows the reactive power demand of the induction generators, the reactive power generated by the APFC and the reactive power drawn from the utility line. As seen in the figure, the reactive power demand of the induction generators is almost completely compensated by the APFC.

Figure 5.10 shows the phase voltage measured at the point where the APFC is connected.

5.3. SCR Failures at Site

Five SCR failures occurred in the course of 300 kvar APFC operation. All of the SCRs employed during the tests were of the S23 hockey puck series (23 mm wafer diameter) from International Rectifier (IR). Fortunately the package from these units can be readily removed to reveal the wafer and facilitate failure analysis.

Most of the SCRs failed with a gate open condition. The failed device was subject to careful analysis. After opening the package, the wafer from one of these components exhibited excellent device characteristics. When the cathode electrode was removed to test the wafer, debonding of the aluminum wire from the gate terminal was clearly visible. Temporary electrodes were created with washers, an insulating cardboard and a clamp. The device then properly exhibited voltage blocking in both directions, when proper voltage was applied with a 300 V battery. Then a temporary gate terminal was created with a needle. When an appropriate charge was dumped into the gate, the device properly exhibited forward conduction. It was then concluded that the SCR wafer was in good condition and the problem was with the improper bonding of the gate terminal.

International Rectifier (IR) was contacted regarding this problem. The vendor was supplied with an unopened failed part as well as details of the UW firing circuitry. The UW circuitry was approved after performing the analysis. IR accepted full responsibility for the failures. International Rectifier asked that the fifty UW owned parts be exchanged for a new batch of fifty "improved" SCRs.

Unfortunately, after the exchange was completed, gate open failures continued, although seemingly at a reduced rate. The UW group is considering the use of SCRs from a different vendor for future testing.

An additional SCR failure apparently occurred during a lightning storm. This SCR failed in a bidirectional shorted condition. Upon opening the package it was observed that the overheated zone of the SCR

was adjacent to the gate, indicative of (di/dt) failure. The large blocking inductor located on the supply side of the APFC rules out the possibility that (di/dt) failure caused directly by the lightning energy. The problem was identified as false triggering caused by lightning induced EMI.

REFERENCES

1. M. A. El-Sharkawi, S. S. Venkata, T. J. Williams, N. G. Butler, "An Adaptive Power Factor Controller for Three Phase Induction Generators," IEEE Trans. on Power Apparatus and Systems, Vol. PAS-104(7), 1985, pp. 1825-1831.

2. M. C. Wehrey, R. J. Yinger, "Demonstration and Testing of the DAF Indal Ltd., 50-kW Vertical Axis Wind Turbine Generator- A Fourteen Month Experience," Report by Southern California Edison Co., 1983.

3. T. Moore, "Wind Power: A Question of Scale," EPRI Journal, May 1984, pp. 6-16.

4. Wind Power Parks: 1983 Survey. Palo Alto, California: Electric Power Research Institute, August 1984, AP-3578.

5. A. S. Mikhail, "Wind Power for Developing Nations," Solar Research Institute, July 1981, SERI/TR-762-966.

6. J. J. Asmussen, "Wind Power, Its Promises, and Problems", Energy Communications, Vol. 7(6), 1981, pp.495-580.

7. N. Mohs, "Blowing in the Wind," Discover, June 1985, pp. 69-74.

8. S. S. Venkata, E. C. Boardman, "Investigations of Small Wind Turbine Induction Generators," Bonneville Power Administration Report No. DOE/BP-137, Portland, Oregon, Dec. 1982.

9. R. Natarajan, "Investigations on Induction Generators for Wind Energy Conversion Systems," Ph.D. Dissertation, University of Washington, Seattle, Washington, Department of Electrical Engineering, Sept. 1986.

10. S. S. Venkata, R. Natarajan, M. A. El-Sharkawi, N. G. Butler, "Investigations on Intermediate-size Wind Electric Conversion Systems Employing Induction Generators. Part I: Estimation of Energy Components," IASTED Conference on Energy, Power and Environmental Systems, Santa Barabara, California, May 29-31, 1985.

11. R. Natarajan, S. S. Venkata, M. A. El-Sharkawi, N. G. Butler, "Economic Feasibility Analysis of Intermediate-Size Wind Electric Energy Conversion Systems Employing Induction Generators," ibid and International Journal of Energy Systems (Accepted for publication).

12. S. S. Venkata, R. Natarajan, M. A. El-Sharkawi, N. G. Butler, Reliability Evaluation of Induction Generators Wind Electric Energy Conversion Systems," Proc. of European Reliability Conference, Copenhagen, Denmark, June 16-20, 1986, pp. 47-54.

13. T. J. Williams, "Adaptive Reactive Power Compensator for Wind Generators," M. S. Thesis, University of Washington, Department of Electrical Engineering, Oct. 1983.

14. M. A. El-Sharkawi, S. S. Venkata, T. J. Williams, N. G. Butler, "An Adaptive Power Factor Controller for Three-Phase Induction Generators," IEEE Trans. on Power Apparatus and Systems, pp. 1825-1831, July 1985.

15. S. S. Venkata, M. A. El-Sharkawi, C. C. Liu, "Reactive Power Management Device Assessment," EPRI Final Report, Advanced Power System Division, Palo Alto, California, Dec. 1986

16. M. A. El-Sharkawi, S. S. Venkata, S. V. Vadari, M. L. Chen, N. G. Butler, R. J. Yinger, "Development and Field Testing of an Adaptive Power Factor Controller," 1987 IEEE PES Winter Meeting, New Orleans, Louisiana, Feb. 1987. (To appear in IEEE Transactions on Energy Conversion).

17. S. V. Vadari, "Failure Mode Effects Analysis of Large-Sized Electronic Circuits Using Dynamic Equivalency Techniques," M.S. Thesis, University of Washington, Department of Electrical Engineering, March, 1986.

18. M. L. Chen, "Adaptive Power Factor Controller," M.S. Thesis, University of Washington, Department of Electrical Engineering, Feb. 1987.

19. IEEE Power Engineering Society "IEEE Recommended Practice for Electric Power Distribution for Industrial Plants," IEEE STD. 141-1976.

20. J. J. Asmussen, "Wind Power, its Promises and Problems", Energy Communications, Vol: 7, No. 6, 1981, pp. 495.

21. H. E. Jordan, Energy-Efficient Motors and Their Applications, (Book): New York, Reinholdt, 1983.

22. Westinghouse Energy-Efficient Induction Generators, Technical Information, Westinghouse Electric Company, No. SA 11007 B81.

23. Primeline Induction Generators, Technical Information, Marathon Electric Company, No. SB 322, March 1984.

24. A. Fitzgerald, L. Kingsley and S. Umans, Electric Machinery (Book): New York, McGraw-Hill Book Company, 1983.

25. E. C. Boardman, S. S. Venkata, N. G. Butler, "The Effect of Directional Rotation in Single Phase Induction Generators", IEEE Trans. on Power Apparatus and Systems, Vol. PAS-103, No. 8, Aug. 1984, pp. 2222-2230.

26. N. N. Hancock, Matrix Analysis of Electric Machinery, (Book), Pergamon Press, Second Edition, 1974.

27. H. Majmudar, Electromechanical Energy Converters, (Book): Allyn and Bacon Inc., 1965.

28. IEEE Industry Applications Society, IEEE Standard Test Procedures for Polyphase Induction Motors and Generators, IEEE STD. 112, 1984.

29. Technical Analysis Guide, Palo Alto, California: Electric Power Research Institute, 1984.

30. IEEE Reliability Group, Reliability Data Handbook, IEEE STD. 500, 1984.

31. A. M. Polovko, Fundamentals of Reliability Theory (Book): New York, Academic Press, 1965.

32. S. S. Venkata, M. Chinnarao, E. W. Collins, E. U. Ibok, "Reliability of Mine Electrical Power System Transients Protection, Reliability Investigations", U.S. Bureau of Mines Report, Vol. II, West Virginia University, Morgantown, W.V., 1979.

33. H. W. Dommel, W. S. Meyer, "Computation of Electromagnetic Transients," Proceedings of IEEE, Vol. 62, pp. 983-993, July 1974.